

**ADVANCED ROBOTIC VOLTAMMETRIC DRUG
ANALYSIS IN A 24-WELL MICROTITER PLATE**

Somjai Teanphonkrang



A Thesis Submitted in Partial Fulfillment of the Requirements for the

Degree of Master of Science in Chemistry

Suranaree University of Technology

Academic Year 2012

การวิเคราะห์ยาแบบโรบอติกโวลเทมเมตริกขั้นสูงในไมโครไทดเตอร์เพลต 24 หลุม

นางสาวสมใจ เตียนพลกรัง



วิทยานิพนธ์นี้เป็นส่วนหนึ่งของการศึกษาตามหลักสูตรปริญญาวิทยาศาสตรมหาบัณฑิต

สาขาวิชาเคมี

มหาวิทยาลัยเทคโนโลยีสุรนารี

ปีการศึกษา 2555

**ADVANCED ROBOTIC VOLTAMMETRIC DRUG ANALYSIS IN A
24-WELL MICROTITER PLATE**

Suranaree University of Technology has approved this thesis submitted in fulfillment of the requirements for a Master's Degree.

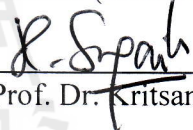
Thesis Examining Committee


(Assoc. Prof. Dr. Jatuporn Wittayakun)

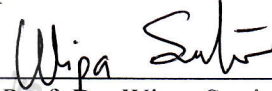
Chairperson


(Assoc. Prof. Dr. Albert Schulte)

Member (Thesis Advisor)


(Prof. Dr. Kritsana Sagarik)

Member


(Assoc. Prof. Dr. Wipa Suginta)

Member


(Asst. Prof. Sanchai Prayoonpokarach)

Member


Prof. Dr. Sukit Limpijumngong

Vice Rector for Academic Affairs


(Assoc. Prof. Dr. Prapun Manyum)

Dean of Institute of Science

สนใจ เตียนพลกรัง : การวิเคราะห์ยาแบบโรโบติกโวลแทมเมตริกขั้นสูงในไมโครไตเตอร์
เพลต 24 หลุม (ADVANCED ROBOTIC VOLTAMMETRIC DRUG ANALYSIS IN A 24-
WELL MICROTITER PLATE) อาจารย์ที่ปรึกษา : รองศาสตราจารย์ ดร.อัลแบร์ท ชูลเทอ,
169 หน้า.

ได้มีการรายงานจากหลายกลุ่มในการนำท่อนาโนคาร์บอนซึ่งมีคุณสมบัติเป็นตัวเร่งทางเคมีไฟฟ้ามาใช้เป็นเครื่องมือวิเคราะห์ในการตรวจวัดทางโวลแทมเมตริกเพื่อตรวจสอบยาปฏิชีวนะ สารต้านอนุมูลอิสระ และยาแก้ปวด วิทยานิพนธ์นี้รายงานเกี่ยวกับการใช้ท่อนาโนคาร์บอนกับวิธีทางเคมีไฟฟ้าแบบอัดโนมิติ ที่ออกแบบมาเป็นพิเศษสำหรับความสะดวกในการวัดโดยใช้ไมโครไตเตอร์เพลตขนาด 24 หลุม การตรวจสอบระบบโรโบติกกับสารที่ใช้งานทางชีวภาพสามชนิดคือ วิตามินซี นอร์ฟล็อกซาซิน และไซโปรฟล็อกซาซิน และพาราเซตามอล แสดงความสัมพันธ์เชิงเส้นระหว่างการเปลี่ยนแปลงของกระแสโวลแทมเมตริกกับความเข้มข้นของวิตามินซี นอร์ฟล็อกซาซิน ยาไซโปรฟล็อกซาซิน และพาราเซตามอลที่ 10 มิลลิโมลาร์ 10 100 และ 150 ไมโครโมลาร์ ตามลำดับ ขณะที่ปริมาณต่ำสุดที่ตรวจวัดสาร วิตามินซี นอร์ฟล็อกซาซิน ยาไซโปรฟล็อกซาซิน และยาพาราเซตามอล เป็น 0.05 มิลลิโมลาร์ 0.3 1.6 และ 1.56 ไมโครโมลาร์ ตามลำดับ นอกจากนี้ยังได้ทำการตรวจวิเคราะห์เชิงปริมาณของสารตัวอย่างที่อยู่ทั้งในรูปสารละลายบริสุทธิ์ และในรูปเม็ดยาที่ทราบความเข้มข้นของทั้งสี่ตัวอย่างโดยใช้วิธีทางเคมีไฟฟ้าแบบโรโบติกโวลแทมเมตริกในไมโครไตเตอร์เพลตขนาด 24 หลุม ผลการทดลองพบว่าการวัดมีค่าความเบี่ยงเบนไปจากค่าจริงไม่เกินร้อยละ 5 และอัตราการกลับคืนใกล้เคียงร้อยละ 100 สำหรับการวัดแบบโรโบติกที่ถูกนำมาใช้สำหรับการประเมินค่าความเข้มข้นของนอร์ฟล็อกซาซิน ที่เติมลงไปในตัวอย่างเป็นซ้ำ และในการศึกษาด้านเภสัชจลนพลศาสตร์ ด้วยวิธีโรโบติกให้ผลการวัดที่ดีกับการตรวจหา ยาแก้ปวดพาราเซตามอล ผลการทดลองที่ได้รับแสดงถึงการพัฒนาระบบการวิเคราะห์ตัวอย่างครั้งละหลายๆ ตัวอย่างพร้อมกัน จึงเป็นระบบที่มีศักยภาพในการนำไปใช้งานที่ต้องการการวิเคราะห์ตัวอย่างครั้งละจำนวนมากๆ โดยเฉพาะในอุตสาหกรรมยา และการทดลองในระดับคลินิก นอกจากนี้การวัดโดยระบบอัดโนมิติให้ความสะดวก สบาย ประหยัด และลดข้อผิดพลาดของการทำการทดลอง

สาขาวิชาเคมี

ปีการศึกษา 2555

ลายมือชื่อนักศึกษา _____

ลายมือชื่ออาจารย์ที่ปรึกษา _____

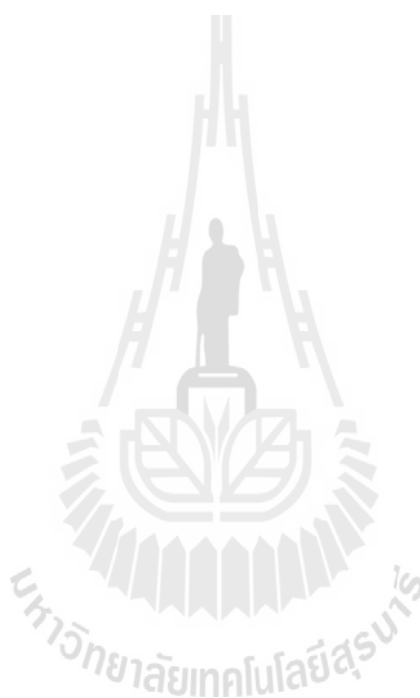
SOMJAI TEANPHONKRANG : ADVANCED ROBOTIC VOLTAMMETRIC
DRUG ANALYSIS IN A 24-WELL MICROTITER PLATE

THESIS ADVISOR : ASSOC. PROF. ALBERT SCHULTE, Ph.D. 169 PP.

ELECTROANALYSIS/ VOLTAMMETRY/ AUTOMATION/ DRUG ANALYSIS/
ANTIBIOTICS/ANTIOXIDANTS/ ANALGESICS

Carbon nanotube (CNT) modified electrodes with electrocatalytic activity have been reported by a number of groups as analytical tools for the voltammetric detection of antibiotics, antioxidants and analgesics. Here, we report the implementation of the CNT-based drug voltammetry into a robotic electrochemical device that is specially designed for the convenient execution of chronological measurements in a 24-well microtiter plate. Automated calibration measurements of three biological-active species, namely ascorbic acid (AA), norfloxacin (NFX), ciprofloxacin (CFX) and paracetamol (PCT), revealed a linearity of the differential pulse voltammetry (DPV) current for concentrations of AA, NFX, CFX and PCT up to 10 mM, 10 μ M, 100 μ M and 150 μ M, respectively. The limits of detection were estimated as 0.05 mM for AA and as 0.3, 1.6 and 1.56 μ M for NFX, CFX and PCT, respectively. In standard solutions or tablet samples of known compound content, all four analytes could be well quantified with the DPV microtiter plate assay, with the deviation of concentrations from true values ranged within $\pm 5\%$ and the recovery found to be close to 100%. An equally good performance level was also obtained when robotic DPV was used for assessment of NFX levels in the spiked serum samples. In a pharmacokinetic experiment robotic DPV was able to monitor actual PCT levels in test urine in appropriate manner. The results obtained from the work of this thesis demonstrated success with the establishment of robotic drug screening. For larger number of samples as they are likely in pharmaceutical and clinical laboratories assets of

the novel methodology are the convenience of execution as well as cost effectiveness and the minimization of manual operating error.



School of Chemistry

Student's Signature _____

Academic Year 2012

Advisor's Signature _____

ACKNOWLEDGMENTS

I would like to express my gratitude to my supervisor Assoc. Prof. Dr. Albert Schulte for giving me the opportunity to work on this project. His guidance, support and ideas made this work interesting for me and gave me a lot of inspiration. Throughout the work he provided his valuable time for guiding and correcting me, which helped making this thesis successful.

I also would like to thank all the other lecturers in the School of Chemistry and School of Biochemistry at Suranaree University of Technology (SUT) for passing on to me their knowledge in Chemistry and their experience in Chemistry laboratory techniques, which I found useful for my project development.

I would like to express my gratitude to the principle investigators of the Biochemistry-Electrochemistry Research Unit, namely Assoc. Prof. Dr. Wipa Suginta and Dr. Panida Khunkaewla for their efforts in offering a well-equipped laboratory facility of high standard. Thanks also go to Prof. Dr. Mathias Winterhalter and Dr. Helge Weingart for their project involvement and provision of antibiotic research samples and to Prof. Dr. Wolfgang Schuhmann and Mrs. Sandra Schmidt for their support with nice SEM images of bare and CNT-modified pencil lead working electrodes. To my university SUT, I thank for thesis fee exemption and for my financial support through project grant allocations to my supervisor.

I wish to extend my warmest thanks to my colleagues at the Biochemistry-Electrochemistry Research Unit, SUT for helping me to get through occasionally difficult

times, and for all the emotional support, friendship, entertainment and care that they provided.

Finally, special thanks go to my parents for continuing support, kind understanding and all the love they gave to me through my life.

Somjai Teanphonkrang



CONTENTS

	Page
ABSTRACT IN THAI	I
ABSTRACT IN ENGLISH	II
ACKNOWLEDGEMENTS	IV
CONTENTS	VI
LIST OF TABLES	X
LIST OF FIGURES	XI
LIST OF ABBREVIATIONS	XIX
CHAPTER	
I INTRODUCTION	1
1.1 Robotic electrochemistry/electroanalysis.....	1
1.2 Research objectives	3
II TECHNICAL BACKGROUND AND LITERATURE REVIEW.....	4
2.1 Principles of common electroanalytical detection schemes.....	4
2.1.1 General remarks	4
2.1.2 Electrochemical impedance spectroscopy	15
2.2 Micro- and macroelectrodes.....	20
2.3 Electroanalysis of drugs.....	23
2.4 Carbon electrodes	31
2.5 Robotic electrochemistry and electroanalysis.....	36
2.5.1 Available publications.....	36

CONTENTS (Continued)

	Page
III RESEARCH METHODOLOGY	39
3.1 Experimental and methods	39
3.1.1 Materials and chemicals	39
3.1.2 Instrumentation	40
3.1.3 Electrodes	41
3.2 Research methodology	42
3.2.1 Preparation of CNT-modified pencil lead electrodes (PLEs)	42
3.2.2 Characterization of CNT-modified PLEs	45
3.2.3 Manual and robotic drug electroanalysis	46
3.2.3.1 Manual and robotic ascorbic acid (AA) voltammetry	46
3.2.3.2 Manual and robotic antibiotic voltammetry	49
3.2.3.3 Manual and robotic analgesic voltammetry	53
IV RESULTS AND DISCUSSION	55
4.1 Characterization of CNT-modified PLEs	55
4.1.1 Scanning electron microscopy (SEM)	55
4.1.2 Electrochemical impedance spectroscopy (EIS)	56
4.1.3 Voltammetry trials with bare and CNT-modified PLEs	62
4.2 Establishment of robotic drug electroanalysis in 24-well microtiter plates	64
4.2.1 Work with respect to the target analyte ascorbic acid	64
4.2.1.1 Conventional ascorbic acid voltammetry tests,	

CONTENTS (Continued)

	Page
calibration measurements and sample analysis	64
4.2.1.2 Robotic ascorbic acid voltammetry: Establishment, calibration measurements and sample analysis	69
4.2.2 Work respect to the target analyte (NFX).....	78
4.2.2.1 Conventional NFX voltammetry tests, calibration measurements and sample analysis	78
4.2.2.2 Robotic NFX voltammetry in the microtiter plate format: Establishment, calibration measurements and sample analysis	82
4.2.3. Work with respect to the target analyte ciprofloxacin (CFX)...	93
4.2.3.1 Conventional CFX voltammetry tests, calibration measurements and sample analysis	93
4.2.3.2 Robotic CFX voltammetry in the microtiter plate format: Establishment, calibration measurements and sample analysis	98
4.2.4 Work with respect to the target analyte PCT.....	106
4.2.4.1 Conventional PCT voltammetry tests, calibration measurements and sample analysis	106
4.2.4.2 Robotic PCT voltammetry in the microtiter plate format: Establishment, calibration measurements and sample analysis	111

CONTENTS (Continued)

	Page
V CONCLUSIONS AND OUTLOOK	123
REFERENCES	125
APPENDICES	140
APPENDIX A SOLUTION PREPARATIONS FOR DRUGS SCREENING	141
APPENDIX B SCHEMES OF THE 24-WELL MICROTITER PLATE LOADS	145
APPENDIX C DESIGN OF SOFTWARE FOR THE EXECUTION OF ROBOTIC ELECTROCHEMICAL ANALYSIS IN 24-WELL MICROTITER PLATES	154
CURRICULUM VITAE	169

LIST OF TABLES

Table		Page
2.1	Physical electrochemistry and equivalent circuit element.....	18
4.1	Impedance parameters were obtained the analysis of the equivalent circuit fit of the impedance spectra of bare and CNT-modified PLEs.....	61
4.2	Ascorbic acid quantification in model (spiked) and real vitamin C tablet samples.....	78
4.3	Norfloxacin (NFX) quantification in spiked model samples, in NORFA tablets (400 mg/tablet) and intentionally spiked serum sample.....	93
4.4	Ciprofloxacin (CFX) quantification in spiked model samples and in COBAY tablets (500 mg/tablet).....	106
4.5	Paracetamol (PCT) quantification in spiked model samples, dissolved Tylenol tablet samples, and in urine samples after tablet intake.....	122

LIST OF FIGURES

Figure		Page
2.1	An electrochemical workstation with a three electrode configuration.....	5
2.2	Schematic diagram of a potentiometric measurement with an ion selective electrode (ISE).....	7
2.3	Conductometric cells for assessments of solutions with low and high conductivity.....	8
2.4	The cyclic voltammetry wave form and the shape of the cyclic voltammogram for a reversible charge transfer reaction.....	10
2.5	Potential wave forms and the resulting voltammograms for normal pulse voltammetry (A1 and A2), differential pulse voltammetry (B1 and B2) and square wave pulse voltammetry (C1 and C2).....	14
2.6	Electrochemically accessible potentials (the “potential window”) of platinum, mercury and carbon electrodes in various supporting electrolyte.....	15
2.7	Block diagram of the instrumentation used for electrochemical impedance spectroscopy (EIS) measurements.....	16
2.8	The small amplitude of sine wave voltage (stimulating signal) and current (measured response) as a function of time for a typical EIS recording in three electrode configuration	17
2.9	Electrochemical impedance spectra of a series and parallel combination of a resistor and a capacitor.....	19

LIST OF FIGURES (Continued)

Figure	Page
2.10 Equivalent circuit and plot of the impedance of model an electrochemical cell.....	20
2.11 Illustration of the cyclic voltammetry of a redox species ($M^{(n+)+} + e^- \longleftrightarrow M^{(n-1)+}$) at a microelectrode or a macroelectrode.....	22
2.12 Illustration of the common types of microelectrodes and their diffusion fields.....	22
2.13 Chemical structure of L-ascorbic acid and the reaction scheme for its redox reaction.....	27
2.14 Chemical structures of norfloxacin, NFX, and the reaction scheme for the oxidation reaction.....	28
2.15 Chemical structures of ciprofloxacin, CFX, and the reaction scheme for the oxidation reaction.....	29
2.16 Chemical structures of paracetamol, PCT, and the reaction scheme for the redox reaction.....	31
2.17 Popular carbon-based electrode materials.....	34
2.18 Schematic diagram representing the principle of the electrophoretic deposition of CNTs.....	35
2.19 Cyclic voltammogram of 1 mM potassium ferricyanide at a pencil lead working electrode in standard measuring solution and acquired in the available electrochemical robotic system.....	36
2.20 The device for automatic sequential electrochemistry in the individual	

LIST OF FIGURES (Continued)

Figure	Page
wells of a 24-well microtiter plate	38
3.1 Pencil lead electrode design and fabrication	44
3.2 Schematic diagram of the procedure used for the preparation of CNT-modified PLEs	44
3.3 Schematic of the arrangement used for beaker-type voltammetry and electrochemical impedance spectroscopy at CNT-modified PLEs	45
3.4 An electrochemical workstation with a three electrodes configuration, for test and calibration measurement of AA in the CV and DPV mode	47
3.5 Electrochemical robotic workstation for robotic voltammetric analysis of AA with CNT-modified PLEs	48
3.6 Schematic representation of the microtiter plate load as used for degradation tests with AA in the robotic electrochemical device	50
3.7 Schematic representation of the microtiter plate load for the robotic voltammetric degradation the of NFX	52
3.8 Schematic representation of the microtiter plate load for the robotic voltammetric degradation test of CFX	52
3.9 Schematic representation of the microtiter plate load for the robotic voltammetric degradation test of PCT	54
4.1 SEM images of a bare PLE (a), and CNT-modified PLEs (b): (c), (d), and (e) at different magnifications	56
4.2 Schematic description of the PLE/CNT/electrolyte system and the	

LIST OF FIGURES (Continued)

Figure	Page
corresponding electronic equivalent circuit (the “Randles” circuit).....	58
4.3 Electrochemical impedance spectra of (a) a bare PLE and (b) a CNT- modified PLE measured in an electrolyte with 1 mM Fe(CN) ₆ ^{3-/4-} in 0.1 M KCl.....	61
4.4 Cyclic voltammograms at a bare and a CNT-modified PLE in 1 mM K ₃ Fe(CN) ₆ in 0.1 M KCl.....	63
4.5 Differential pulse voltammograms at bare PLE and CNT-modified PLEs in 1 mM Fe(CN) ₆ ³⁻ in 0.1 M KCl.....	64
4.6 Cyclic voltammograms and differential pulse voltammograms of 5.0 mM AA in 0.1 M KCl at a bare and a CNT-modified PLE working electrode.....	66
4.7 A set of DPVs of 0.1 to 10 mM concentration of AA in 0.1 M KCl.....	67
4.8 Quantification of AA in spiked model samples by the precalibration method.....	68
4.9 Quantification of AA in a sample of a dissolved AA tablet by the precalibration method.....	69
4.10 Schematic representation of automated robotic electrochemical AA screening.....	70
4.11 Electrode and analyte stability test.....	72
4.12 Robotic electrochemical AA calibration measurements in 24-well microtiter plate.....	73
4.13 The microtiter plate load used for automated voltammetric quantification of	

LIST OF FIGURES (Continued)

Figure	Page
AA (real sample)	74
4.14 Robotic voltammetric quantification of AA (model sample) in microtiter plate wells by the precalibration method.....	74
4.15 Robotic voltammetric quantification of AA (real sample) in microtiter plate wells by the precalibration method.....	76
4.16 Conventional cyclic and DPVs of 100 μ M NFX in 0.1 M acetate/ 0.1 M KCl buffer (pH 4.5).....	79
4.17 Manually recorded DPVs of various concentration of NFX in 0.1 M acetate buffer (pH 4.5).....	80
4.18 Quantification of NFX in a model sample with adjusted 2 μ M levels by the standard addition method	82
4.19 Quantification of NFX in a dissolved NFX tablet sample by the standard addition method.....	83
4.20 NFX stability test in the robotic electrochemical system.....	85
4.21 Robotic NFX calibration measurements in a 24-well microtiter plate.....	86
4.22 Schematic representation of the load of a microtiter plate as used for a robotic NFX calibration measurement.....	86
4.23 Schematic display of the load of a microtiter plate as used for the concentration determination of a model (spiked) NFX sample with an adjusted level of 2.0 μ M.....	89
4.24 Microtiter plate-based quantification of NFX in a spiked, 2.0 μ M, NFX	

LIST OF FIGURES (Continued)

Figure	Page
model sample by the automated standard addition method.....	90
4.25 Microtiter plate-based quantification of NFX in a dissolved tablet (real) sample by the automated standard addition method.....	91
4.26 Robotic voltammetric quantification of NFX in spiked serum sample in microtiter plate wells by the standard addition method.....	92
4.27 CVs (a) and DPVs (b) of 10 μM CFX in 0.1 M phosphate (buffer pH 4.0)/ 0.1 M KCl at a bare PLE and a CNT-modified PLE working electrode.....	95
4.28 DPVs in solutions of increasing CFX concentrations as used for calibration curve acquisition and analysis.....	96
4.29 Quantification of CFX in a spiked model sample by application of the manually performed standard addition method.....	97
4.30 Quantification of CFX in a dissolved CFX tablet sample by application of the manually performed standard addition method.....	98
4.31 The electrochemical detection of 50 μM of the CFX in a microtiter plate well, with an electrode assembly incorporating a CNT-modified PLE (WE), an Ag/AgCl (RE) and a Pt spiral (CE).....	99
4.32 Robotic CFX calibration measurement in a 24-well microtiter plate format.	100
4.33 The microtiter plate load for CFX calibration measurement.....	101
4.34 Schematic display of the load of a microtiter plate as used for the concentration determination of a model (spiked) sample.....	102

LIST OF FIGURES (Continued)

Figure	Page
4.35 Microtiter plate-based quantification of CFX in spiked, 10.0 μ M CFX model samples by the automated standard addition method.....	103
4.36 Microtiter plate-based quantification of CFX in commercial CFX tablet samples by the automated standard addition method.....	105
4.37 Comparison of CVs (a) and DPVs (b) of 100 μ M PCT in 0.1 M KH_2PO_4 / 0.1 M KCl (pH 4.5) acquired with bare and CNT-modified PLEs.....	108
4.38 DPVs for increasing concentrations of PCT in 0.1 M KH_2PO_4 /0.1 M KCl (pH 4.5).....	110
4.39 Quantification of PCT in spiked model samples by manually performed DPV in the standard addition mode.....	110
4.40 Quantification of PCT a dissolved tablet sample by manually performed DPV in the standard addition mode.....	111
4.41 Response stability test for robotic PCT voltammetry.....	112
4.42 Robotic PCT calibration measurements in a 24-well microtiter plate.....	114
4.43 The microtiter plate load as used for robotic electrochemical PCT calibration measurements.....	114
4.44 The microtiter plate load as used for robotic electrochemical PCT determination with automated standard addition method in charge of quantification.....	115
4.45 Robotic voltammetric quantification of PCT in microtiter plate wells using the strategy of standard addition method for final computation.....	116

LIST OF FIGURES (Continued)

Figure	Page
4.46 Microtiter plate load as used for PCT determination in tablet sample solutions via robotic DPV and the standard addition method.....	117
4.47 Robotic voltammetric PCT level assessment of tablet samples.....	118
4.48 PCT DPVs acquired in different urine samples before and after uptake of a 1000 mg dose of PCT through tablet consumption.....	119
4.49 The microtiter plate load as used for robotic electrochemical PCT determinations in urine samples with automated standard addition method in charge of quantification.....	120
4.50 Robotic voltammetric urine PCT level assessment in microtiter plate format	121

LIST OF ABBREVIATIONS

V	Volt
E	Potential
I	Current
I_F	Faradaic current
I_C	Capacitive current
i_p^c	Cathodic peak current
i_p^a	Anodic peak current
A	Ampere
R	Resistance
C	Capacitance
G	Conductance
Z	Impedance
W	Warburg impedance
Y	Admittance
Ω	Ohm
ω	Omega
π	Pi
f	Frequency
Φ	Phase
l	Distance
\emptyset	Diameter

LIST OF ABBREVIATIONS (Continued)

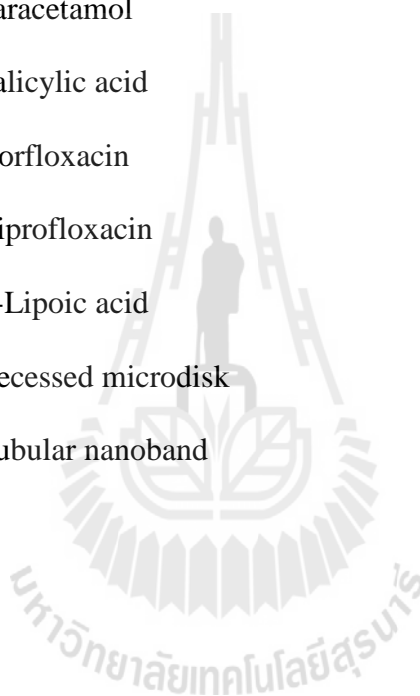
ρ	Specific resistivity
S	Siemens
e^-	Electron
μA	Microampere
L	Liter
mL	Milliliter
μL	Microliter
M	Molar
mM	Millimolar
μM	Micromolar
g	Gram
mg	Milligram
μg	Microgram
ppm	Parts-per-million
ppb	Parts-per-billion
ISE	Ion selective electrode
WE	Working electrode
CE	Counter electrode
RE	Reference electrode
CV	Cyclic voltammetry
NPV	Normal pulse voltammetry
DPV	Difference pulse voltammetry

LIST OF ABBREVIATIONS (Continued)

SWV	Square wave voltammetry
SV	Stripping voltammetry
HPLC	High performance liquid chromatography
FIA	Flow injection analysis
NMR	Nuclear magnetic resonance
GC/MS	Gas chromatography /mass spectrometry
SPET	Soil phase extraction
LC/MS	Liquid chromatography /mass spectrometry
CE	Capillary electrophoresis
EIS	Electrochemical Impedance Spectroscopy
R_s	Solution resistance
R_{CT}	Charge transfer resistance
C_{DL}	Double layer capacitance
AC	Alternating current
DC	Direct current
EC	Electrochemistry
PLE	Pencil lead electrode
GCE	Glassy carbon electrode
MWCNTs	Multiwall carbon nanotubes
CFE	Carbon fiber electrode
CPE	Carbon paste electrode
C_{60}	Carbon-60

LIST OF ABBREVIATIONS (Continued)

SPE	Screen printed electrode
EDP	Electrophoretic deposition
AA	Ascorbic acid (Vitamin C)
ASP	Aspirin
PCT	Paracetamol
SAL	Salicylic acid
NFX	Norfloxacin
CFX	Ciprofloxacin
ALA	α -Lipoic acid
RMD	Recessed microdisk
TNB	Tubular nanoband



CHAPTER I

INTRODUCTION

1.1 Robotic electrochemistry/electroanalysis

Analytical chemistry is important since the early days of chemistry and deals with the separation, identification and quantification of chemical species (“the analytes”) in samples of all sorts. Qualitative analysis only identifies the presence of an analyte of choice while quantitative analysis further determines the concentration of the particular compound with a suitable analytical method. Modern analytical chemistry is dominated by sophisticated instrumental analysis, namely spectroscopic and spectrometric, thermal, mass-sensitive and electrochemical techniques. Powerful spectrochemical analysis is usually related with complex, bulky and expensive optical equipment and there is a current trend to look for alternatives that offer more simple and cost-effective solutions for qualitative and quantitative analysis in e.g. environmental, pharmaceutical or food samples.

One alternative with that potential is electroanalysis which uses the relation of the potential (volt) and current (amps) in an electrochemical cell for analyte identification and quantification. Modern electrochemical equipment is comparably cheap and, thanks to the enormous progress in the field of electronics in the past decades, able to offer a superb sensitivity based on an ultralow pico- to femto-ampere current measurement capability. Electrochemical workstations are also available in highly miniaturized

versions that are operated with laptop-based software and transportable electrochemical cells. The latter is especially beneficial when aiming on field studies with instrumentation handled outside of the normal laboratory setting and this condition is not so easy to gain with the instrumentation for optical spectroscopy. The mentioned technical assets of electrochemistry equipment were a good motivation for working in this thesis on a subject that aimed at automation of electroanalysis to gain a convenient and cost-effective operation.

Focus was actually the automated electrochemical drugs analysis in 24-well microtiter plates. In the following, the approach of robotic electrochemical drug screening will be briefly outlined. The device for this type of measurements has been made available in the laboratory through previous work within Ph.D. on the convenient and reliable quantification of antioxidant levels in food samples (Intarakamhang, Leson, Schuhmann and Schulte, 2011 and Intarakamhang and Schulte, 2012) and of heavy metals in water and soil (Intarakamhang and Schulte, 2013).

Task of this M. Sc. thesis work was to further adapt the existing robotic electrochemical device to the needs of a highly sensitive pharmaceutical compound determination. Important issues to address included the optimization of working electrode for best voltammetric detection of the drugs of choice and the generation of special software scripts that execute in reproducible manner programmed electrochemical drug detection. Chosen as model types of drugs for the proof-of-principle study were ascorbic acid, two antibiotics, more specifically norfloxacin[®], a first generation of synthetic fluoroquinolones, and its derivative ciprofloxacin[®], and one analgesic (paracetamol[®]). For these four drugs the quantification was established in the electrochemical microtiter

plate format. Recovery rates, sensitivities and limits of detection were determined and the reproducibility explored using model samples made by dissolving purchased powders of the target drugs. Also measured were samples originating from the dissolution of tablets containing vitamin C[®], norfloxacin[®], ciprofloxacin[®] or paracetamol[®] in suitable buffers. In either case a comparison between the provided content on the box of the commercial product and the measured values allowed judgments on the quality of the proposed analytical procedure. And final test measurements in serum (NFX) and urine (PCT) delivered information on the suitability for applications in a more challenging situation that was expected to expose the sensors to interfering compounds likely to be present in the sample matrix.

1.2 Research objectives

The prime target of this thesis work was the development of a new strategy for an improved voltammetric analysis of pharmaceutical compounds. Technical assets of the developed scheme should be:

- (1) simplicity,
- (2) convenience for work with larger sample numbers,
- (3) good analytical performance, and
- (4) cost-effectiveness.

All the named four assets were aimed at with the technical solution of robotic electrochemical measurements in the wells of microtiter plates and through system optimization to the needs of automated drug voltammetry.

CHAPTER II

TECHNICAL BACKGROUND AND LITERATURE

REVIEW

2.1 Principles of common electroanalytical detection schemes

2.1.1 General remarks

Electrochemical techniques are routinely used for very sensitive detection of a variety of important analytes such as environmental pollutants, drugs and food contents. They are competitive in terms of precision, accuracy and sensitivity when compared, for instance, with optical methods. However, electrochemical instrumentation is cheaper, smaller and easier to operate and less complex than the apparatus for trace spectroscopy, which is a prominent alternative methodology for ultra-low level analysis. Because of its excellent cost-to-performance ratio and simplicity, electrochemical analysis matured in the past few decades into a more and more frequently applied analytical assay for heavy metal screening, drug analysis, environmental pollutant assessment, and water quality and industrial process control. The establishment of the strong position of electroanalysis was further supported by the immense progress with the electronics of the equipment that forms the basis of modern electrochemical work stations as shown in Figure 2.1. Improvements in the design and better electronic circuitries led to the appearance of potentiostats with pA detection and ns time resolution capability, properties that are ideal when aiming at electrochemical ultra-trace analyte quantification.

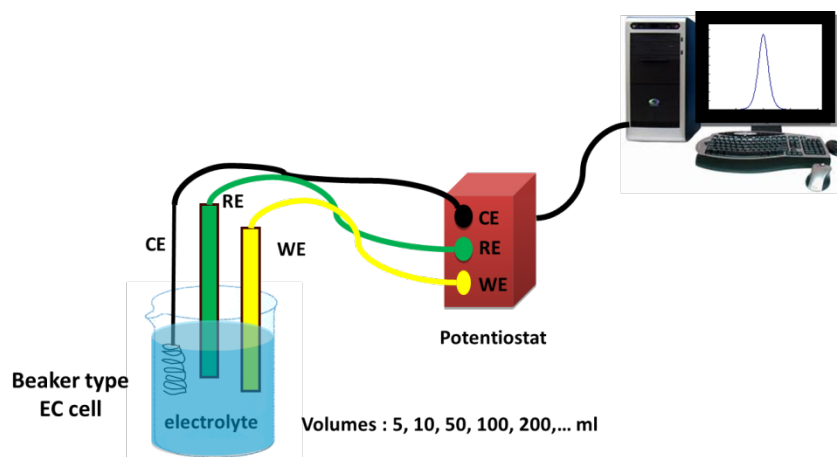


Figure 2.1 An electrochemical workstation with a three electrode configuration. Important components are the electrochemical cell with a working (WE), counter (CE) and reference electrode (RE) and the personal computer with appropriate software for the control of current (I) or potential (E) vs. time or I vs. E measurements and data acquisition and storage.

Within the family of electrochemical techniques available for trace analysis are the techniques of potentiometry, conductometry and voltammetry. The principles of these individual schemes will be briefly explained in the following.

Potentiometry gains information on the composition of a sample from the specific potential appearing between two electrodes, one of which is a common reference electrode such as the saturated Ag/AgCl reference electrode and the other, for instance, an ion-selective electrode (“indicator electrode,” ISE’s) specific for a certain target ion. Potentiometry is a classical analytical technique with the developing roots going back all the way to the end of the nineteenth century. However, the invention of new, better selective ionophores and more sensitive and stable electronic components for accurate and noise-free voltage measurements in the more recent past have tremendously

expanded the range of analytical applications of potentiometric measurement. ISE's, see Figure 2.2 for a schematic, and are currently intensively used in many fields, including clinical diagnostics, industrial process control, environmental monitoring, and physiology (Wang, 2006). They are typically membrane-based sensors, consisting of a selective ion-conducting polymer material, which separates as a membrane the sample from the inside of an electrode glass capillary. The inside of the capillary has a filling solution containing the ion of the interest at a known and constant activity. The membrane is usually water insoluble and mechanically stable. The composition of the membrane is designed to yield a potential that is primarily due to the outside exposure to the ion of interest. The trick is to find membranes that will selectively interact at the in- and outside with the analyte ion in terms of (chelating) affinity binding, leaving their counter ions behind. This process causes a transmembrane potential to appear in the case that the outside (sample) concentration is not equal to the inside (reference) level. The transmembrane potential is measured against a standard reference electrode and usually dependent on the concentration of the analyte ion in the sample solution. Calibration plots can thus be constructed and used for quantification. Assets of potentiometric measurements are a high selectivity and the ability to detect and quantify target analyte ions in complex matrices with a multitude of other substances (Wang, 2000).

An important characteristic property of an electrolyte solution is its capability to conduct electrical current. The electrolyte conductance is in fact possible through movement of positive (cation) and negative (anion) ions, which originate from the dissociation of strong or weak electrolytes.

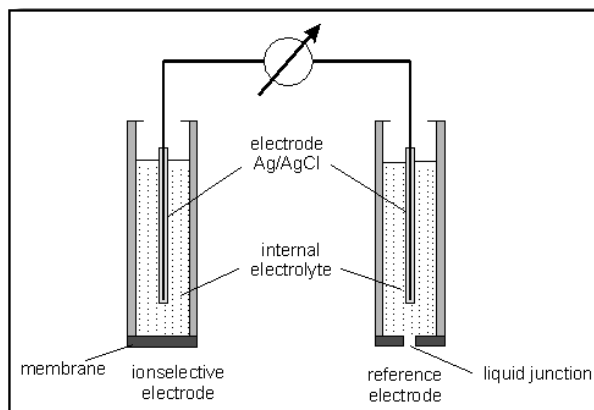


Figure 2.2 Schematic diagram of a potentiometric measurement with an ions selective electrode (ISE) (Wang, 2006).

The conductance of the electrolyte solution is measured in a small specially designed vessel with two electrodes, which is known as the conductance cell (see Figure 2.3). Conductance cells are usually made of glass with a set of sealed platinum plate electrodes, which are fixed in distance and covered with platinum black to avoid unwanted electrode polarization. For measurements in poorly conducting solutions, electrodes are placed close to one another in a fixed distance while in more conductive solutions a larger distance is preferred to avoid too high current flow during the resistance measurement (Koryta, Dvorak and Kavan, 1993).

$$R = \rho \cdot \left(\frac{l}{A}\right). \quad (\Omega) \quad (2.1)$$

R is the solution resistor, l is the distance between the electrodes, A is their area and ρ is specific resistivity ($\Omega \text{ m}$). The reciprocal of the resistivity ρ is called electrical conductivity (κ , $S \text{ m}^{-1}$). At the same time the reciprocal of the resistance of an electrolyte solution is the conductance, the unit of which is Siemens (S ; Ω^{-1}).

$$\kappa = \rho^{-1} \quad (\text{S m}^{-1}) \quad (2.2)$$

$$G = R^{-1} = \kappa \times \frac{A}{l} \quad (\text{S m}^{-1}) \quad (2.3)$$

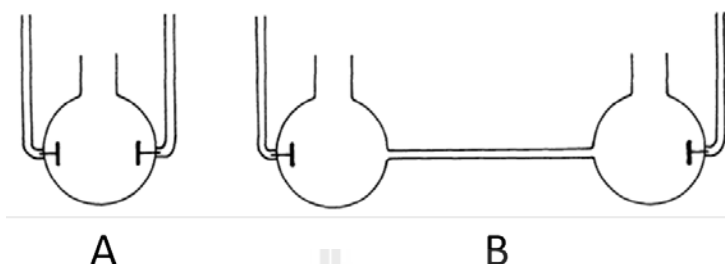


Figure 2.3 Conductometric cells for assessments of solutions with (A) low, and (B) high conductivity (Koryta et al., 1993).

As the area and distance of electrodes for a specific conductance cell are fixed, the value l/A is fixed, too and the parameter is defined as the cell constant, C . The conductance G can be computed from a resistance measurement that is gained by the application of voltage and acquisition of current and subsequent use of Ohm's Law. Then, with the known value of the cell constant, the specific conductivity κ can be calculated and related to the concentration, c , of the electrolyte solution to finally get the molar conductance Λ_m as parameter descriptive of the concentration-dependent electrolyte conductivity (Koryta et al., 1993).

$$\Lambda_m = \left(\frac{\kappa}{c} \right) \quad (\text{S m}^2 \text{ mol}^{-1}) \quad (2.4)$$

Conductometry is a method of analysis that can provide relative measures of important physiochemical properties including the dissociation constant, the hydrolysis stage and the activity, which is a parameter used at high electrolyte concentration to

consider attractive ion pair formation through interionic electrostatic force and the effect of deviation from linearity in conductivity vs. concentration plots (Bagotsky, 2006). An important application of conductance cells is conductometric titration where the clearly visible change in solution resistance (conductance) is used as indicator for the equivalence point and analyte quantification (Yamanaka, Yoshida, Koga, Ise and Hashimoto, 1998).

Voltammetry is used as powerful electroanalytical scheme for trace analysis as well as for studies of the mechanism of electrode reactions of various sorts. In a typical voltammetric measurement a constant, stepped, pulsed or gradually varying potential is applied via a potentiostat between the so-called working (WE) and a reference electrode (RE). While the working electrode is polarized to the desired potential, the current response (flow of charge between the working and the counter electrode) of the electrochemical cell is continuously measured as a function of time (Wang, 2000).

A first type of a voltammetric analysis is cyclic voltammetry (CV), which is the most widely used electrochemical technique for acquiring qualitative information on the redox potential of redox couples and the reversibility of the electrochemical charge transfer reaction on the WE surface but can also well serve quantitation purposes. With CV, as shown in Figure 2.4A, the applied potential is swept linearly between a starting (V_1), a turning (V_2), and a final potential, which may or may not be identical to starting potential. During such a potential cycle the potentiostat continuously measures the current as a function of time and records the actual potential as well. Constructed can then be with appropriate software instantaneously (“online”) plots of current, I , versus potential, V (“the cyclic voltammogram”). Figure 2.4B shows the expected CV response

for a measurement that has been observed with in three electrodes configuration, this is with a WE, RE and CE immersed in a solution containing a dissolved reversible redox couple by means of a single potential cycle and setting the potential limits V_1 and V_2 anodic and cathodic of the apparent reduction potential of the dissolved redox species.

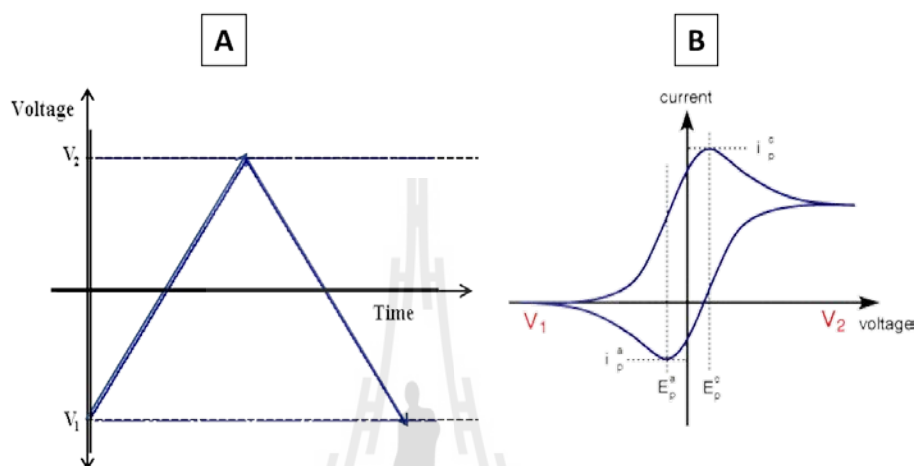


Figure 2.4 (A) The cyclic voltammetry wave form and (B) the shape of the cyclic voltammogram for a reversible charge transfer reaction. i_p^c and i_p^a are the cathodic and anodic peak current, respectively.

As cyclic voltammetry requires a continuous gradual change of the electrode potential, there is always a superimposed capacitive (charging) current (I_C) present that disturbs the analytically relevant faradaic redox current (I_F). To eliminate the unwanted capacitive current and to improve the signal-to-noise ratio of the measurements ($=I_F/I_C$), a unique technique using called pulse voltammetry was introduced. Pulse voltammetry takes advantage of differences in the speed of the decay between the capacitive charging and the faradaic charge transfer current during a short potential step (or “pulse”). While a charging current decays exponentially with time, a faradaic current

(for the diffusion-controlled situation) decays only as a function of the square root of time. Accordingly, the rate of decay of the capacitive current is considerably faster than the decay of the faradaic current. The charging current is actually negligible at a time of about $5 R_u \times C_{dl}$ after the potential step where $R_u \times C_{dl}$ reflects the time constant for the electrochemical cell, and may range from μs to ms . Therefore, at the end of a long enough potential pulse, the measuring current consists solely of the faradaic current and collection of the total current value at the end of the potential pulse allows discrimination between the faradaic and the charging current (Skoog, Holler and Nieman, 1997).

There are several types of pulse voltammetry that differ in the design of the pulse profiles and the way of data collection. The first choice in the family of pulse voltammetry is normal pulse voltammetry (NPV). NPV consists of a series of pulses of increasing amplitude, with the potential returning to the initial value after each pulse (Figure 2.5A1). Consider for the following interpretation the electrochemically induced reduction of an oxidized dissolved species assuming moderately fast unhindered electron transfer kinetics. If the initial (starting) potential is well positive of the redox potential of the species, the application of small amplitude pulses does not cause any faradaic reactions; hence there is no faradaic current response and because of the elimination via the pulse technique, also no capacitive current. The total current thus is at about zero line (Figure 2.5A2). However, when the pulse amplitude is high enough to bring the potential close to the redox potential, then there is a faradaic reaction induced at the working electrode and a current response at the end of the potential pulse will be observed. The magnitude of the current may depend on both the rate of diffusion of the electroactive species and the kinetics of electron transfer. At some level, the pulse potentials are sufficiently negative of the redox potential and the electron transfer reaction occurs

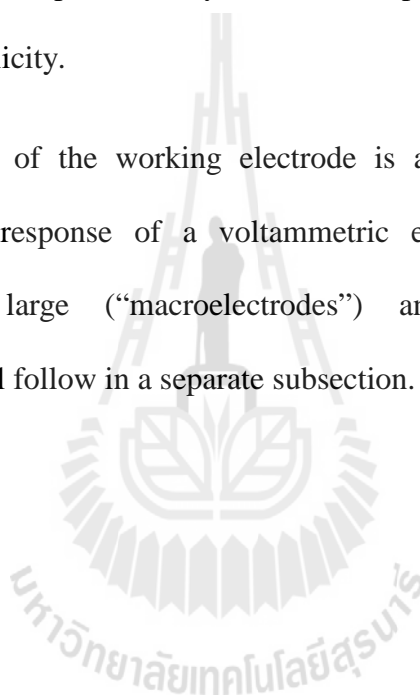
rapidly enough to make the faradaic current depending merely on the rate of diffusion. A diffusion limited current is obtained and becomes visible as a plateau at the end part of the sigmoidal shaped normal pulse voltammogram.

Differential pulse voltammetry (DPV) is another development of the pulse strategy and an extremely useful technique for measuring very low levels of organic and inorganic redox active species. In DPV, the pulse amplitude is fixed and superimposed on a linear potential ramp (Figure 2.5B1). Again consider the reduction of redox species at a working electrode potential around the redox potential. The difference, ($\Delta I = I_2 - I_1$) between the current sampled before (I_1) and just the end of a pulse (I_2) reaches a maximum, and is comparatively small for other electrode potentials. The outcome is a voltammogram with a symmetric peak (Figure 2.5B2). The principle of square wave pulse voltammetry (SWV) is similar to DPV but with SWV the wave form is composed of a symmetrical square step superimposed on a continuously growing potential (Figure 2.5C1). Current as measured on the reverse half-cycle (I_r) is subtracted from the current measured on the forward half-cycle (I_f). The difference, $\Delta I = I_f - I_r$, is displayed as a function of the applied potential, which leads to the typical bell-shaped SWV voltammogram (Figure 2.5C2) (Bard and Faulkner, 2001).

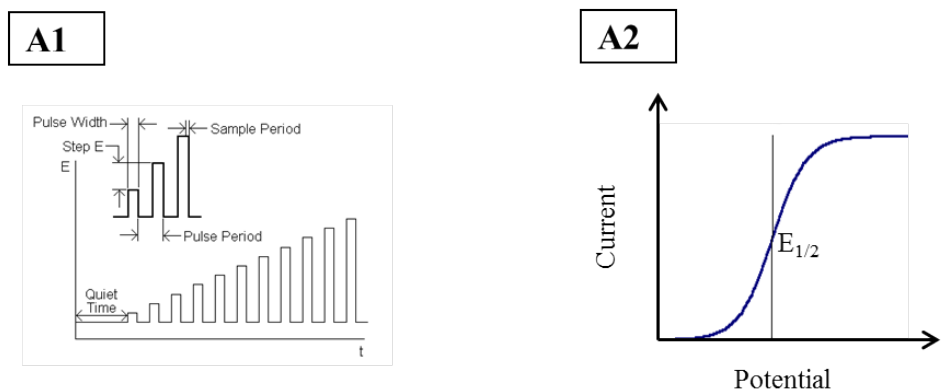
Main determinants of the performance of any voltammetric quantification of analyte species are the quality and type of potentiostat, the choice of optimal parameters for the chosen techniques, and the quality of the inert working electrode. Modern working electrodes most often are made of inert materials such as noble metals (Pt, Ir, Pt/Ir, Au etc.), the various available types of inert carbon (e.g. carbon pastes, glassy carbon, carbon fibers, pyrolytic carbon powder, fullerenes, carbon nanotubes,

graphitic pencil lead, etc.) or they are noble metal or carbon electrodes that are modified with thin films of mercury or bismuth or other beneficial surface deposits. In general, the working electrode should be suitable for a high signal-to-noise ratio in the given electrolyte as well as reproducible and stable in the voltammetric response. Other important considerations for the choice of the working electrode include the width of the electrochemically assessable potential window (Figure 2.6), the base material's electrical conductivity, the surface reproducibility, mechanical properties and issues concerning cost, availability and toxicity.

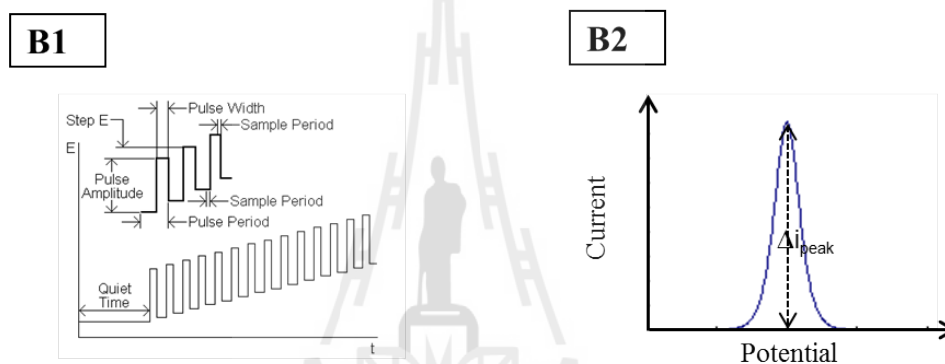
The size of the working electrode is also a factor that can strongly influence the current response of a voltammetric experiment. Comments on the differences between large (“macroelectrodes”) and small (“microelectrodes”) voltammetric sensor will follow in a separate subsection.



Normal pulse voltammetry



Differential pulse voltammetry



Square wave pulse voltammetry

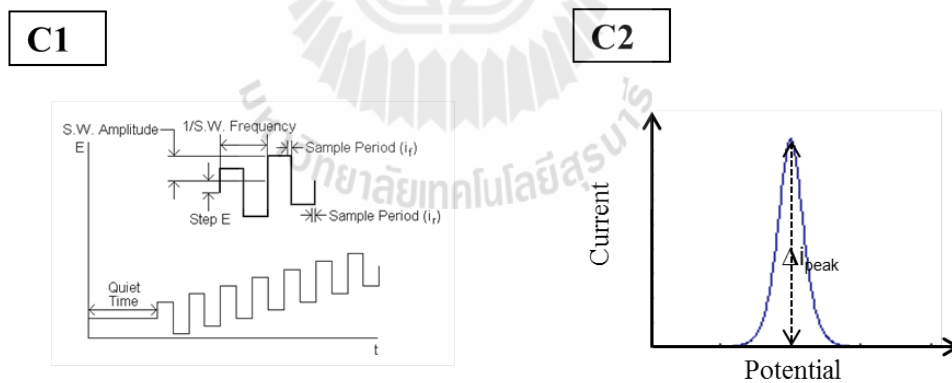


Figure 2.5 Potential wave forms and the resulting voltammograms for normal pulse voltammetry (A1 and A2), differential pulse voltammetry (B1 and B2), and square wave pulse voltammetry (C1 and C2).

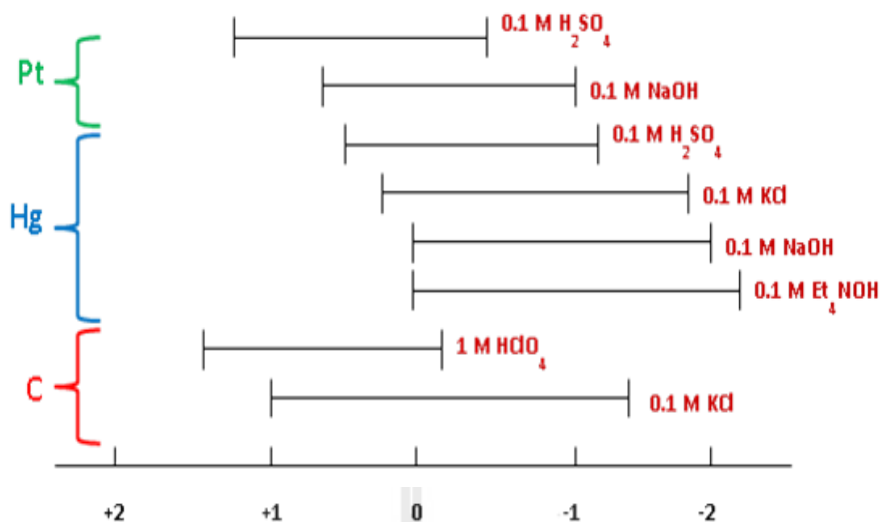


Figure 2.6 Electrochemically accessible potentials (the “potential window”) of platinum, mercury and carbon electrodes in various supporting electrolyte (Wang, 2000).

2.1.2 Electrochemical impedance spectroscopy

In the early 1970s, research electrochemists and material scientists discovered the power of electrochemical impedance spectroscopy (EIS) as a tool for studying electrochemical systems (Gabrielli, 1995). EIS is a technique that employs an electrochemical workstation in a three-electrode configuration. Implemented are working electrode (WE), counter electrode (CE) and reference electrode (RE), respectively, to characterize the surface condition or adsorbed species at the interface via application of an alternating voltage (current) and recording the systems current (voltage) response (Figure 2.7) (Loveday, Peterson and Podgers, 2004).

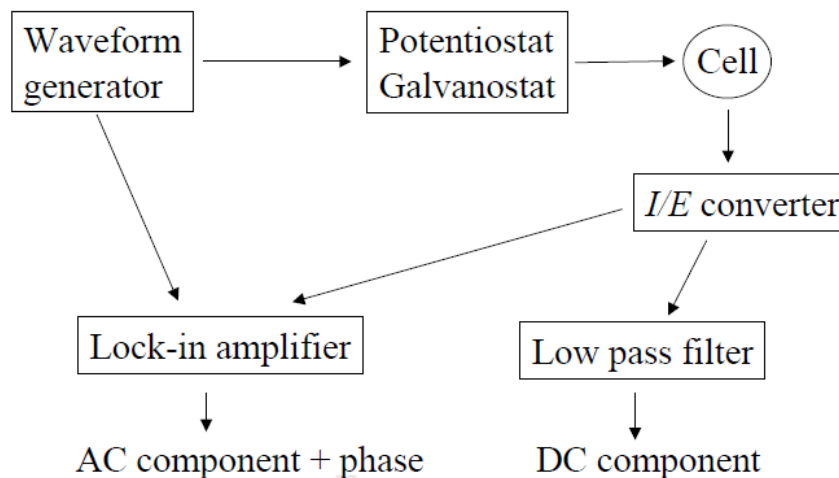


Figure 2.7 Block diagram of the instrumentation used for electrochemical impedance spectroscopy (EIS) measurements (Loveday et al., 2004).

Important for EIS is that the electrode/electrolyte interface undergoing electrochemical or chemical reactions can be described by an analogous electronic circuit consisting of specific combination of resistors and capacitors. What actually is being measured with potentiostatic EIS is the current response of the electrochemical cell towards the application of a sine wave potential. Varied in the measurements is the frequency of the stimulating potential sine wave and constructed are then EIS spectra that are plots of properties such as the impedance magnitude or the real/imaginary part of impedance as function of the frequency of the sine wave stimulus. Dependent on the nature of the electrochemical cell, and this is ideally dominated by the properties of the working electrode (“the electrode of interest”), there may or may not be a phase shift between the stimulating potential and the caused current sine wave (Figure 2.8) while the frequency of the two signals usually is the same.

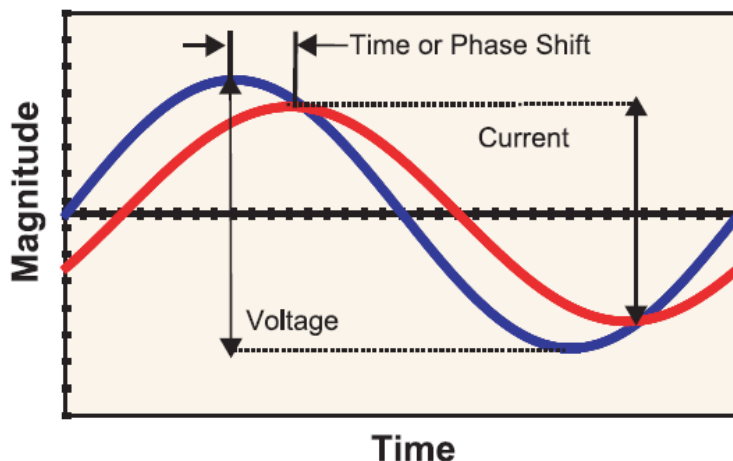


Figure 2.8 The small amplitude sine wave voltage (stimulating signal) and current (measured response) as a function of time for a typical electrochemical impedance spectroscopy recording in three electrode configurations. Note the phase shift between the two traces (Loveday et al., 2004).

EIS data is commonly analyzed by fitting them to an equivalent electrical circuit model. Most of the circuit elements in the model are electrical elements such as resistors, capacitors, and inductors. To be useful, the elements in the model should have a basis in the physical electrochemistry of the system. For example, most models contain a resistor that models the cell's solution resistance. Some knowledge of the impedance of the standard circuit components is therefore quite useful. Table 2.1 lists the common circuit elements, the equation for their current versus voltage relationship, and their impedance.

Table 2.1 Physical Electrochemistry and Equivalent Circuit Elements.

Component	Current Vs. Voltage	Impedance
resistor	$E = IR$	$Z = R$
inductor	$E = L \, di/dt$	$Z = j\omega L$
capacitor	$I = C \, dE/dt$	$Z = 1/j\omega C$

Very few electrochemical cells can be modeled using a single equivalent circuit element. Instead, EIS models usually consist of a number of elements in a network. Both serial (Figure 2.9A) and parallel (Figure 2.9B) combinations of elements occur. Fortunately, there are formulas that describe the impedance of circuit elements in both parallel and series combination. For linear impedance elements in series the equivalent impedance can be calculated from:

$$Z_{eq} = Z_1 + Z_2 + Z_3. \quad (2.5)$$

For linear impedance elements in parallel the equivalent impedance is calculated from:

$$\frac{1}{Z_{eq}} = \frac{1}{Z_1} + \frac{1}{Z_2} + \frac{1}{Z_3}. \quad (2.6)$$

Two examples are given to illustrate the point of combining circuit elements. For a 1 and a 4 Ω resistor connected in series, the impedance of combination is the same as the total impedance and is calculated as:

$$Z_{eq} = Z_1 + Z_2 = R_1 + R_2 = 1 \, \Omega + 4 \, \Omega = 5 \, \Omega. \quad (2.7)$$

Both resistance and impedance increase when the resistors in series. Now suppose that we connect two 2 μF capacitor in series then basic physics total capacitance of the combined capacitors is 1 μF . Impedance goes up, but capacitance goes down when

capacitors are connected in series. This is a consequence of the inverse relationship between capacitance and impedance.

$$\begin{aligned} Z_{eq} &= Z_1 + Z_2 = 1/j\omega C_1 + 1/j\omega C_2, \\ &= 1/j\omega(2e-6) + 1/j\omega(2e-6), \\ &= 1/j\omega(1e-6). \end{aligned}$$

To model diffusion-related impedance, Warburg impedance, W , is included in the dummy cell that models an electrochemical cell (Figure 2.10A). This Randle circuit models a cell where polarization is due to a combination of kinetic and diffusion processes. The Nyquist plot for the Randle cell is shown in Figure 2.10B. The Bode plot for the same data is shown in Figure 2.10C. The lower frequency limit was down to 1 mHz to better illustrate the differences in the slope of the magnitude and in the phase between the capacitor and the Warburg impedance.

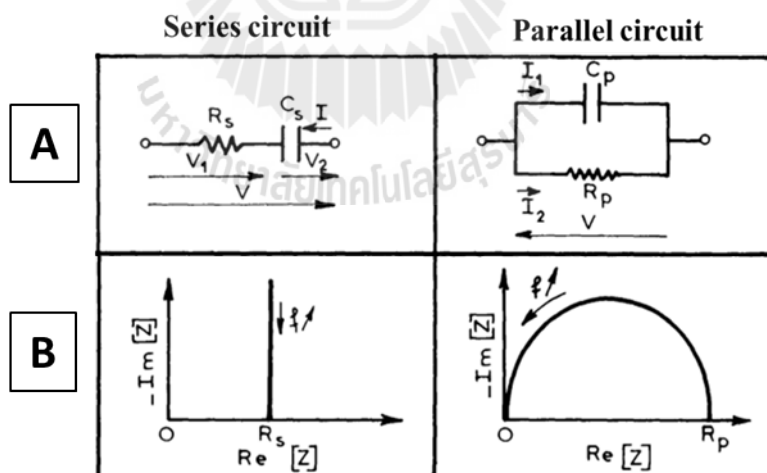


Figure 2.9 Electrochemical impedance spectra of a series and parallel combination of a resistor and a capacitor. (A) Schematic of the electrical circuit and (B) the Nyquist plots for the circuits in (A) (Gabrielli, 1995).

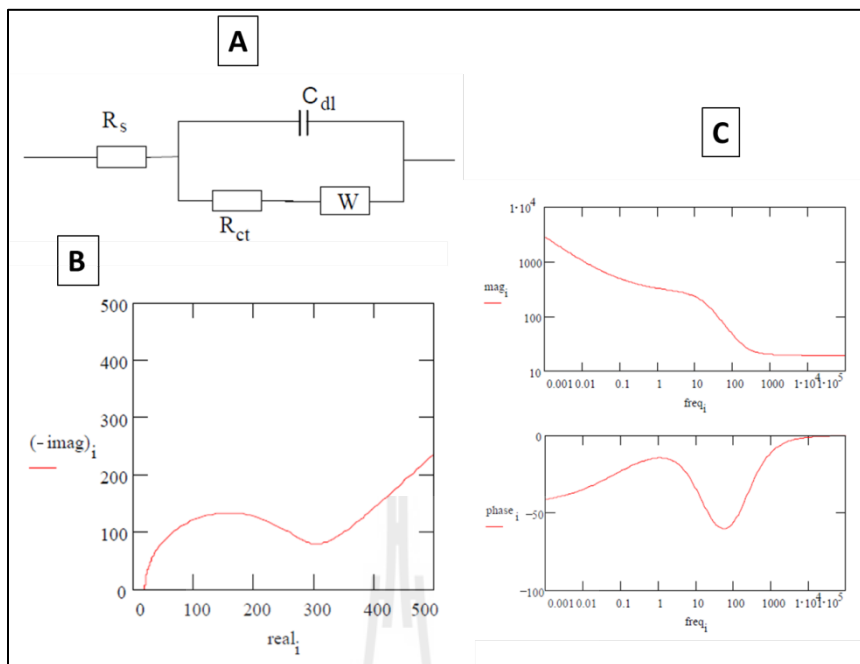


Figure 2.10 Equivalent circuit and plot of the impedance of an electrochemical cell were R_s is the solution resistance, R_{ct} the charge-transfer resistance C_{dl} the double-layer capacitance and W the Warburg impedance. (A) Equivalent circuit (Randles cell); (B) plot in the complex plane (Nyquist plane); and (C) plot in the Bode plane (Gamry instruments, 2010).

2.2 Macro- and microelectrodes

Macroelectrodes are electrodes with a relatively large active surface area, e.g. platinum disk electrodes with diameters of the insulated metal plane of a few mm or cylindrical electrodes made of metal rods of mm diameters and length. Microelectrodes, on the other hand, have active geometric dimensions in the low micrometer range. The reduction in the characteristic size is cause for a change of the behavior of the sensors in voltammetric measurements. Figure 2.11 shows the schematic representation of two cyclic voltammogram of an electroactive species, one recorded at a micro- and the other

at a macroscopic working electrode. The macroelectrode CV has a typical peak shape with current initially increasing before reaching a maximum and a declining phase. For the microelectrode (top), the current reaches at potentials exceeding the redox potential a steady state level and a sigmoidal voltammogram is observed. Reasons for this dissimilarity in appearance of the macro- and microelectrode CV are the properties in the mass transport of redox species toward the electrode surface via diffusion. For microelectrodes, the mass transport is radial while for macroelectrodes planar diffusion delivers the species to the active surface. With radial diffusion significantly more redox species is brought to the electrode surface compared to pure planar diffusion and depletion at higher rates of consumption as happening at the larger potentials is avoided for microelectrodes. Accordingly, microelectrodes display the so-called diffusion-limited steady state current; visible as current plateau in the microelectrode CV. Worth mentioning here that microelectrodes are common with geometries shown in Figure 2.12. That figure also represents the expected shape of the related diffusion fields (Pletcher, 1991).

Owing to their small total electrode surface areas the total measured currents at microelectrodes are small and usually in the range of nano- to picoamperes. On the other hand, the electrode capacitance is reduced as this parameter scales with the active electrode area and thus the RC time constant valid for the electrochemical measurement is beneficially reduced. Electrochemical transitions of redox active species from oxidized to reduced state and vice versa can be monitored with microelectrodes with up to microsecond time resolution which is good for an assessment of fast electron transfer reactions. Another effect of the small electrode area and the reduced capacitance is the minimization of capacitive currents and, together with improved faradaic currents due to

enhanced diffusion; an improvement in the ratio of faradaic to capacitive currents (i_F/i_C) is gained when using microelectrodes for electroanalysis. If not only the active electrode surface but also the total tip dimension is kept small to make needle type microelectrodes, then special measurements of local concentration profiles in the vicinity of micro/nanopores, and corrosion pits, etc. and the detection at small objects, such as living biological cells or liposomes etc. become possible.

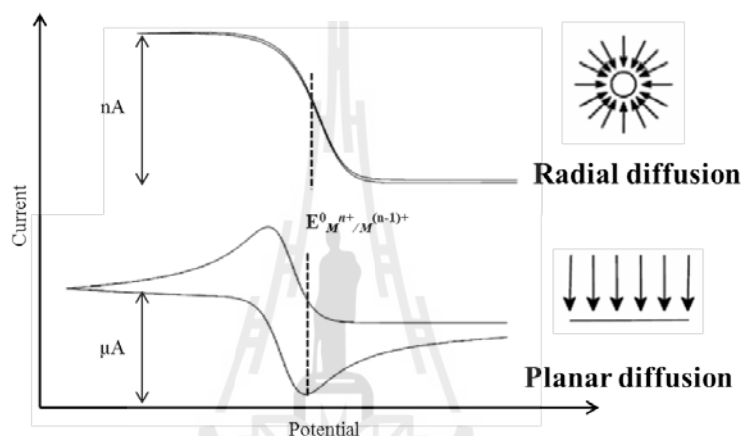


Figure 2.11 Illustration of the cyclic voltammetry of a redox species ($M^{(n+)+} e^- \rightleftharpoons M^{(n-1)+}$) at a microelectrode (top) or a macro electrode (bottom).

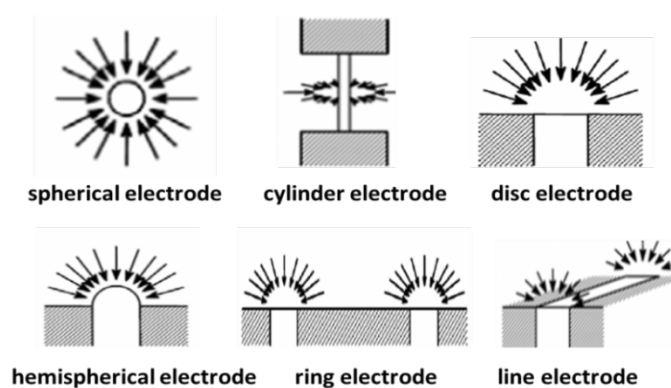


Figure 2.12 Illustration of the common types of microelectrodes and of their diffusion fields (Pletcher, 1991).

Attractive applications of microelectrodes and macroelectrodes are trace electroanalysis and the detection of extremely small amount of electroactive species (analytes) in sample solutions in the low ppm to ppt range. The electrodes are then often employed jointly with the schemes of pulse voltammetry to gain (additionally) the benefits going along with pulse techniques. How this is relevant for this thesis work is described in the next section, which deals with pharmaceutical electroanalysis.

2.3 Electroanalysis of drugs

Electrochemical pharmaceutical analysis deals with a wide range of chemical compounds. Only requisite for the suitability of an electrochemical detection of pharmaceuticals is that the molecules are redox active through the presence of electroactive functional groups and phenol-, nitro-, quinone-, nitroso-, amine and thiol entities are just a few examples of the many existing electroreducible or oxidizable substituents. Thesis goal was the implementation of drug electroanalysis into a workstation for robotic electrochemical measurements. To do this for the entire set of electroactive drugs would have been an impossible task and for a proof of principle of the concept of robotic drug electroanalysis work was limited to a selection of three types of drugs, namely (1) antioxidants (here: ascorbic acid), (2) antibiotics (here: norfloxacin, NFX, and ciprofloxacin, CFX), and (3) analgesics (here: paracetamol, PCT). Some remarks on the conventional methodologies for the detection of the chosen compounds are presented in following paragraphs.

Chromatographic methods with spectroscopic or electrochemical technique are standard for the determination of drugs in pharmaceutical environmental, clinical samples

(Wong, 1989). In 1989, for instance, high performance liquid chromatography (HPLC) with coulometric electrochemical detection was used for AA analysis, which is an important content of a variety of fruit and vegetables extracts, many beverages and various pharmaceutical supplements (Washko, Hartzell and Levine, 1989). Also, HPLC (Nayyssonen, Pikkarainen, Parviainen, Heinonen and Mononen, 1988), flow injection analysis (FIA) (Leon and Catapano, 1993) and ion exchange strategies (Chang, Hsu, Kao and Yang, 1982) have been reported for the determination of pharmaceutical AA species.

A study of Spraul demonstrated the utilization of reversed-phase HPLC coupled to NMR-spectroscopy for the determination and identification of PCT, the most frequently used painkiller on the pharmaceutical market and the medicine related to the highest number of incidences of drug poisoning that the emergency care units of hospitals have to deal with (Spraul, Hofmann, Lindon, Farrant, Seddon, Nicholson and Wilson, 1994). Liquid chromatography coupled to high-field ¹H-NMR spectroscopy showed its power for drug metabolite detection and characterization as, for instance, the identification of paracetamol metabolites in urine and bile was successfully achieved (Spraul et al., 1994). A derivative spectrophotometric method was developed for the assay of a ternary mixture of aspirin (ASP), paracetamol (PCT) and salicylic acid (SAL) (Fawzi, 2006). A determination of drug residuals in water worked with gas chromatography mass spectrometry (GC/MS) (Stumpf, Ternes, Wilken, Rodrigues and Baumann, 1999). Drugs in waste as well as in river and drinking water have been assessed with a method including solid phase extraction (SPE) and final detection by LC-electro-spectroscopy/MS/MS (Ternes, Hirsch, Mueller and Haberer, 1998 and Ternes, Bonerz and Schmidt, 2001). Fluoroquinolone identification and quantification in pharmaceutical preparations or biological samples have been proven possible via

spectrophotometry and spectrofluorometry (Salem, 2005) and by capillary electrophoresis (CE) (Lin, Deng, Liao, Sun, Lin and Chen, 2004). Although spectroscopic methods with chromatographic separation are routinely applied because of their reasonable sensitivity and selectivity and an ability to work well in the presence of interferences, the methodologies certainly have the drawbacks of being time-consuming, complicated in execution and expensive and demanding in terms of chemical use and instrumentation (Huang, Shentu, Chen, Liu and Zhou, 2008).

Electrochemical detection schemes, on the other hand, are often simpler in workflow, less demanding in consumables and cheap in instrumentation and they have proven an excellent capability for the determination of ultra-low trace-level of drugs, at least for a good collection of examples. Good sources of information on the principles and the status of electrochemical drug analysis are a few recent comprehensive review articles (Vire, Kauffmann and Pafriarache, 1989; Kauffmann and Vire, 1993; Wang, 1999; Ad-el-Aaali, 2004; Uslu and Ozkan, 2007). All possible electrode materials are, in principle, suitable for the establishment of efficient electrochemical drug detection. However, the work of this thesis concerned about the application of pencil lead electrodes (PLEs) for the targeted robotic drug voltammetry in microtiter plates as they already worked well in preceding work of others for the robotic electroanalysis of ascorbic acid, total antioxidant capacities and heavy metals (Intarakamhang et al., 2011, Intarakamhang and Schulte, 2012 and Intarakamhang et al., 2013).

PLEs are made of pencil leads of various diameters as they are commercially available as accessories in book shops or stationeries. An important issue with an eye on drug detection is the fact that bare PLEs often do not possess an appropriate sensitivity

for the compound of interest and response to the drug of choice has to be established through the involvement of a catalytically active surface modification (Patriarche, 1986). Very promising properties for the purpose of improving electrodes for the electrochemical detection of biologically relevant species were confirmed for CNT surface deposits (Banks and Compton, 2006, Zagal, Griveau, Ozoemena, Nyokong and Bedioui, 2009, Jacobs, Peairs and Venton, 2010 and Vashist, Zheng, Al-Rubeaan, Luong and Sheu, 2011). CNT-modified electrodes usually benefit from both a high surface area of the porous carbon nanotube modification as well as of an ability of CNT filaments to act as electrocatalyst. CNT-modified electrodes have already been suggested as sensors for the detection of the four target drugs of this thesis and the literature will be reviewed in the following text.

AA, to start with, is an electron donor and as such a redox active compound (Figure 2.13). Various analytical schemes for AA including optical and electrochemical assays take advantage of the redox properties of the compound (Pachla, Reynolds and Kissinger, 1985). There is a vast amount of literature available on the benefits of a CNT modification of the working electrodes for AA electroanalysis and the positive effect was observed for modified gold electrodes (e.g. Noroozifar, Mozhgan and Hamed, and Chauhan, Narang and Pundir, 2011), carbon paste electrodes (e.g. Meissam, Mozhgan and Hamed, 2013) and glassy carbon electrodes (Gupta, Jain and Shoor, 2013). Literature on the application of CNT-modified PLEs for this purpose is, to our best knowledge, not yet available in the databases. However, CNT-modified PLEs will be tested here for their performance as sensors in the robotic electrochemical workstation.

AA voltammetry was established in a 24-wells microtiter plate and demonstrated functional with bare PLEs by Intarakamhang et al. in an earlier study (Intarakamhang et al., 2011). Of interest will be whether the CNT modification enhances the methodology in comparison to the standard that is achieved without the nano-graphitic modifier.

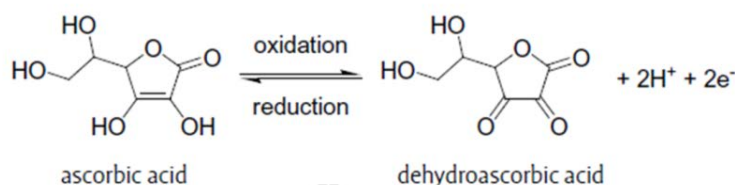


Figure 2.13 Chemical structure of L-ascorbic acid (AA) and the reaction scheme for its redox reaction which may take place in interaction with an electrode via electron transfer across the solid-liquid interface or in a solution reaction in a reaction with a suitable redox partner molecule.

Norfloxacin, NFX ($\text{C}_{16}\text{H}_{18}\text{FN}_3\text{O}_3$) or (1-ethyl-6 fluoro-1, 4-dihydro-4-oxo-7-(1-piperazinyl) quinolone-3-carboxylic acid) (Figure 2.14) is a broad spectrum antibiotic of the class fluoroquinolones. It is against both Gram negative and Gram positive bacteria and used for treatment of infections of the urinary and respiratory tract, and of gastrointestinal and sexually transmitted diseases (Petersen, 1999). Analytical methods that are reported for NFX include schemes based on voltammetric principles. Those methods are simple and offered the required sensitivity and selectivity for accurate quantitative analysis. Jaber and Lounici, for instance, reported the quantification of NFX via differential pulse polarography (Jaber and Lounici, 1994) and adsorptive differential pulse stripping voltammetry was brought to success by Jeber and Lounici (Jeber and Lounici, 1994).

Determination of trace levels of NFX with analytical quality has been considered using CNT-modified working electrodes. Examples are the success with NFX cyclic voltammetry at a multiwalled carbon nanotube (MWCNT) film-coated glassy carbon electrode (GCE) (Huang et al., 2008), and cathodic stripping NFX voltammetry (Solangi, Huhawar and Bhangar, 2005) and enhanced NFX differential pulse voltammetry with copper oxide/MWCNT composite-coated electrodes (Devaraj, Deivasigamani and Jeyadevan 2013).

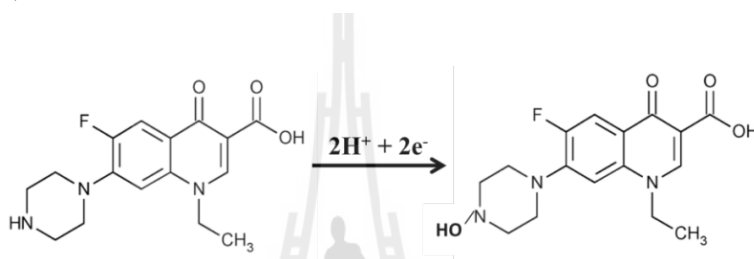


Figure 2.14 Chemical structure of norfloxacin, NFX, and the reaction scheme representing the redox reaction that takes norfloxacin place on the electrode surface via electron transfer across the solid-liquid interface (Huang et al., 2008).

The structure of the other antibiotic target, actually ciprofloxacin, CFX, ((C₁₆H₁₈FN₃O₃) or (1-cyclopropyl-6-fluoro-1, 4-dihydro-4-oxo-7-(1-piperazinyl)-3-quinolone carboxylic acid)) is shown in Figure 2.15. CFX is a synthetic broad spectrum antibiotic used for treating infections caused by a variety of pathogenic microorganisms. In 2007, Zhang et al. reported that the electrochemical detection of CFX can be enhanced by supplementation of the supporting electrolyte/measuring solution with a surfactant (Zhang and Wei, 2007). CFX electroanalysis with CNT modified electrodes was suggested as strategy to improve the analytical performance of the sensing scheme and achieve wider linear ranges and lower detection limits (Fotouhi and Alahyari, 2010).

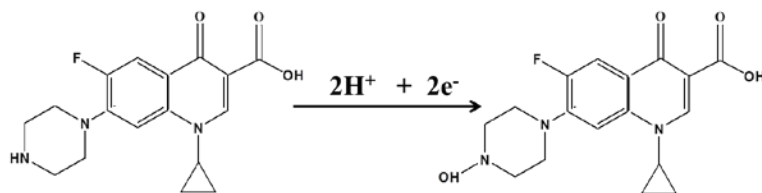


Figure 2.15 Chemical structure of ciprofloxacin, CFX, and the reaction scheme for the redox reaction which may take place in interaction with an electrode via electron transfer across the solid-liquid interface (Zhang and Wei, 2007).

Paracetamol, PCT ($C_8H_9NO_2$) is also known as acetaminophen (N-acetyl-p-aminophenol or 4-acetamidophenol, Figure 2.16). It is a major ingredient in numerous cold and influenza medications and an agent in favor of the lowering of fever. PCT is also an effective and safe analgesic agent and is used worldwide in large quantities to relieve pain associated with headache, toothache, backache, arthritis, migraine, neuralgia, muscular aches, menstrual cramps, and positive pain (Hardy and Paul, 1997; Zidan, Tee, Abdullah, Zainal and Kheng, 2011). There are many methods for the determination of PCT, alone or in drug mixtures, in commercial formulation or biological samples and electrochemical measurements are among the options (Goyal and Singh, 2006).

Representative examples of electrochemical PCT determination with good performances work with carbon paste electrodes in differential pulse voltammetry mode (ShangGuan, Zhang and Zheng, 2008), with a glassy carbon electrode as cyclic voltammetry sensor (Tungkananurak, K., Tungkananurak, N. and Burns, 2005), with square wave voltammetry at a gold electrode modified by 4-amino-2-mercaptopyrimidine (Jia, Zhang, Li and Wang, 2007), with an implementation into a flow injection analysis and screen printed electrodes with carbon nanotube modification (Fanjul-Bolado, Lamas-

Ardiasana, Hernandez-Santos and Costa-Garcia, 2009), and with square wave voltammetry at single wall carbon nanotube modified pyrolytic graphite electrodes (Goyal, Gupa and Ghatteaje, 2010). Recently, nanoparticle modified electrodes have been proposed for the quantitative determination of PCT in pharmaceutical preparations including electrodeposited Au, Cu, Ru attachment of metal nanoparticles (Nair, John and Sagara, 2009; Boopathi, Won and Shim, 2004; Fanjul-Bolado et al., 2009) or C₆₀ deposits (Tan, Bond, Ngooi, Lim and Goh, 2003) and already mentioned CNT modifications (Goyal and Singh, 2006; Goyal et al., 2010) of electrodes, all offering high sensitivity with low detection limit. Zidan et al. used bismuth oxide (Bi₂O₃) nanoparticles to modify the surface of a glassy carbon electrode and make a sensitive sensor for electrochemical NFX measurements (Zidan et al., 2011).

Based on the reported success case for the determination of the four target analytes (AA, NFX, CFX, and PCT), this thesis work focused on the implementation of CNT-modified PLEs as working electrode into a robotic electrochemical device. The next subsection is dedicated to an introduction of carbon as working electrodes material and different types of carbonaceous sensors will be described.

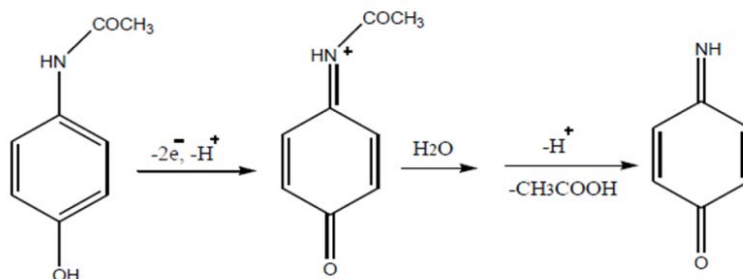


Figure 2.16 Chemical structure of paracetamol, PCT, and the reaction scheme for the redox reaction which may take place in interaction with an electrode via electron transfer across the solid-liquid interface (Zidan et al., 2011).

2.4 Carbon electrodes

Graphite-type carbon is a widespread engineering material and available in the forms ranging from commonly known graphite powder, pencil lead, ceramic-type glassy carbon to high-tech carbon fibers (Morgan, 2005) and the recently renowned Noble Prize-winning fullerenes, carbon nanotubes and graphene (Guldi, Rahman, Sgobba and Ehli, 2006). In normal graphite-type carbon the individual carbon atoms are arranged and formed into planar sheets of bridged hexagonal atomic rings. Typically, many of these sheets are stacked together in a parallel arrangement with movable π electrons sandwiched between individual carbon layers, which are the basis for the reasonable conductivity of graphite. The conductivity paired with chemical inertness and versatility made graphitic carbon attractive as an electrode material (Richard and McCreery, 2008). The actual type of carbon and an eventual chemical pretreatment have a profound effect on the analytical performance when the material is used as the precursor for sensors. Popular carbon electrode materials are glassy carbon, carbon paste, carbon fibers, screen

printed carbon, vapor deposited carbon films, and thin film coatings of fullerenes, carbon nanotubes and grapheme. Some examples of carbon electrodes are displayed in the photographs in Figure 2.17.

The widespread use of carbon as advanced electrode material for sensors in electroanalysis is based on a broad available potential window and low background currents, a rich surface chemistry that can be used for chemical electrode modification, a low price, chemical inertness and the related suitability for various sensing and detection applications. Variants of successfully employed graphitic or carbonaceous voltammetric working electrodes include: 2.17(A). The screen printed electrode (SPE) (Figure 2.17 (A)) that is prepared by spreading carbon inks in structured patterns on microscope slide-like polymer plates (Nascimento and Angnes, 1998; Dominguez, Alonso-Lomillo and Arcos Martinez, 2007, Li, M., Li, Y., Li, D-W; Long, 2012). The innovative strips are now manufactured in mass production for sale and developed into routinely used tools for electrochemical analysis in environmental, clinical or food sample. The carbon pencil lead electrode (PLE) (Figure 2.17 (B)) made from rods that are normally part of writing pencils. Inserted in appropriate holders with a few mm of the conductive pencil lead exposed, PLEs are normally used as electrodes with a cylindrical geometry (Blum, Leyffer and Holze, 1996; Campos Prado Tavares, 2008; Yardim, 2011). The carbon fiber electrode (CFE) (Figure 2.17 (C)) that has carbon fibers of micrometer diameter being used as conductive structure embedded in either glass or polymer insulations to form what was earlier described as microelectrodes (Huffman and Venton, 2009). Carbon fibers are mass produced for engineering applications where it serves as the fibrous strengthening component of reinforced plastics as used for tennis rackets, airplane wings, surf boards etc. (Csöregi, Gorton, 1993; Marko-Varga, 1993). The glassy carbon

electrode (Figure 2.17 (D)) which usually is disk-shaped with the ceramic-type glassy carbon embedded in a glass or polymer insulation (GCE) (Bokros, 1977). And the carbon nanotube electrodes (CNT) (Figure 2.17 (E)), which is attempting to take advantage of the remarkable electrical and mechanical properties of the modern material (Yogeawaran and Chen, 2008; Hecht, Hu and Irvin, 2011).

As working electrodes for the voltammetry in this study were chosen PLE electrodes made of 0.5 mm diameter pencil leads as commercially available as accessories in book shops or stationeries. To improve the capability for the detection of ultra-low levels of target analyte species (here: AA, NFX, CFX, PCT), the PLEs are meant to be modified with surface attached CNTs with electrocatalysis activity (Crespo, Macho, Bobacka and Rius, 2009). A strategy that turned out to be very effective in the deposition of CNT layers on various substrate electrodes is their electrodeposition on either the anode or cathode of an electrochemical cell, depending on the CNT properties (Campbell, Sun and Crooks, 1999). CNT electrodeposition was recently reported by Boccaccini et al. (2006) who used an electrophoretic procedure in a two-electrode electrochemical cell (see Figure 2.18) to attract CNTs to the cathode of a two-electrode electrochemical cell and keep the tubes after arrival fixed on the cathode surface via van der Waals attraction (Boccaccini et al., 2006; Zhu, Sujari and Ghani, 2012). A pure dip coating procedure for CNT modification is not expected to create the desired defect-free and uniform CNT electrode deposits. Therefore the more promising procedure of CNT electrodeposition was expected to be the better method of choice and, as detailed later, the PLEs working electrodes for the robotic electrochemical drug detection were comout to be electrocoated with thin but well-adhering CNT films.

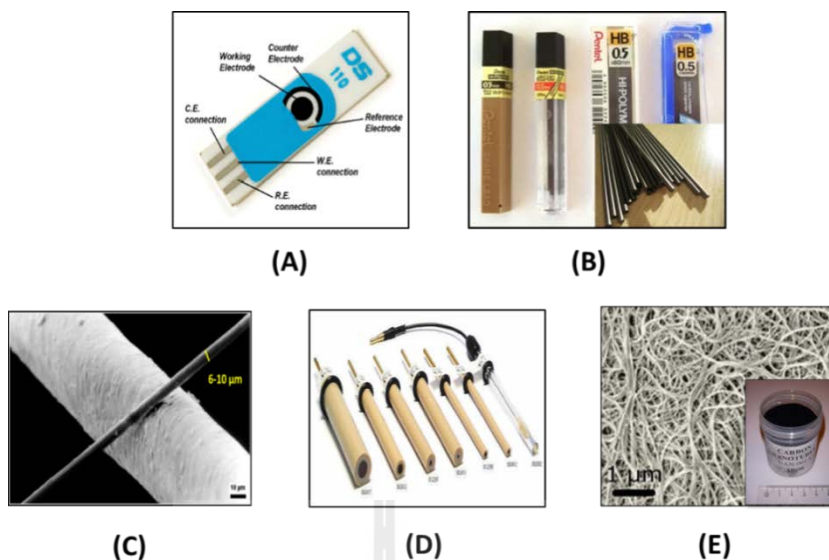


Figure 2.17 Popular carbon-based electrode materials are: (A) Screen printed carbon, (B) pencil lead, (C) Carbon fiber, (D) Glassy carbon, and (E) Carbon nanotubes.

Shown as a first proof that PLEs can in principle be operated in the workstation for automated voltammetry in 24-well microtiter plates is a CV of ferricyanide that was acquired with such an electrode in an individual well of a microtiter plate (Figure 2.19). In the Results and Discussion section the quality for the automated electroanalysis of AA, NFX, CFX and PCT will be described and discussed more specifically.

An electrochemical robotic system using standard microtiter plates as reaction wells for potentiostatic and high-throughput electroanalysis was conceived and realized using step motor driven positioning in combination with fixable software (Erichsen et al., 2005). In routine laboratory work, when compared to manual systems, the robotic device is easy to learn and operate, has a high sensitivity and reproducibility and offer short operating time under automatic control. The system is adaptable to work under inert-gas in aqueous and organic solvents, and maybe modified to add or remove solution by

integrated syringe pumps. The performance of the system is demonstrated by redox screening of a Ru-complex (hexaammine ruthenium (III) chloride) or Fe-complex (potassium ferricyanide) standard solution and by electroanalysis with organic or inorganic compound. An example is shown in Figure 2.19.

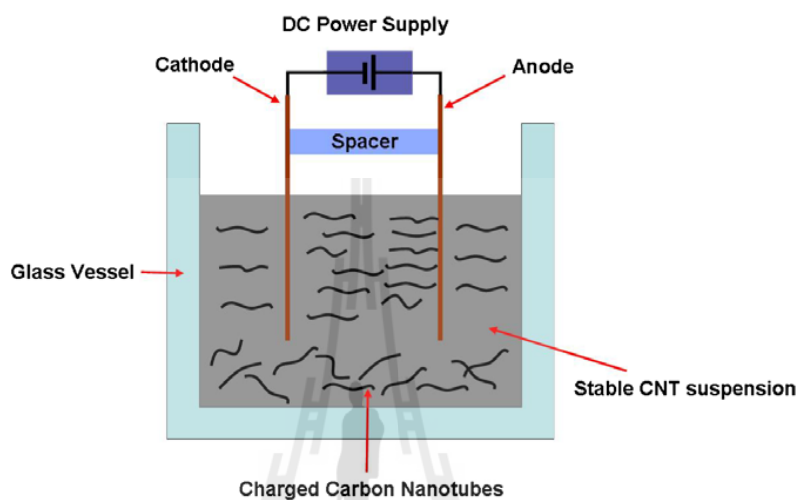


Figure 2.18 Schematic diagram representing the principle of the electrophoretic deposition of COOH-modified CNTs on the cathode of an EPD cell with a cylinder-type working electrode (Boccaccini et al., 2006).

In this thesis, aim was the adaptation of the existing setup for automated electrochemical measurements in 24-wells microtiter plates (Erichsen et al., 2005) to the screening of pharmaceutical drugs which are meant to be antioxidants, antibiotics, and analgesics, in first place. In particular for the antibiotics NFX and CFX and for the analgesics PCT work with CNT as working electrode is a requisite because the voltammetric signals at the bare PLE would be probably too weak for low trace measurements. The next section describes the state of the art of the instrumentation for

robotic (automated) electrochemical measurements in sequentially addressable microtiter plates.

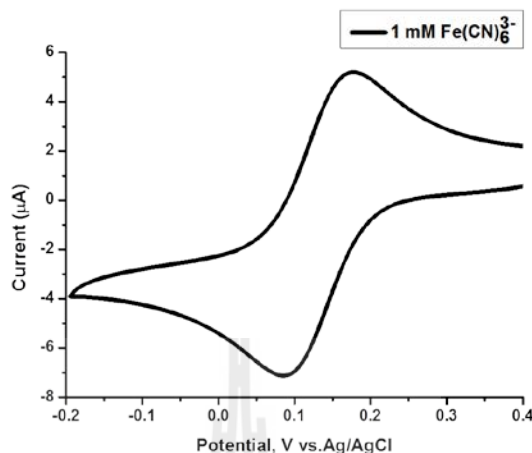


Figure 2.19 Cyclic voltammogram of 1 mM potassium ferricyanide at a pencil lead working electrode in standard measuring solution and acquired in the available electrochemical robotic system.

2.5 Robotic electrochemistry and electroanalysis

2.5.1 Available publications

Recently, an electrochemical robotic system using the vials of standard 24- or 96-well microtiter plates as measuring containers for potentiostatic and galvanostatic electrosynthesis or electroanalysis was conceived and realized by others using stepper motor-driven positioning stages in combination with a movable three-electrode assembly, 24-well microtiter plate wells as electrochemical cells, a potentiostat and flexible software (Erichsen et al., 2005; Lindner, Lu, Mayer, Speiser, Tittel and Warad, 2005; Markle, Speiser, Tittel and Schuhmann, 2005). A schematic of the system for automated (robotic) electrochemistry is displayed in Figure 2.20. The electrode

assemblies used for particular experiments are specifically designed to fit suitably without physical contact into the wells of the microtiter plate and they are adapted in terms of their electrochemical properties to the needs of the target analytical application. Automatic execution of sequences of measuring and positioning steps is then used to address one well after the other and carry out at halts in the well solution either electrosynthetic procedures or apply electroanalytical techniques for detection of species.

Electrode assemblies may, for instance, incorporate as reference electrode a simple Ag/AgCl wire, a cylinder or disk-shaped metal or carbon macro or microelectrode as the working electrode and a Pt wire spiral as the counter electrode. For the automation of voltammetric experiments in the individual plate wells tailored software scripts have to be written that allow variation of the parameters controlling both the motion of the electrode assembly and the measuring procedure and data management. Additional features such as syringe pumps for solution delivery to the well, temperature control units for the well solutions, and a microtiter plate shaker may be incorporated if needed. So far, the robotic electrochemical approach has been applied to the preparation and testing of a library of metalloporphyrin-based nitric oxide sensors (Ryabova, Schulte, Erichsen and Schuhmann, 2005), for screening of the catalytic activity of large sets of organometallic ruthenium (II) complexes of different structures (Lindner et al., 2005), for combinatorial automated micro electrosynthesis of organic compound collections (Marerke et al., 2005), for automated glucose biosensor fabrication (Reiter, Ruhlig, Ngounou, Neugebauer, Janiak, Vilkanauskyte and Schuhmann, 2004), the measurements of ascorbic acid (AA) levels of fruit juices vitamin C tablets, and herbal plant extracts (Intarakamhang et al., 2011), for the quantification of free radical scavengers (antioxidant) in food samples (Intarakamhang and Schulte, 2012) and for

robotic stripping voltammetry of the heavy metals lead and cadmium in water and soil samples (Intarakamhang et al., 2013). In an extension of the already accomplished success cases, the focus here will be on an adaptation of the methodology for convenient non-manual drug electroanalysis.

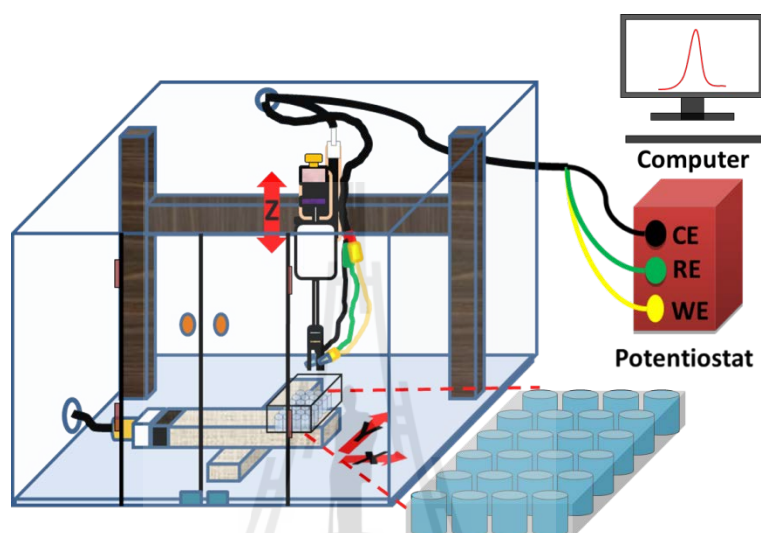


Figure 2.20 The device for automatic sequential electrochemistry in the individual wells of a 24-well microtiter plate of the system. Central parts are: (1) a computer-controlled EC workstation, (2) an assembly of working, counter and reference electrode, (3) an x, y, z micropositioning system, and (4) the personal computer with special software for automated operation of the workstation.

CHAPTER III

RESEARCH METHODOLOGY

3.1 Experimental and methods

3.1.1 Materials and chemicals

Chemical	Supplier
Single-wall carbon nanotubes P3-SWNT	Carbon solution, Inc. California, USA.
Pencil leads $\varnothing = 0.5$ mm HB	Pentel [®] , Japan.
Potassium chloride, anhydrous KCl	Carlo ErbaReagentiSpA, Rodano, Italy.
Hydrochloric acid, HCl	Carlo ErbaReagentiSpA, Rodano, Italy.
Nitric acid, HNO ₃	Carlo ErbaReagentiSpA, Rodano, Italy.
Sodium acetate, CH ₃ COONa	Carlo ErbaReagentiSpA, Rodano, Italy.
Acetic acid, CH ₃ COOH	Carlo ErbaReagentiSpA, Rodano, Italy.
Potassium hydrogen phosphate, KH ₂ PO ₄	Carlo ErbaReagentiSpA, Rodano, Italy.
Potassium ferricyanide, K ₃ Fe(CN) ₆	Acros, New Jersey, USA.
Hexaamine ruthenium (III) chloride, Ru(NH ₃) ₆ Cl ₃	Acros, New Jersey, USA.
Disodium hydrogen phosphate, Na ₂ HPO ₄	Carlo ErbaReagentiSpA, Rodano, Italy.
Sodium hydroxide, NaOH	Carlo ErbaReagentiSpA, Rodano, Italy.
L(+) Ascorbic acid	Sigma Aldrich, Kansas, USA.

3.1.1 Materials and chemicals (Continued)

Chemical	Supplier
Norfloxacin [®] , C ₁₆ H ₁₈ FN ₃ O ₃	Research sample from a collaborator from Jacobs University Bremen, Germany.
Norfar (400 mg) (a Norfloxacin drug)	Qualimed, Thailand.
Ciprofloxacin [®] , C ₁₇ H ₁₈ FN ₃ O ₃	Research sample from a collaborator from Jacobs University Bremen, Germany.
Cobay (500 mg) (a Ciprofloxacin drug)	Millimed, Thailand.
4-Acetamidophenol, C ₈ H ₉ NO ₂	Acros, New Jersey, USA.
Tylenol (500 mg) (a paracetamol drug)	Jansen-Cilag/DKSH, Thailand

3.1.2 Instrumentation

- A function generator (Agilent[®] 3322A 20 Hz function/arbitrary wave form generator); it was used for the electrophoretic deposition of the carbon nanotube electrode modification via constant DC voltage application in 2-electrode cell configuration.
- An electrochemical workstation from Gamry Instruments (potentiostat Model Reference 300[®], Gamry Instruments, Warminster, PA USA); it was used for characterization of electrodes via electrochemical impedance spectroscopy (EIS) and cyclic voltammetry.

- A robotic electrochemical workstation including a potentiostat PalmSens Instruments (Palm Instruments BV, Amsterdam, Netherland) and micropositioning via three computer-controlled positioning devices the enabled precise vertical (z) positioning of an assembly of the WE, CE and RE and horizontal (x/y) movements of a standard 24-well microtiter plate. All electrochemical experiments were carried out through the operation of a three-electrode electrochemical sensor interface. The system was used for manual and automated voltammetric experiments, drug characterization, and calibration and sample measurements.
- A scanning electron microscope (SEM) for inspection of the morphology of PLE-modified CNT networks.
- A high-speed micro centrifuge, Hitachi CF16RX II, Osaka, Japan.
- A Denver balance TC 205, Denver Instruments, Colorado, USA.
- An ultrasonic bath for laboratory purpose, CREST, USA.
- A hotplate & magnetic stirrer, IKA H3400-HS07, Japan.
- A mixer UZUSIO for laboratory use, VTX-L3000 LMX, USA.
- A refrigerator/freezer, Sanyo 10.2-cu, Thailand.

3.1.3 Electrodes

- Bare PLEs (\varnothing 0.5 mm) HB electrode, Pentel[®], Japan. (Preparation: see below)

- A CNT-modified PLE; the electrode was prepared from a bare pencil lead as described below (see also Figure 3.1-3.2 in 3.2.1).
- A counter electrode: a platinum wire drilled to a coiled structure at the bottom.
- A reference electrode: a home-made miniaturized pseudo Ag/AgCl reference electrode. A silver wire was cleaned by polishing with a fine grade emery paper and subsequent rinsing with distilled water. Then, an about 2 cm long part at the end of the wire was placed into a mixture of 0.1 M in HCl and 3 M in KCl and 10 volt was applied with a laboratory power supply for 10 min, using a platinum wire as cathode. During the electrolysis a greyish AgCl deposit was formed on the silver wire surface to make the requisite Ag/AgCl system for use as reference electrode up.

3.2 Research methodology

3.2.1 Preparation of CNT-modified pencil lead electrodes

The steps for the preparation of CNT-modified PLE working electrodes are shown in Figures 3.1-3.2. At the beginning of the procedure, a 6 cm long piece of a pencil lead is sealed into a heat shrinking tube, however, with leaving about 2 mm at the bottom and 4 cm at the top end exposed. The 2 mm piece of pencil lead at the bottom end is used as a cylindrically shaped working electrode (the “PLE”) while the exposed area at the top is meant to be for making electrical contact to the potentiostat cable with a crocodile clamp. After completion, the PLE was cleaned by a 1 min immersion into 4 M

HNO₃ (Demetriades, Economou and Voulgaropoulos, 2004), with subsequent thorough rinsing with distilled water. The electrolyte for the voltage-induced deposition of CNTs on the surface of the bare PLE was a 20 mg/ml suspension of CNT in water. Deposits of CNTs on the pencil lead electrode surface were achieved by applying a positive DC voltage of 1 V for 10 minutes to the precursor electrode (Boccaccini et al., 2006). The positive voltage supports anodic electrophoretic attraction of the negatively charged carboxylated CNTs, which via van der Waals forces are kept in place at the carbon surface. Freshly CNT-modified PLEs were allowed to dry after the deposition procedure at room temperature and then got rinsed with distilled water and stored until future use. A thorough characterization of the PLE-modified CNTs was performed by using a combination of electron microscopy (Boccaccini et al., 2006; Fu et al., 2009; Tsierkezos and Ritter, 2010; Yang, Unnikrishnan and Chem, 2011; Zidan, Tee, Abdullah, Zainal and Kheng, 2011), impedance spectroscopy (Yang and Wu, 2001; Esseghaire, Helali, Fredj, Tlili and Abbelghani, 2008; Tsierkezos and Ritter, 2010; Truong, Chikae, Ukita and Takamura, 2011; Yang et al., 2011) and voltammetry (Ghoneim, Radi and Beltagi, 2000; Zhang and Wei, 2007; Huang et al., 2008 and ShangGuan et al., 2008; Raof, Kiani, Ojani and Valiollahi, 2011; Goyal et al., 2010), respectively.

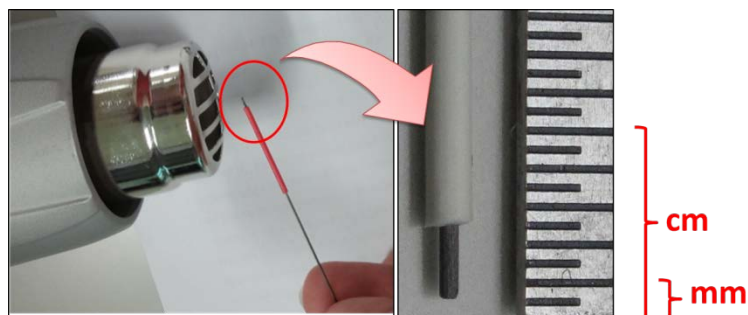


Figure 3.1 Pencil lead ($\text{Ø } 0.5 \text{ mm}$) is sealed into heat shrinking tube, with leaving about 2 mm at the bottom and 4 cm at the top end exposed. The top end is for instrument connection while the bottom end serves as cylindrical working electrode.

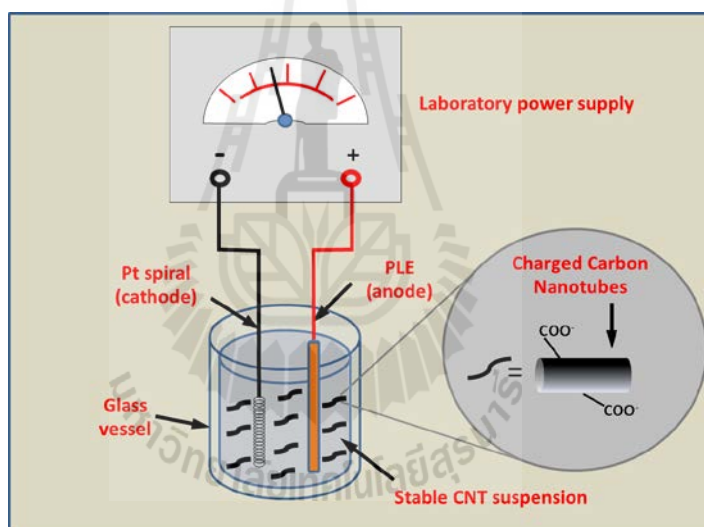


Figure 3.2 Schematic diagram of the procedure used for the preparation of CNT-modified PLEs. Applying a positive DC voltage of 1 V for 10 minutes leads to thin film deposition of a well-adhering CNT layer that facilitates electrochemical drug measurements in the robotic electrochemical workstation.

3.2.2 Characterization of CNT-modified PLEs

The layer of the catalytic CNTs on the surfaces of PLEs obtained via the electrophoretic deposition procedure is very thin. Microscopic observation of the attachment of the nanometric filaments is therefore difficult in normal microscopes and scanning electron microscopy on the bare and modified versions of PLEs thus a requisite for the visualization of the presence of the CNT deposit. The microscopic surface characterization of CNT-modified PLEs were accompanied by an electrochemical impedance spectroscopy, EIS, tests and an electrochemical inspection via cyclic and differential pulse voltammetry, respectively in electrolytes containing a reversible redox mediator (e.g. 1 mM $\text{K}_4\text{Fe}(\text{CN})_6/\text{K}_3\text{Fe}(\text{CN})_6$ in 0.1 M KCl solution). If not otherwise mentioned, a pseudo Ag/AgCl wire was used as reference and a Pt spiral wire as counter electrode for these measurements. The electrochemical configuration used is shown in Figure 3.3.

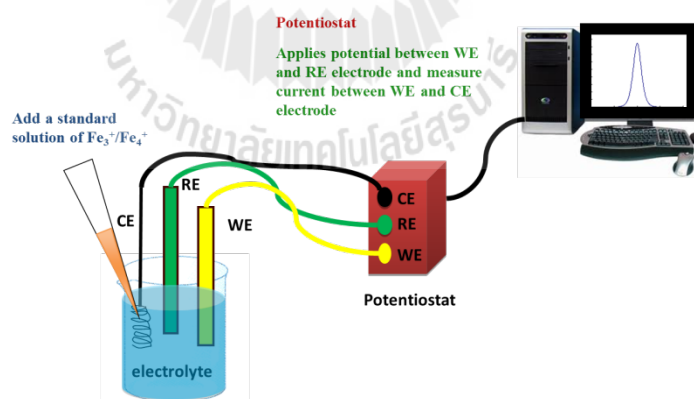


Figure 3.3 Schematic of the arrangement used for beaker-type voltammetry and electrochemical impedance spectroscopy measurement with CNT-modified PLEs.

3.2.3 Manual and robotic drug electroanalysis

3.2.3.1 Manual and robotic ascorbic acid (AA) voltammetry

AA is an antioxidant and has been selected as one of the model compounds for the establishment of robotic electrochemical drug screening. It is present in fruits, vegetables, milk, beverages and pharmaceutical products, and after body uptake through consumption opposes oxidative cell stress by decreasing the level of cell damaging reactive oxygen species (Padaytty, 2003). The basic voltammetry of AA on PLEs in a robotic electrochemical workstation is literature-known (Intarakamhang et al., 2011) and the published conditions were used as starting point for setting the optimal parameters for the novel automated detection at CNT-modified PLEs. AA concentrations in the 0.1 M KCl measuring solution were varied in order from a 1 M stock AA to construct typical calibration curves, which usually are plots of the voltammetric peak currents, I , vs. the actual concentration of species in the electrolyte. The details of the proposed electrode design were varied to optimize the analytical performance. Changed were, for instance, the number of repetitions and the amplitude of the voltage of the electrophoretic CNT deposition. This variation of critical parameters was expected to vary the amount of catalytically active CNT on the pencil lead surface. Initial test and calibration measurements as well as AA quantification via CV and DPV were performed in the conventional beaker-type cell configuration as shown in Figure 3.4.

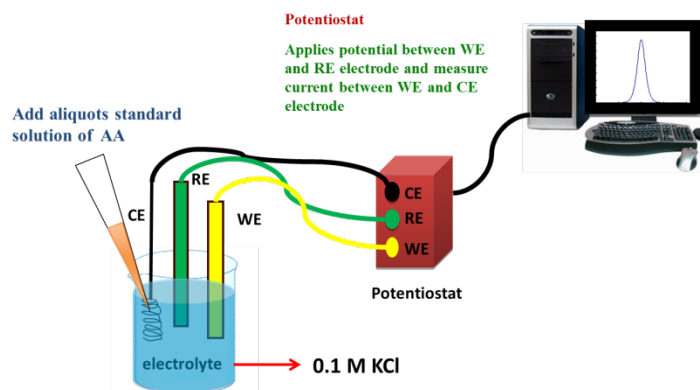


Figure 3.4 The electrochemical workstation with a three electrode configuration for test and calibration measurement of AA in the CV and DPV mode.

Prior to use, the CNT-modified PLEs were always electrochemically activated in 0.1 M KCl by DPV, with a potential scan between -0.2 to 1.0 V until stable signals were observed. Then AA was adjusted in the beaker-type electrochemical cell within the concentration range of 0.1 to 10 mM for the calibration measurements. The oxidation peak current of AA at CNT-modified PLEs usually came up at about 0.2 V. Quantified were the AA contents in model and real samples, and the analysis followed the calibration method. All electrochemical experiments were carried out at room temperature. In between individual measurements, CNT-modified PLEs were transferred to the 4 M HNO₃ solution again to remove any adsorptive substances sticking to the PLE and give a reproducible clean electrode surface.

After the identification of the optimal parameters set for the conventional beaker-type voltammetric analysis, AA assessments were carried out with these conditions but via the robotic-type of approach as shown in Figure 3.5.

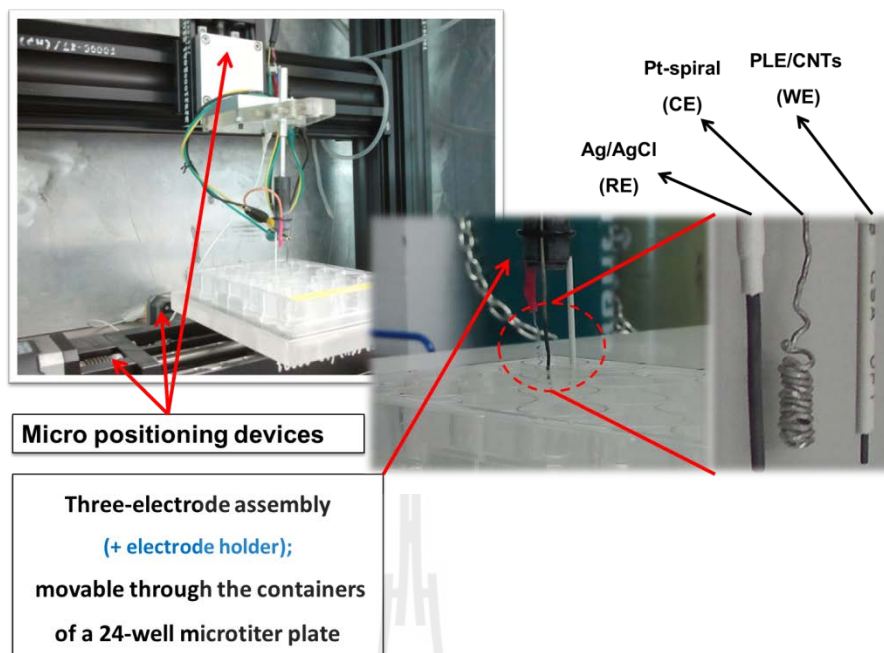


Figure 3.5 Close up views of the electrochemical robotic work-station for robotic voltammetric analysis of AA with the CNT-modified PLEs.

The electrochemical robotic system used in sample container this study was operated with a standard 24-wells microtiter plate sample container for voltammetric electroanalysis. It had a stepper motor-driven positioning of the three-electrode assembly in charge of the in-well voltammetry. Flexible software modules allowed movements of the electrode assembly through the plate wells and at halts in the well solutions either electrochemical electrode conditioning, electrode dip cleaning, or the electrochemical measurements in the cyclic or differential pulse voltammetry mode.

A complete analytical run through all microtiter plate wells can take up to 4 hours, depending on how fast electrode assembly positioning is adjusted and what tasks the assembly attempts in the individual plate containers. The stability of the analyte thus is critically important for success with accurate quantification. The liability

of AA for degradation was tested with adapted microtiter plate well loads. All wells were, for instance, loaded with 10 mM AA and the related DPVs were recorded automatically. An assessment of the peak current as a function of times during e.g. a 3 hours robotic measurement could then be used for predictions of the stability of AA in the system. The load of a stability test in the electrochemical microtiter plate format is shown in Figure 3.6.

All other microtiter plate loads that were used for calibration and model and real sample content measurements in the robotic electrochemical workstation are listed in Table B.1 in the Appendix B of this thesis. For all measurements the electrode assembly used for plate well voltammetry implemented an Ag/AgCl wire as reference electrode, a coiled Pt wire as counter electrode, and a CNT-modified PLE as the working electrode. The assembly was guided through the plate wells in predefined sequence by specially designed software scripts as provided in the Table C.3 (see in Appendix C).

3.2.3.2 Manual and robotic antibiotic voltammetry

NFX and CFX are the two antibiotics that have been selected as model compounds for the establishment of robotic electrochemical drug screening. Basic information on the electroanalysis, in particular the voltammetry, of NFX and CFX was available in the literature (Huang et al., 2008; Zhang and Wei, 2007) and the published conditions for voltammetric measurements were used here as starting point for the trials with CNT-modified PLEs. In course of the trials parameter optimization was carried out.

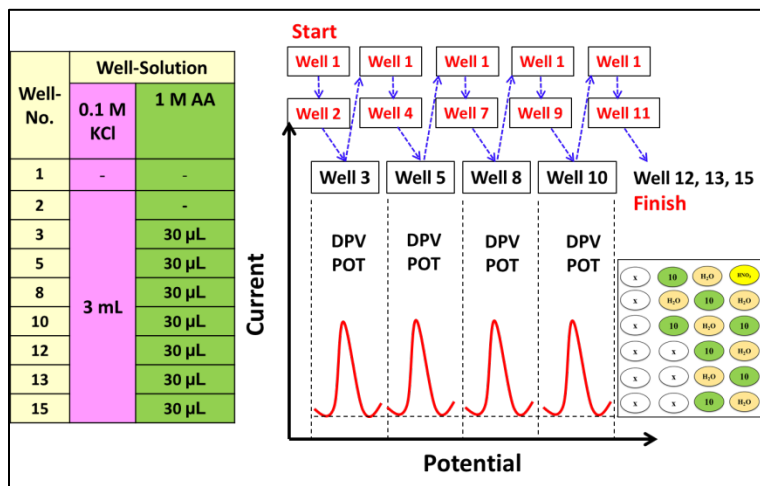


Figure 3.6 Schematic representation of the microtiter plate load as it was used for degradation tests with AA in the robotic electrochemical device.

The concentration of NFX and CFX in the measuring solution, actually a 0.1 M acetate buffer also 0.1 M PBS, was varied via defined additions of a 1 mM stock solution of NFX and CFX, respectively. Trials in solutions of different analyte levels allowed constructing calibration curves as plots of the voltammetric peak currents, I_p , vs. the actual concentration of species in the measuring buffer. Test and calibration measurements as well as NFX and CFX quantification in real and model samples were approached via DPV, initially in the conventional beaker-type cell configuration and then later in the robotic electrochemical workstation in automated manner.

The PLE working electrodes of the three electrode assembly were first electrochemically activated in 0.1 M acetate buffer (pH 4.5) by using a CV scan from 0 to 1.2 V with a scan speed 20 mV s^{-1} (for NFX measurement) and electrochemically activated in 0.1 M phosphate buffer (pH 4.0) by using a CV scan from 0.3 to 1.3 V with a scan speed 20 mV s^{-1} (for CFX measurement). The oxidation peak

current was located at 0.9 V and 1.0 V vs. Ag/AgCl for NFX and CFX, respectively. The magnitude of the peak currents was computed and used as signal for quantification. NFX and CFX concentrations were determined in model and real samples, usually by the standard addition method and all assessments were carried out at room temperature. After individual measurements, CNT-modified PLEs were refreshed and cleaned via dipping (or electrochemical cleaning or ultrasonic vibrator) into 4 M HNO₃ solution to remove adsorbed substances and reach a reproducible electrode surface.

After determination of the optimal parameter set for the voltammetric antibiotic analysis in conventional beaker-type trials, the electrochemical antibiotic quantification was carried out via the robotic-type approach as shown in Figure 3.5. The operation of the robotic electrochemical system for the detection of antibiotics system was as used for AA microtiter plate electroanalysis (refer to 3.2.3.1). Again, it was important to get an idea about the stability of the two antibiotics. A possible degradation of NFX and CFX was examined via tests in microtiter plates, with individual plate containers containing 8 μM and 50 μM of NFX and CFX, respectively. DPV were recorded at defined time points, the corresponding peak currents determined and plotted as a function of time. Times for a complete microtiter plate run were 3 h and 2 h for NFX and CFX, respectively. The solutions were loaded following the microtiter plate design as displayed in Figures 3.7 and 3.8. Information regarding solution preparation for the calibration and model and real sample measurements are listed in Tables B.2, B.3 and B.4 and B.5 and B.6 (see in Appendix B).

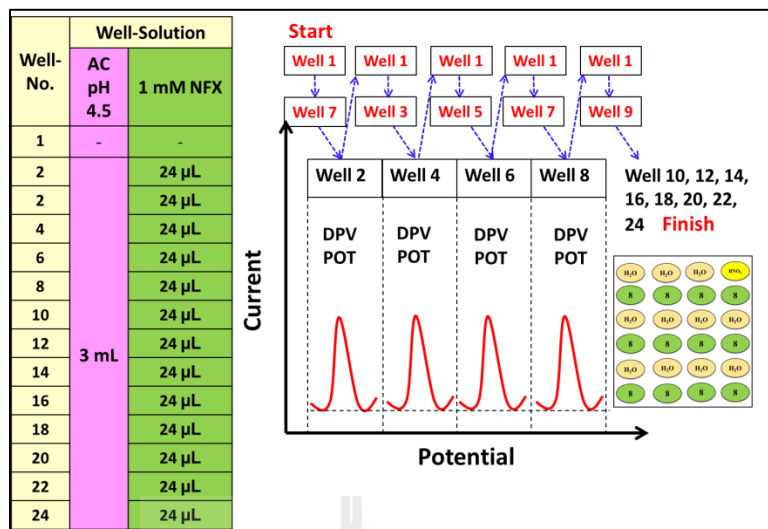


Figure 3.7 Schematic representation of the microtiter plate loads for the robotic voltammetric degradation study of NFX.

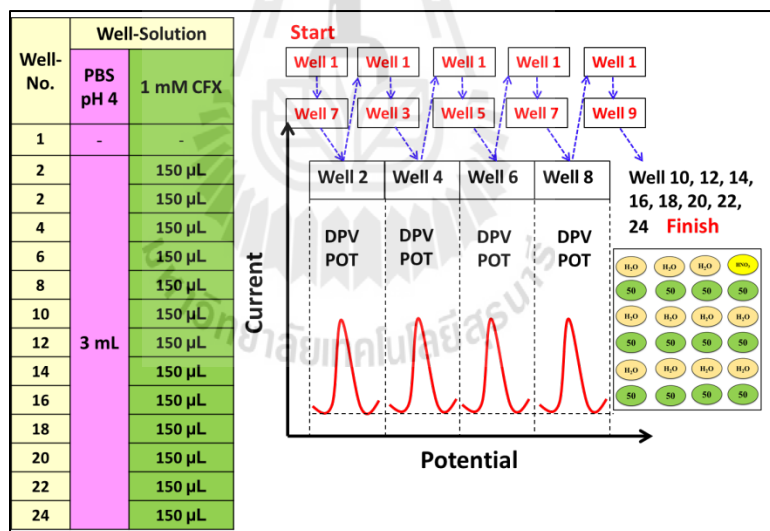


Figure 3.8 Schematic representation of the microtiter plate loads for the robotic voltammetric degradation study of CFX.

3.2.3.3 Manual and robotic analgesic voltammetry

PCT is a frequently used drug and was another compound serving as a model for performance tests of the system for robotic electrochemical drug screening. Information on PCT voltammetry was available in the literature and the published conditions (from references listed in Chapter II) were used as starting point for initial measurements at CNT-modified PLEs and then parameter optimization was applied. PCT was usually measured in a 0.1 M KH_2PO_4 buffer (pH 4.5) solution and the levels were varied to be able to construct calibration curves as plots of the voltammetric PCT peak currents, I_p , vs. the actual PCT concentration in the electrolyte. As for the AA and NFX/CFX case, test and calibration measurements as well as PCT quantification via DPV were initially done in a normal beaker-type cell configuration (refer to Figure 3.4).

For successful PCT electroanalysis, the PLE working electrode of the three electrode assembly was first electrochemically activated in 0.1 M KH_2PO_4 (pH 4.5) by using a CV scan from 0 to 1.2 V with a scan speed 20 mVs^{-1} . PCT levels in the measuring solutions were for calibration purpose adjusted via additions of desired aliquots of the standard solution of PCT, usually within the concentration range from 5 to $150 \mu\text{M}$. The PCT oxidation peak appeared at 0.51 V vs. Ag/AgCl the recorded DPVs and the current magnitude was used for the construction of calibration curves. Model (spiked buffer solutions) and real samples analysis happened in the standard addition method; all experiments were carried out at room temperature. After every measurement, CNT-modified PLEs were dipped into 4 M HNO_3 solution to remove adsorptive substances and give a reproducible clean electrode surface.

Identification of optimal parameters for the voltammetric PCT analysis took place via measurements in beaker-type electrochemical cells. With optimal conditions, PCT assessments then were carried out via robotic-type electroanalysis as earlier presented in Figure 3.5. Robotic electrochemical detection of PCT used identical system configuration as earlier presented for the AA (3.2.3.1) and antibiotic (3.2.3.2) trials. PCT degradation tests were performed in microtiter plate wells, with each well loaded with a 20 μM PCT. PCT DPV peak currents were extracted and plotted as function of times for the measurements which lasted 1 h for this analyte. The microtiter plate load for the PCT stability test is provided in Figure 3.9. More information on solution preparation for calibration trials, for measurements of the PCT content of commercial tablets and of urine samples are provided in the lists in Tables B.7, B.8 and B.9 (seen in Appendix B).

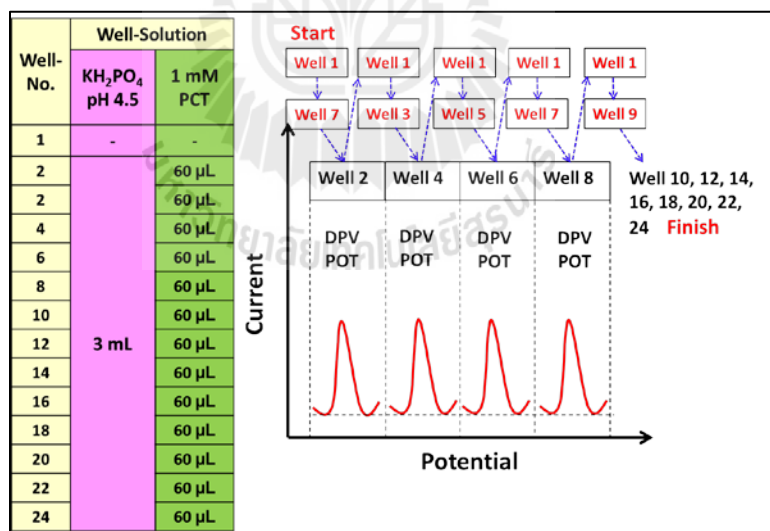


Figure 3.9 Schematic representation of the microtiter plate loads for the robotic voltammetric degradation study of PCT.

CHAPTER IV

RESULTS AND DISCUSSION

4.1 Characterization of CNT-modified PLEs

OF key importance for success with the proposed robotic drug electroanalysis in standard microtiter plates was the quality of the CNT-modified PLE working electrode in the movable electrode assembly that was guided through the plate wells by the positioning hard- and software of the system. Their surface morphology and electroactivity was therefore thoroughly characterized by a combination of scanning electron microscopy (SEM), electrochemical impedance spectroscopy (EIS), cyclic voltammetry (CV) and differential pulse voltammetry (DPV). The observations proved an integrity and suitable performance level and relevant details are given in the next section.

4.1.1 Scanning electron microscopy (SEM)

The fine structure of CNT-modified PLEs was characterized using the high-resolution power of a SEM. Confirmed was a uniform but ultrathin CNT film deposition on the PLE substrate. Figure 4.1 shows the SEM images of a bare and a CNT-modified PLE. When comparing the low magnification micrographs of the two types of PLE rods (Figures 4.1a-b), the CNT modification is not really visible and one could even think that no CNT deposit is present on the apparently modified version.

However, in the higher resolution SEM images the CNT treatment becomes clearly evident as a uniform and nanoporous network of the nanotubes that covers the cylindrical surface of the PLE (Figure 4.1c-e). The electrodeposited CNT film apparently adheres well to the underlying carbonaceous surface of the PLE which is an important feature to avoid delamination in course of long-term measurements and loss of the functional layer. As later indeed confirmed by the accompanying electrochemical tests, the exposed active surface area of CNT-modified PLEs seemed to be high as a consequence of the observed well-pronounced nanoporosity.

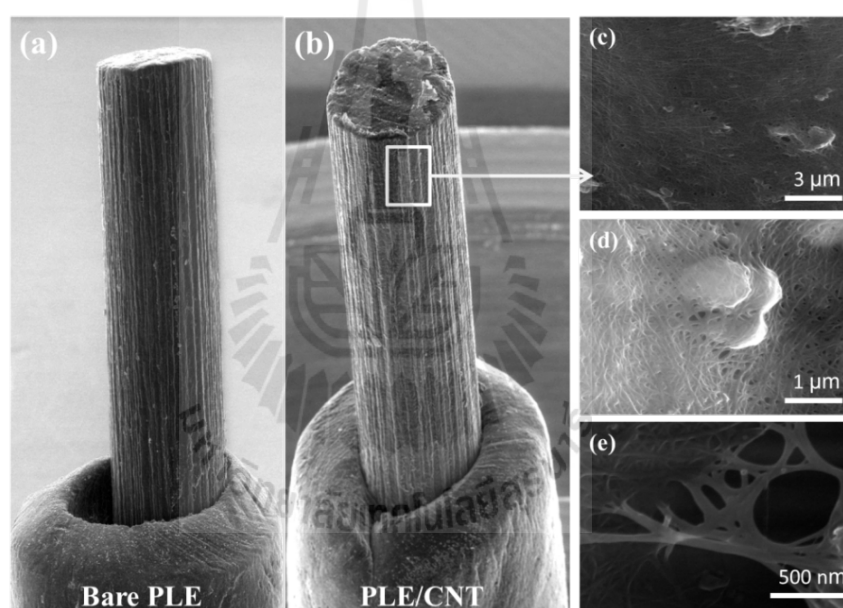


Figure 4.1 SEM images of a bare PLE (a), and a CNT-modified PLE (b), (c), (d), and (e), are zooms of the structure in the white square in (b).

4.1.2 Electrochemical impedance spectroscopy (EIS)

EIS tests with bare (control) and CNT-modified PLEs were performed in the presence of a reversible redox mediator couple, which was added to the

measuring buffer in both oxidized and reduced forms and in equivalent concentration. Impedance spectra for the electrodes in faradaic interaction with the redox mediator, namely ferricyanide/ferrocyanide in 0.1 M KCl, were recorded in the potentiostatic EIS mode and analyzed as usual (Yang et al., 2011). The inset of Figure 4.2 is a schematic representation of the Randle equivalent circuit model that was used to interpret the experimental data. In the Randles electrochemical cell R_s is the solution resistance (or electrolyte resistance), R_{CT} is the faradaic charge transfer resistance related to the redox interaction of the $[\text{Fe}(\text{CN})_6]^{3-/4-}$ couple with the solid/liquid electrode/electrolyte interface, C_{DL} is the electrical double layer capacitance and Z_w , finally, is the Warburg impedance element which accounts for the mass transport limitation of iron species consumed at the electrode surface via reduction or oxidation and the need for diffusional compensation.

Through the application of a small-amplitude alternating potential to an electrochemical cell and the acquisition of the time-dependent current response it is possible to derive values for R_s , R_{CT} , C_{DL} and Z_w in an EIS experiment. A comparison of the parameter set between different electrodes then can be used to judge, for instance, on their quality in terms of ease to perform an electron exchange with a dissolved redox species and surface roughness and/or porosity. Higher R_{CT} indicate more difficult electrode-induced oxidation or reduction and larger C_{DL} values may point towards larger active electrode surface as capacitance typically scales with area. Here, EIS has been used as an efficient way to derive information on the enhancement of surface porosity of PLE electrode through the placement of a nanoporous CNT network and also on the gain in electrocatalytic activity through CNT deposition expressed as manifestation of a reduced charge transfer resistance.

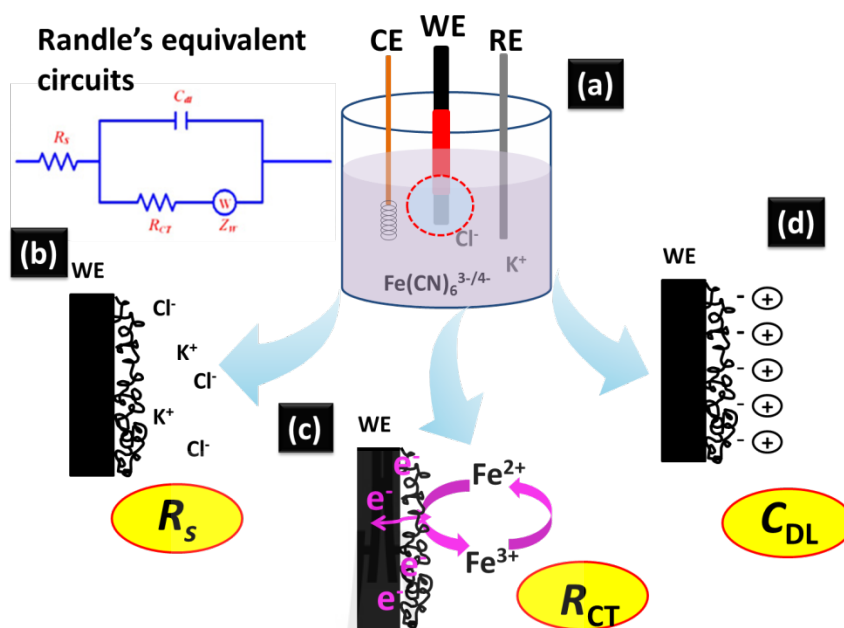


Figure 4.2 (a) Schematic description of the PLE/CNT/electrolyte system and the corresponding electronic equivalent circuit (the “Randles” circuit). (b) Within the solution, ionic conductance is responsible for current flow through the electrochemical cell and this parameter is represented in the Randles circuit as solution resistance R_s , (c) at the CNT/PLE surface a faradaic redox reaction in terms of electron exchange takes place and gives reason for the charge transfer resistance R_{ct} in the Randles circuit, and (d) always present at an electrode in an electrolyte is the Helmholtz double layer, and this physical electrode attribute is encountered for in the Randles cell by the capacitance C_{dl} .

Typical EIS spectra of the different electrodes are shown in Figure 4.3. Figure 4.3(a) displays in one graph the Nyquist plots valid for a bare (black trace) and CNT-modified (red trace) PLE in ferrocyanide/ferricyanide-containing KCl electrolyte. Visible for the bare PLE is a semicircle part that refers to the combination

of the solution resistance (here the resistance of the 0.1 M KCl) and the charge transfer resistance for the redox reaction of the iron species at the electrode surface. Also visible is at the low (right) side of the frequency spectrum is the onset of the linear line that is expected to appear due to the diffusional delivery of $[\text{Fe}(\text{CN})_6]^{3-/4-}$ and the associated Warburg impedance (Z_w) (Yang et al., 2011). The Nyquist plot for the CNT-modified PLE looked different to the one from the bare PLE in that the diameter of the semicircle was much compressed and on the same scale appeared almost like a line. As explained in an earlier section, Nyquist plots allow extraction of values for the solution and charge transfer resistance: the semicircle has to be extrapolated to the x-axis, and the axes crossing points of the circle have to be determined. Then the value for the higher frequency crossing point is the solution resistance while the crossing point at the low frequency side is the sum of the solution and charge transfer resistance. Easier access to the two parameters of interest is possible by a look to the Bode plots of the impedance spectrum as displayed in Figure 4.3(b) (black trace, bare PLE; red trace, CNT-modified PLE). Here, the y-axis crossing points are reflecting the charge transfer resistance while the extrapolation of the high frequency plateau towards y axis provides at the intersection the solution resistance. Clearly visible by a comparison of the two Bode plots is that the charge transfer resistance is lowered by a decade when modifying a PLE with a nanoporous thin-film CNT network. The solution resistance appears the same for the two measurements which is of course sensible as the solutions for the trials were the same and a variation in electrolyte conductivity was unlikely. With already determined values for the solution and charge transfer resistance the double layer capacitance values for the two types of electrodes can be computed by extracting the frequencies

of the maxima in the Nyquist plots and using $C_{DL} = \frac{1}{R_{CT} \times 2\pi \times f_{max}}$ for computation.

Because of the nanoporosity of the CNT coatings, modified PLEs were routinely correlated with the higher capacitance.

Table 4.1 is providing the outcome of the analysis of EIS with bare and CNT-modified PLEs and informs about the observed dropping in the charge transfer resistance induced by the intentional CNT electrode surface modification and about the increase in the double layer capacitances associated with that treatment. Reproducibly, the R_{CT} values were found to decrease by an order of magnitude. The bare PLE from Figure 4.3, for instance, had an R_{CT} of $= 722.6 \pm 7.5$ k Ω while the CNT-modified version had an R_{CT} of $= 78.2 \pm 4.5$ k Ω . The extracted results suggested that a CNT-modified PLE could oxidize and reduce the ferro-/ferricyanide redox supplement of the electrolyte easier as bare PLE electrode. In addition, CNT-modified electrodes had larger double layer capacitances and accordingly larger surface areas. They were thus expected to produce for the same analyte concentration higher current signals in cyclic and pulse voltammogram, which is, in particular in conjunction with pulse voltammetry where capacitive currents are eliminated, a very beneficial property in term of the analysis of samples with trace contents of the species of interest.

Table 4.1 Impedance parameters were obtained by the analysis of the equivalent circuit fit of the impedance spectra of bare and CNT-modified PLEs.

Parameter	Electrode						average	
	1		2		3		PLE	PLE/CNT
	PLE	PLE/CNT	PLE	PLE/CNT	PLE	PLE/CNT		
R_S	148 Ω	116 Ω	137 Ω	123 Ω	154 Ω	117 Ω	146.3 \pm 8.6 Ω	118.7 \pm 3.8 Ω
$R_S + R_{CT}$	871 k Ω	74.0 k Ω	867 k Ω	83.0 k Ω	869 k Ω	78.0 k Ω	869.0 \pm 2.0 k Ω	78.3 \pm 4.5 k Ω
R_{CT}	722 k Ω	73.9 k Ω	730 k Ω	82.8 k Ω	715 k Ω	77.9 k Ω	722.6 \pm 7.5 k Ω	78.2 \pm 4.5 k Ω
C_{DL}	2.2 pF	21.5 pF	2.2 pF	19.2 pF	2.2 pF	20.4 pF	2.2 \pm 0.0 pF	20.4 \pm 1.2 pF

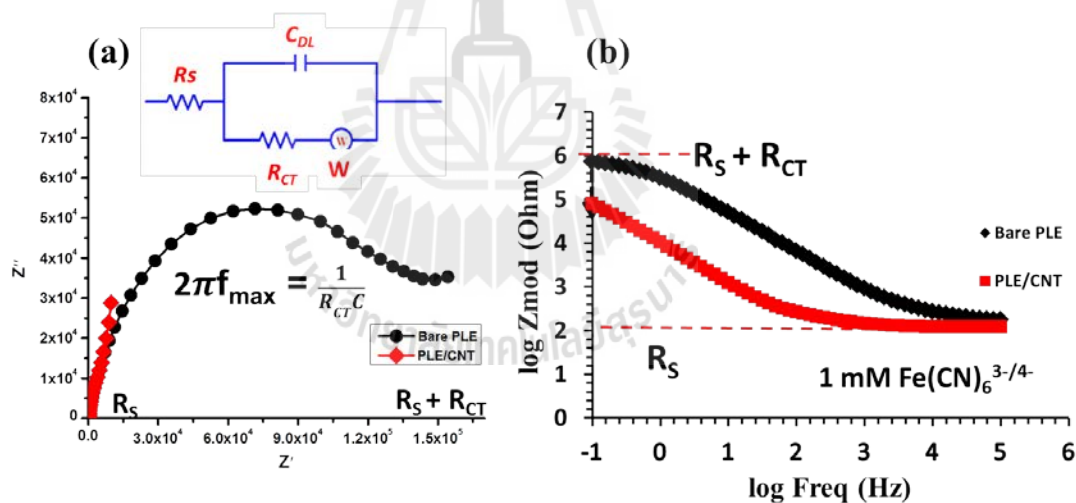


Figure 4.3 Electrochemical impedance spectra of (black) bare PLE and (red) a CNT-modified PLE measured in an electrolyte with 1 mM $\text{Fe}(\text{CN})_6^{3-/4-}$ in 0.1 M KCl. The spectra (Nyquist plot in (a); Bode plot in (b)) were acquired in the potentiostatic EIS mode with an applied DC voltage of 0.3 V and for a frequency range of 0.1 to 100 kHz.

4.1.3 Voltammetry trials with bare and CNT-modified PLEs

The obvious benefits of a CNT modification of PLEs that have been identified via SEM and EIS assessment, namely the increase in active electrode area through CNT film porosity and the decrease in charge transfer resistance through CNT electrocatalytic behavior, were expected to lead to an improved voltammetry. This is because the shape and peak size of voltammograms is dominated by both the ease with which electroactive species can undergo reduction and oxidation on an electrode surface and the active electrode area available for the interfacial redox process. Cyclic voltammograms for the oxidation and reduction of $\text{Fe}(\text{CN})_6^{3-}$ in 0.1 M KCl on bare and CNT-modified PLEs working electrode were recorded in the potential range 0.0 to 0.4 V vs. Ag/AgCl (sat KCl) and representative examples are shown in Figure 4.4. At the bare PLE (black curve) the cathodic and anodic peak potential appears at about 0.15 V with i_p^c of 29 mA and 0.25 V with i_p^a of 21 mA, respectively. In the CV of the CNT-modified PLE (red curve), on the other hand, the cathodic and anodic peak potential look similar in shape; however, the two peak currents are increased by a factor of about 2.4. The peak current enhancement for the reversible electrochemical conversion of $\text{Fe}(\text{CN})_6^{3-}$ at the CNT-modified PLE is likely to be caused by the increased surface area offered by the applied CNT layer. A positive effect of the electrocatalytic property of CNT, as observed in the EIS study, cannot be excluded. However, the $\text{Fe}(\text{CN})_6^{3-}/\text{Fe}(\text{CN})_6^{4-}$ redox couple is a reversible system that already runs at high efficacy in term of charge transfer in a CV or DPV experiment, even at bare carbon or metal electrode surface. The contribution of the CNT modification interns of electrocatalytic enhancement is the probably not the major for the response improvement.

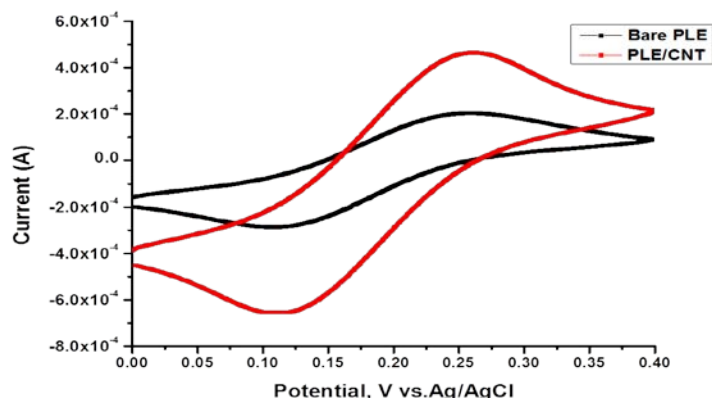


Figure 4.4 Cyclic voltammograms at a bare (black) and a CNT-modified (red) PLE in 1 mM $\text{K}_3\text{Fe}(\text{CN})_6$ in 0.1 M KCl. Starting potential for the acquisition of the CV was 0.4 V vs. Ag/AgCl, turning potential was 0 V vs. same reference, and final potential was equal to starting potential. The scan was completed with a scan rate of 50 mV s^{-1} .

The positive impact of a CNT modification became also evident when recording differential pulse voltammograms with bare and modified PLEs. DPV examples are shown in Figure 4.5 and they revealed a clearly better performance of the CNT-modified PLE sensor. Again and for the same reason as for CV, the peak currents were more than twice as much as for the bare PLE. Based on above findings and in good accordance with observations published by others it can be said that the CNT modification provided an exquisite platform for application of PLE electrodes to (pulse) voltammetric analysis of redox active analyte species. All analytical trials approaching electrochemical drug analysis thus used the CNT-modified version of PLEs as working electrodes and, as shown later, this choice contributed positively to the achievement of the goal of robotic drug electroanalysis in microtiter plate wells. Work related to the analysis of pharmaceutical drugs in conventional electrochemical

cell arrangement and in the robotic electrochemical system is described in the next sections.

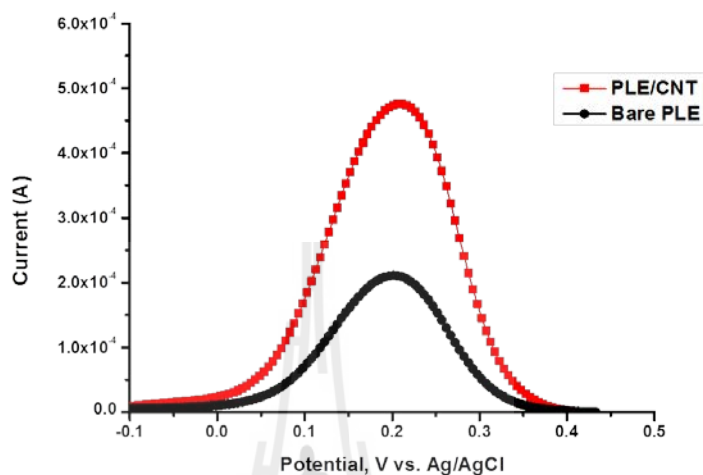


Figure 4.5 Differential pulse voltammograms at bare PLE (black) and CNT-modified (red) PLEs in 1 mM $\text{Fe}(\text{CN})_6^{3-}$ in 0.1 M KCl. Starting potential for the acquisition of the DPV was 0.4 V vs. Ag/AgCl, final potential was 0 V, same reference. The scan was completed with a scan rate of 50 mV s^{-1} . The parameters for the acquisition of the DPV were: E_{step} : 5 mV, E_{pulse} : 50 mV, t_{pulse} : 0.07s.

4.2 Establishment of robotic drug electroanalysis in 24-well microtiter plates

4.2.1 Work with respect to the target analyte ascorbic acid

4.2.1.1 Conventional ascorbic acid voltammetry tests, calibration measurements and sample analysis

In a first set of AA trials, cyclic voltammograms and differential pulse voltammograms for 5.0 mM AA in 0.1 M KCl as supporting

electrolyte were recorded at bare and CNT-modified PLEs working electrodes. Representative examples of the electrochemical measurements are shown in Figure 4.6. In agreement with the literature the CV revealed an irreversibility of the AA electro-oxidation and a cathodic peak was neither presented in bare nor the CNT working electrode case. Interestingly, the peak potential for anodic AA oxidation shifted noticeably to a less positive potential when the working electrode was changed from bare to a CNT-coated one. And at the same time the magnitude of the peak current increases by about 30% of the value for the bare electrode. These observations are in line with the effects that were observed as ferricyanide was the probing electro-active compound for the properties of a CNT modification of PLEs: 1. there is an electrocatalytic effect brought in by the CNT and allows easier oxidation (= oxidation at lower positive potentials as driving force) and 2. there is an increase in electrode surface area and thus a higher current for the same analyte concentration.

As differential pulse voltammetry lessens the magnitude of the capacitive portion of the analytically explored current through an electrochemical cell, this methodology and not cyclic voltammetry was applied for working out AA calibration curves and for AA quantification in samples. The optimum parameters for the acquisition of DPVs for the software platform of the employed potentiostat were the following: E_{pulse} , 50 mV; E_{step} , 4 mV; and t_{pulse} , 0.07 s. Figure 4.7 displays a representative collection of DPV curves that were obtained when recording DPVs in a solution of increasing concentration of AA with a CNT-modified PLE in charge as working electrode. For the construction of calibration plots (here: I_p vs. [AA]) baseline-corrected current values were determined individually for all DPVs in the trial and then plotted versus the partnering AA levels. Routinely the magnitude of the

oxidation peak current (i_p^a) increased with increasing concentration (c) of added AA. Good linearity with R values above 0.99, however, was restricted to the first part of the calibration curve and usually ranged up to 10 mM. The calibration curve experiment was repeated 3 times for the linear range from 0.1 mM to 10 mM. The linear range regression equation here is $i_p^a = 0.556c + 0.4219$, $R = 0.9959$, where i_p^a is the oxidation peak current (μA) and C is the AA concentration (mM); the detection limit of AA was found to be 0.05 mM.

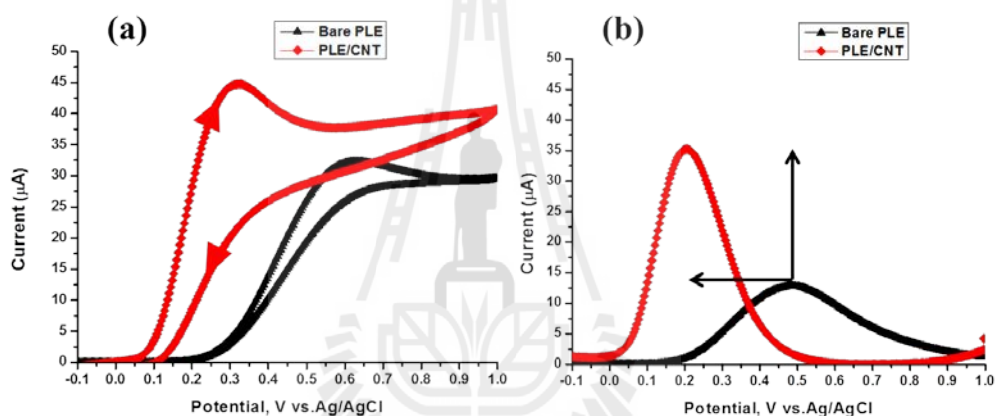


Figure 4.6 (a) Cyclic voltammograms and (b) differential pulse voltammograms of 5.0 mM AA in 0.1 M KCl at a bare (black curve) and CNT-modified (red curve) PLEs working electrode. The CV was recorded with a starting potential of -0.1 V, a turning potential of 1.0 V and a final potential of -0.1 V and a scan rate 25 mVs^{-1} . The DPV scan went from -0.1 V to 1.0 V and used E_{step} as 4 mV, E_{pulse} 50 mV, and t_{pulse} 0.07 s. (All potentials vs. Ag/AgCl pseudo reference electrode).

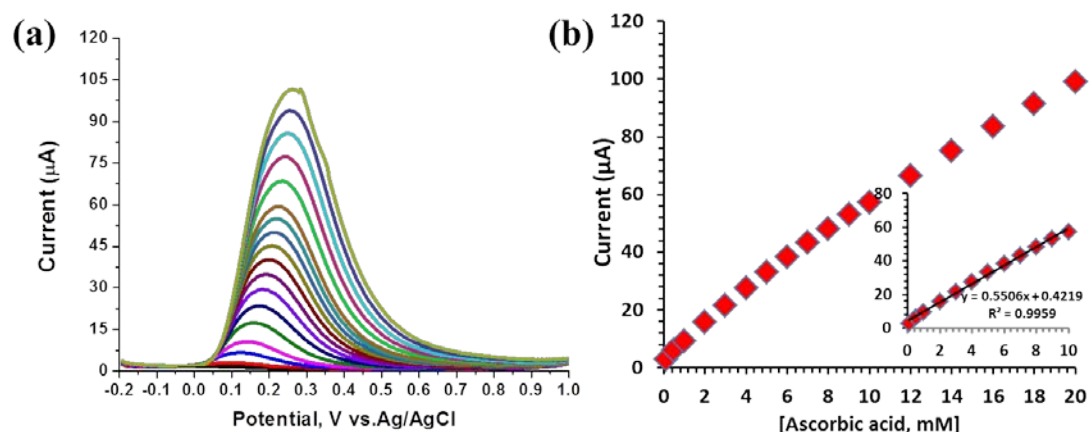


Figure 4.7 (a) A collection of DPVs of 0.1 to 10 mM concentration of AA in 0.1 M KCl (pH 6.73). For this particular example (b), the linear range extended with an R value of 0.9959 from about 0.1 to about 10 mM; parameter set for DPV: potential: -0.2 - 1.0 V, E_{step} 4 mV, E_{pulse} 50 mV, scan rate 25 mV/s and t_{pulse} 0.07 s.

The availability and use of the calibration curves allowed sample quantification of AA. Figure 4.8 (a) is a typical display of DPVs, one for an AA model sample with adjusted level of 1 mM analyte and the other one for the blank electrolyte. Based on the linear calibration plot (Figure 4.8(b); $R = 0.9973$), the observed, base line-corrected i_p^a value of 24.02 μA computed for the sample measurement converts to an AA concentration of 0.96 mM. The apparent recovery rate for this particular sample quantification was thus 96%. Repeated measurements on 1 mM AA model samples confirmed a good reproducibility of the analytical scheme in use and the average assay recovery rate turned out to be 96 ± 4.0 ($n = 3$) per cent for the beaker-type execution.

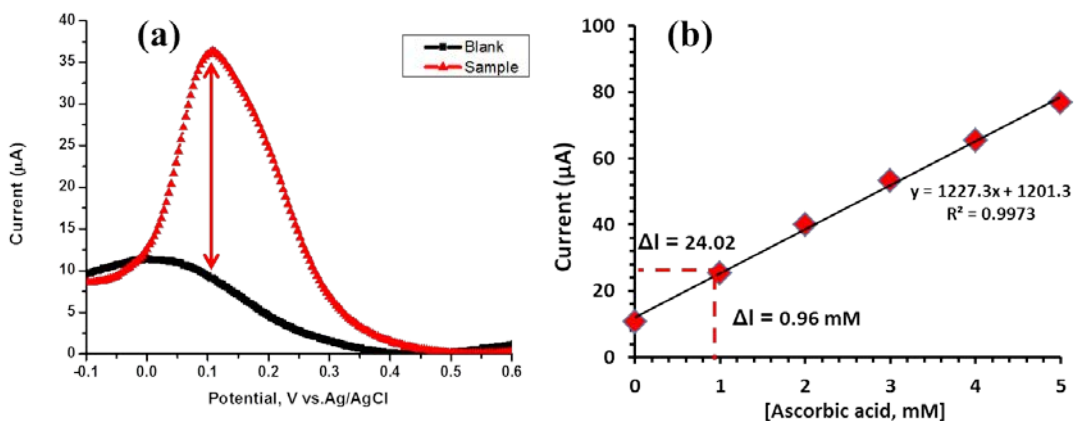


Figure 4.8 Quantification of AA in spiked model samples by the precalibration method. (a) A typical DPV for the 1 mM AA model sample (red trace) and the DPV of the blank electrolyte (black trace). (b) The linear calibration plot (DPVs not shown) with a display of the determination of the analyte level for the sample that gave rise to the DPV in (a).

The AA voltammetry assay as outlined above was finally applied to real sample analysis and measurements were made with solutions of a commercial AA tablets (Hicee 500 mg/tablets) from a local pharmacy shop. Figure 4.9(a) shows the DPV of a typical sample assessment of the tablet sample in the beaker-type electrochemical cell and, assuming AA as the main contributor to the electrochemical signal and taking the dilution factor for sample load into the measuring buffer into account, the peak of 27.12 µA converted to an AA concentration of 491.23 ± 1.07 mg (n = 3) indicating a well acceptable average recovery rate for the determination of about 98% of the listed 500 mg tablet content.

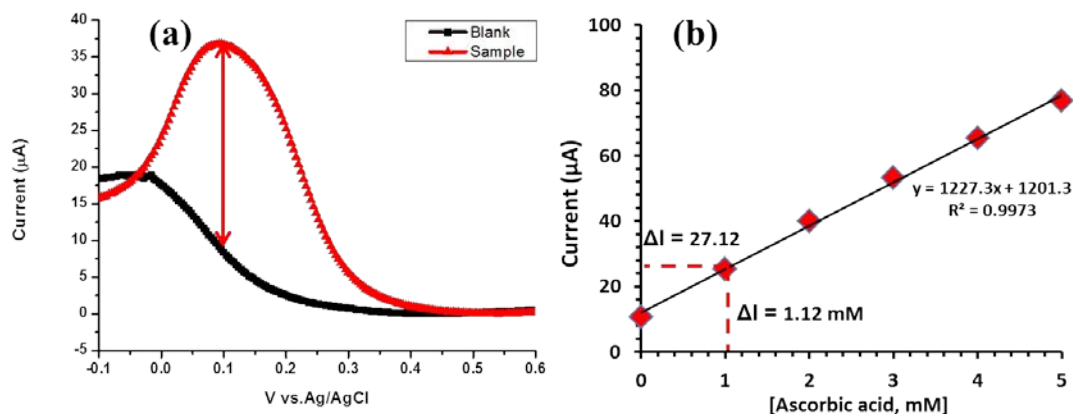


Figure 4.9 Quantification of AA in a sample of a dissolved AA tablet by the precalibration method. (a) A typical DPV for the real sample (red trace) and the DPV of the blank electrolyte (black trace). (b) The linear calibration plot (DPVs not shown) with a display of the determination of the analyte level for the tablet sample that gave rise to the DPV in (a) With dilution taking into account the determined, 12 mM translated into 491.2 mg in the tablet with a listed content of 500 mg.

4.2.1.2 Robotic ascorbic acid voltammetry: Establishment, calibration measurements and sample analysis

Routine chemical analysis in both industrial and academic laboratory settings needs reliable, convenient and cheap methodologies. Moreover, an automation of analytical work provides opportunities to reduce both the cost and the number of manual operations of analytical assessments. As demonstrated in the first section of this chapter manual AA voltammetry at CNT-modified PLEs worked with good performance for the quantitative determination of this analyte. It thus made sense to explore the quality of the sensors also for applications in the robotic electrochemical device that was available in the laboratory through earlier work by

may last hours for completion of one microtiter plate the stability of the working electrode response is a critical issue. The experiment that delivered the data for Figure 4.11 addressed this problem with a design that saw multiple DPVs recorded with a 0.5 mm diameter CNT-modified PLE over a period of 3 hours at intervals of 30 min in a microtiter plate well containing 10 mM AA. The seven DPVs produced the typical bell-shaped I/E curves with a symmetrical current peak at about 0.28 V, relative to the reference electrode, and, more important with respect to AA and electrode stability, the tracks overlaid almost perfectly and peak currents were the same with very minor deviations. Apparently, a degradation of the analyte or an electron transfer-inhibiting coverage of the working electrode surface with products of the electrochemical AA oxidation, were not a problem, at least not over the 3 h period of inspection. Electrode and analyte stability as requisites for functional robotic AA voltammetry in microtiter plates were thus successfully observed.

Next in the proposed system establishment was the proof that an automated acquisition of proper AA calibration curves is possible in the robotic electrochemical device for measurement in microtiter plates. For this purpose 12 AA concentrations ranging from 0.1 to 10 mM were loaded in the wells of a microtiter plate that were designated for holding samples and their DPVs were acquired. The resulting collection of 12 DPV curves is shown in Figure 4.12 and, important to note, they were the result of an automated electrode run through the wells with no operator action other than start of the procedure. As expected from earlier observations, the values of the DPV peak currents, I_p^a , increased progressively with increasing concentration of AA. The linear range of automated AA voltammetry was found to be 0.1 to 10 mM; this was similar to what conventional manual AA voltammetry as

described above could offer. Apparently robotic AA electroanalysis was well functional and the methodology ready for further non-manual quantification of the analyte in model and real samples, a task that is described next.

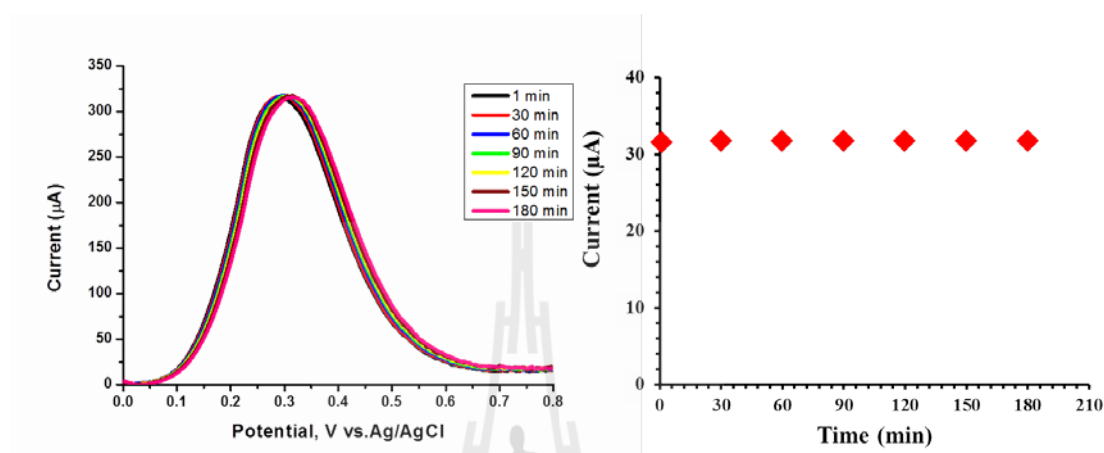


Figure 4.11 Electrode and analyte stability test an ascorbic electrochemical device. A 10 mM AA test solution was placed in a microtiter plate well and, using the electrode assembly of the robotic system with a CNT-modified PLEs (WE), an Ag/AgCl (RE) and a Pt-spiral (CE) for measurements, DPVs were recorded over a period of 3 h at 30 min intervals. Supporting electrolyte was 0.1 M KCl, the scan speed for the DPV was 25 mVs^{-1} and the DPV parameters were as defined earlier.

For AA quantifications via the precalibration strategy, a microtiter plate was routinely loaded with (i) 4.0 M HNO_3 in well #1 for working electrode pretreatment, (ii) distilled water in well #2 and 7 for the electrode assembly cleaning, (iii) measuring electrolyte without AA supplementation (pure 0.1 M KCl) in well #3 for base line according, (iv) a 1 mM AA model sample in wells #4-10 and last but not least, and (v) six real samples made of AA tablets in the wells #11-17. The

adapted load of microtiter plate for measuring in one automatic run a total of 12 sample solution is actually illustrated in Figure 4.13.

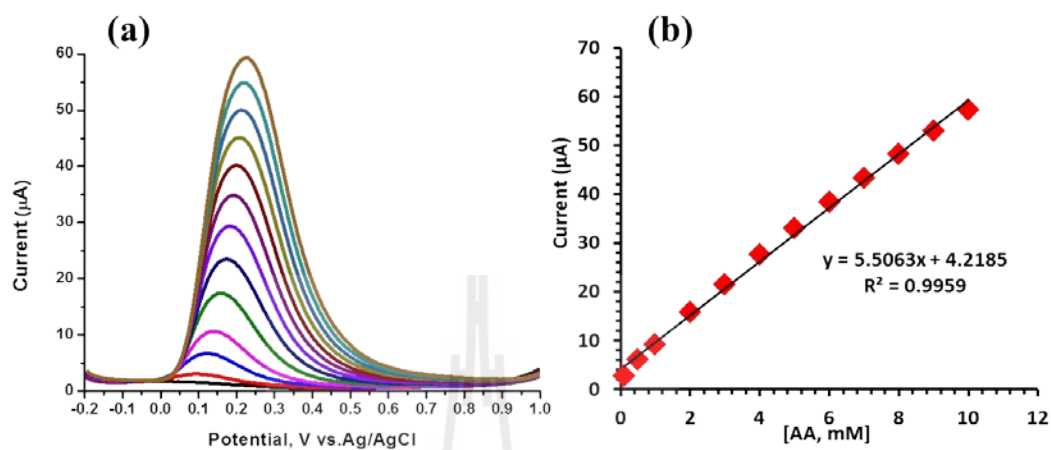


Figure 4.12 Robotic electrochemical AA calibration measurements in 24-well microtiter plate. (a) 12 sample wells of the microtiter plate were filled with analyte solution of 0.1 to 10.0 mM, and (b) sequentially subjected to automated DPV acquisition with the following parameters; scan range -0.2 - 1.0 V vs. Ag/AgCl; E_{step} 4 mV; E_{pulse} 50 mV; scan rate 25 mV s^{-1} ; and t_{pulse} 0.07 s.

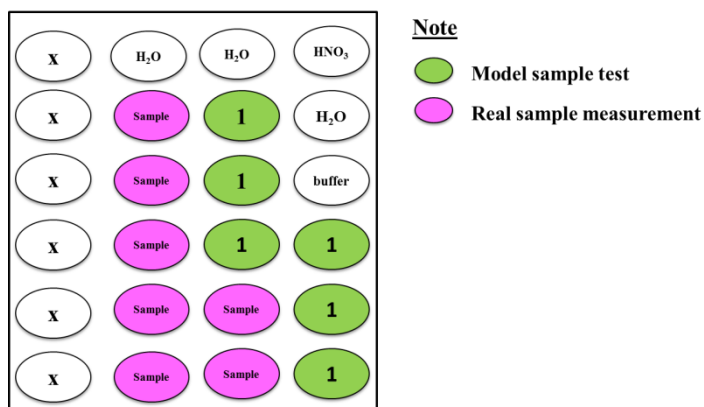


Figure 4.13 The microtiter plate load used for automated voltammetric quantification of 6 model and 6 real AA samples in an individual software-controlled analytical plate run.

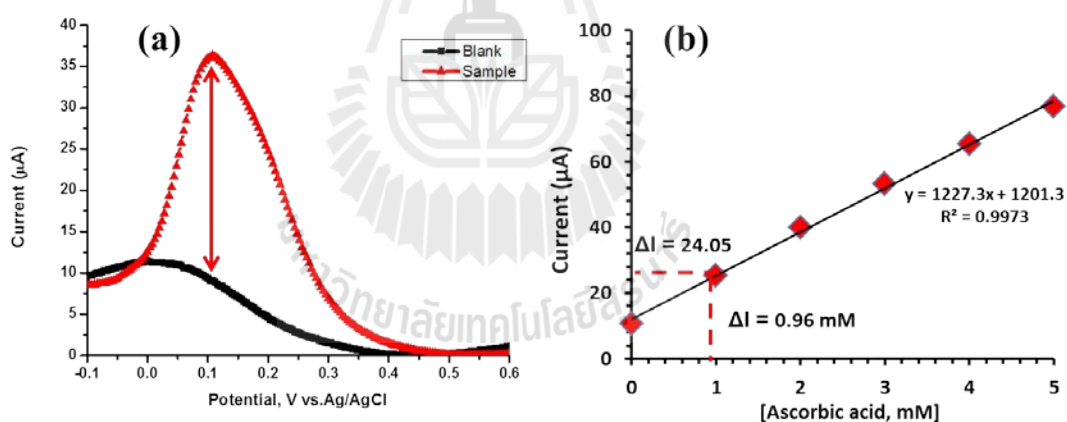


Figure 4.14 Robotic voltammetric quantification of AA in microtiter plate wells by the precalibration method. (a) One of the six model sample AA differential pulse voltammograms acquired in an automated run through a loaded microtiter plate. (b) Calibration plot for adjusted AA concentration from 1-5 mM with the computation of the AA content corresponding to the DPV in (a).

Figure 4.14 is a display of two DPVs as typically obtained in an automatic run through a microtiter plate with a load as shown in Figure 4.13; one is related to a measurement in analyte free buffer (black trace, well # 3) and the other related to acquisition in a well with model solution (red trace, one of the six green-colored wells). Figure 4.14(b) is the linear calibration plot that was constructed in the particular run from the DPVs acquired in Figure 4.12. The quality of the linear calibration plot was good ($R = 0.9973$) and with its help the observed i_p^a value of $24.05 \mu\text{A}$ for the 1 mM model sample could be converted to a measured AA concentration of 0.96 mM . The recovery rate was thus 96% in this particular case. A good average recovery rate of $96 \% \pm 4\%$ was computed when analyzing all six model samples that have been included in the trial. The real sample AA measurements in well #17-23 had a similar success. The observed i_p^a value of $28.10 \mu\text{A}$, for instance, converts to an AA concentration of 1.13 mM (in the well solution) and, after consideration of the dilution factor, into $28.10 \mu\text{A}$ for the tablet content. Analysis of all six real samples of the microtiter plate run revealed an average determined tablet content of $495.61 \pm 1.0 \text{ mg}$, which translates into an average recovery rate $101.0 \pm 4.0 \%$.

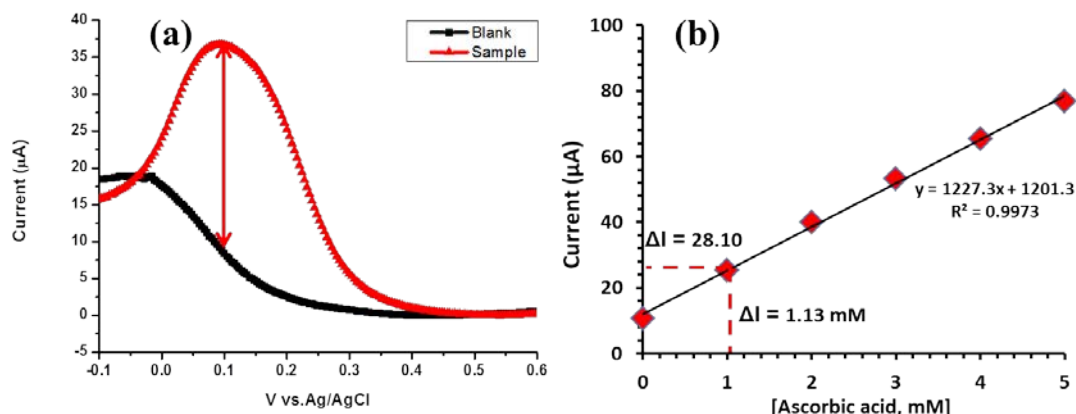


Figure 4.15 Robotic voltammetric quantification of AA in microtiter plate wells by the precalibration method. (a) One of the six real sample AA differential pulse voltammograms acquired in an automated run through a loaded microtiter plate. (b) Calibration plot for adjusted AA concentration from 1-5 mM with the computation of the AA content corresponding to the DPV in (a). Note: Final tablet content calculation had to take the dilution factor into account.

To summarize this sub-section, a sensitive voltammetric assay procedure for AA has been successfully incorporated into a microtiter plate-based robotic electrochemical workstation. Measurement of the target analyte used a suitable sized movable three-electrode assembly with CNT-modified PLEs working electrode, an Ag/AgCl reference and a Pt counter electrode. The tailored software of the specially-designed apparatus allowed computerized electrode (z) and microtiter plate (x, y) micropositioning and timely potentiostate operation. This facilitated a sequential assay by means of the execution of electrode pretreatment and cleaning procedures as well as AA quantification via voltammetry at appropriate periods. With properly adjusted parameters, the robotic AA differential pulse voltammetry achieved a linear

response between 0.1 to 10 mM and a detection limit of 0.05 mM AA. As supported by the data in Table 4.2 the calibration curve method worked well for the automated voltammetric AA quantification. Actually the combination of CNT modification of PLEs with the methodology of robotic differential pulse voltammetry in a microtiter plate format produced reliably and reproducibly accurate assessment of the AA content of spiked model samples and samples originating from dissolving commercial vitamin C tablets. The robustness of the robotic electrochemical AA assay was evident by the good agreement to data from manual voltammetric analysis. The robotic approach is, however, much more convenient as the manual one and it does not need a continuous involvement of laboratory staff during the actual measurement and the engaged person is able to focus on other duties during the time the instrument works the samples off under computer control and performance the microtiter plate assessment. The latter may be an asset of importance for the pharmaceutical and food industry where multiple AA determinations are routine task.

Table 4.2 Ascorbic acid quantification in model (spiked) and real (vitamin C tablet) samples. Comparison of the analytical performance of a manual beaker-type electrochemical assay with the quality of robotic DPV in a 24-well microtiter plate with software controlled scheme execution. For all included trials the number, n, of repetitions of measurements was 6.

Sample	Voltammetry				Recovery	
	Manual		Robotic		Manual	Robotic
	Added	Found	Added	Found		
Model sample test, μM	1.0	0.96 ± 4.0	1.0	0.96 ± 4.0	96.0 ± 4.0	96.0 ± 4.0
Tylenol 500 (mg/tablet)	-	491.23 ± 0.23	-	495.61 ± 1.0	98.23 ± 1.7	101.0 ± 4.0

4.2.2 Work with respect to the target analyte (NFX)

4.2.2.1 Conventional NFX voltammetry tests, calibration measurements and sample analysis

As for AA also for NFX manual voltammetry in beaker-type electrochemical cell arrangement preceded the trials with the compound in the robotic electrochemical system. Representative CVs and DPVs from the manual voltammetric measurements of $100 \mu\text{M}$ NFX in 0.1 M acetate/ 0.1 M KCl buffer, pH 4.5 are shown in Figure 4.16. At a bare PLE working electrode no analytically useful oxidation or reduction peaks appeared in the CV recordings and not much better for this type of measurements was the observation for the CNT-modified PLEs for which at least a

shoulder in the onset of the oxygen evolution current wave indicated NFX electrochemistry (refer to Figure 4.16(a)). Better for both types of electrodes were their DPVs (refer to Figure 4.16(b)). A tiny NFX oxidation peak came up at about 0.9 V vs. reference in the DPV at a bare PLE and this peak got expressed at well improved level and sharper at CNT-coated PLEs. A peak comparison actually revealed an about 15 fold increase that was gained by the presence of the electrocatalytic CNT layer on the surface of the thin PLE cylinder. NFX DPV at a CNT-modified PLE was thus the best option to further be explored as a scheme for the calibration/quantification studies of this important pharmaceutical analyte in either beaker-type electrochemical cells or in the robotic electrochemical system.

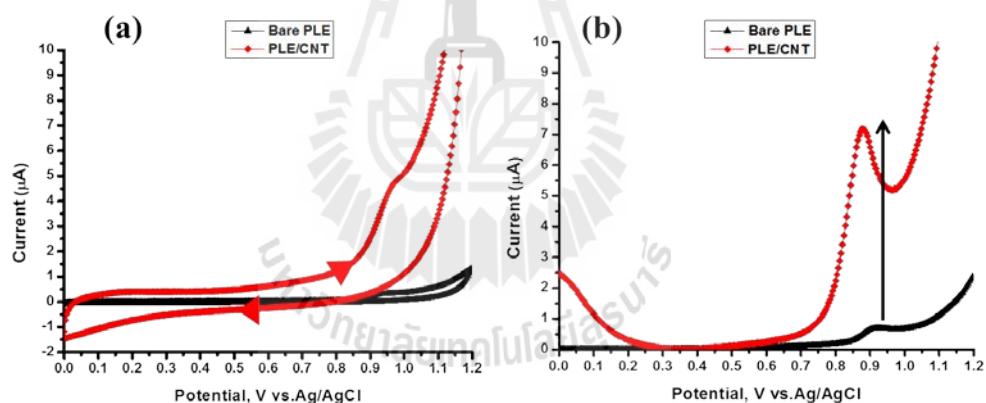


Figure 4.16 Conventional cyclic (a) and differential pulse, and (b) voltammetry of 100 μM NFX in 0.1 M acetate/ 0.1 M KCl buffer (pH 4.5) in a beaker-type electrochemical cell. The black traces refer to voltammograms at a bare PLE while the red traces belong to CNT-modified PLEs. Scan range was 0 to 1.2 V, scan speed was 20 mV s^{-1} , and for the acquisition of the DPV used were $E_{\text{step}} = 4 \text{ mV}$ $E_{\text{pulse}} = 50 \text{ mV}$, $t_{\text{pulse}} = 0.07 \text{ s}$ and $t_{\text{dep}} = 300 \text{ s}$.

For manual NFX calibration measurements an E_{pulse} of 50 mV, E_{step} of 4 mV and t_{pulse} of 0.07 s were used as the optimal parameters for DPV acquisition. Figure 4.17 a shows an example of DPV curves for different NFX concentrations. Usually 300 s was allowed to pass as kind of preconcentration time to accumulate NFX via adsorption of the organic compound on the CNT-modified PLEs before the corresponding DPVs were recorded. A linear relationship with a good regression coefficient (see inset of Figure 4.17(b) as a representative example) was typically observed between the NFX oxidation peak current (i_p^a) and the concentration (c) of the analyte in the range from 1.0 μM to 10 μM . The detection limit of NFX quantification at CNT-modified PLEs was found to be 0.3 μM , with preconcentration time set to 300 s.

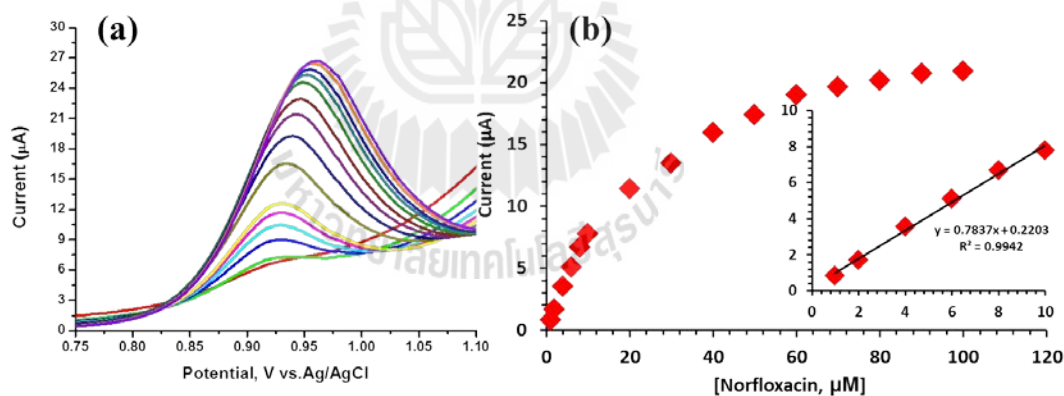


Figure 4.17 Manually recorded DPVs of various concentrations of NFX in 0.1 M acetate buffer (pH 4.5). (b) The calibration curve with peak currents extracted from (a); the linear range extended to about 10 μM . Parameter for DPV acquisition: potential range 0 - 1.2 V, preconcentration time 300 s, E_{step} 4 mV, E_{pulse} 50 mV, scan rate 20mVs^{-1} and t_{pulse} 0.07 s.

The standard addition method was successful for a voltammetric quantification of NFX. Figure 4.18 is a typical NFX sample assessment via DPV with a representative test concentration of 2.0 μM . Shown in part (a) are four original DPVs, one for the bare sample and three for the sample with increasing amounts of standard addition. For this particular case, the analysis of the plot of peak currents vs. added NFX in part (b) revealed a determined NFX sample level of 1.96 μM . As the adjusted sample concentration was exactly 2 μM , the recovery rate for this measurement was 99.0%. For six repetitions of the manual measurement on a 2.0 μM NFX model solution the average recovery rate for the analysis in the standard addition mode was $99.0\% \pm 5.2\%$ (see also Table 4.3).

The established manual analytical procedure with CNT-modified PLEs used for quantitative NFX voltammetry was also applied for inspections of real samples which were made by dissolving commercial NFX tablets from a local pharmacy shop in the measuring buffer. Figure 4.19 shows the set of five DPV recordings that allowed utilization of the standard addition method for an quantification of the drug, present at a 400 mg level per tablet. Taking the dilution of the tablet solution in course of the analysis into account the average measured NFX tablet content was $412.8 \text{ mg} \pm 0.1 \text{ mg}$ ($n = 6$), which translates into an average recovery rate of $103.2\% \pm 3.2\%$ ($n = 6$) (see also Table 4.3).

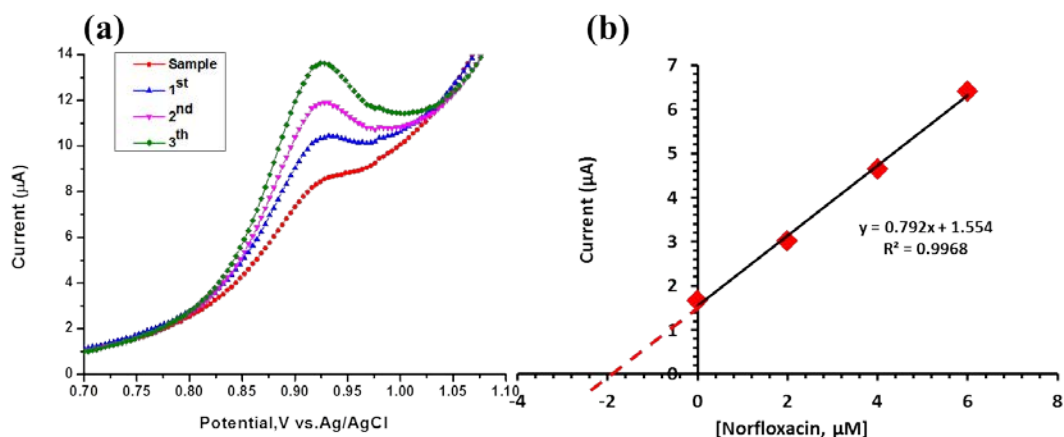


Figure 4.18 Quantification of NFX in a model sample with an adjusted 2 μM level by the standard addition method. Measuring buffer was 0.1 M acetate buffer (pH 4.5) in 0.1 M KCl. (a) A typical set of the NFX DPVs for the bare sample (red trace) and for sample with three sequential additions of small aliquots of a NFX stock solution. (b) Sample NFX quantification in the standard addition mode with the extrapolation of the linear regression line to the x axes and the utilization of the x-axes interception for sample concentration identification.

4.2.2.2 Robotic NFX voltammetry in the microtiter plate format:

Establishment, calibration measurements and sample analysis

From the conventional beaker-type trials it was known that the NFX voltammetry at CNT-modified PLEs delivered good results for the quantification of the compound in spiked model and in dissolved tablet samples. It was thus interesting to see whether this good performance would also be available when executing the analytical scheme in the robotic electrochemical device to

establish a non-manual microtiter plate antibiotic assaying similar to what already was described for the antioxidant AA.

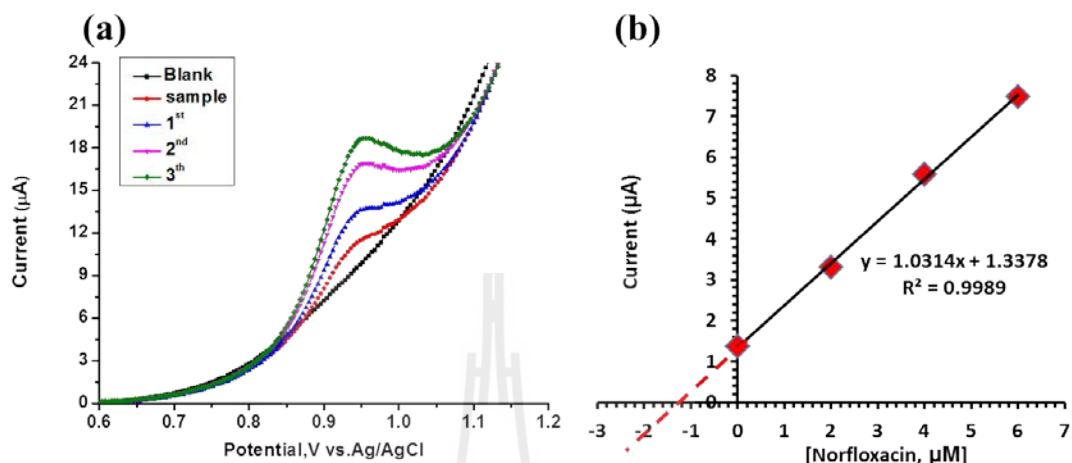


Figure 4.19 Quantification of NFX in a dissolved NFX tablet sample by the standard addition method with voltammetric detection. Measuring buffer was 0.1 M acetate buffer (pH 4.5) in 0.1 M KCl. (a) A typical set of the NFX DPVs for the blank solution (black trace), the bare sample (red trace) and for sample with three sequential additions of small aliquots of a NFX stock solution. (b) Sample NFX quantification in the standard addition mode with the extrapolation of the linear regression line to the x axes and the utilization of the x-axes interception for sample concentration identification.

Start were again tests of the stability of the response of CNT-modified PLEs towards NFX over a period as long as the estimated measuring time of a complete NFX microtiter plate voltammetry run, which actually was considered to be about 3 h in total time. Figure 4.20(a) is the display of a collection of twelve DPVs that were recorded at a CNT-modified PLE during a 3 h automatic voltammetric trial

in a microtiter plate well that contained 8 μM NFX and with measurements carried out at intervals of 15 min. All DPVs expressed the typical bell-shaped NFX peaks resting on the anodic current wave of the oxygen evolution with the peak maximum located at about 0.94, relative to the reference electrode. A small drift in the baseline of the peaks sometimes came up. When, however, plotting the baseline-corrected anodic NFX peak currents as function of measuring time (see Figure 4.20(b)) it became evident that they were reasonably stable, excluding significant loss of electrode activity and/or analyte degradation. An important prerequisite for successful automated NFX electroanalysis in microtiter plate wells was thus fulfilled.

In the next step, the DPV response of the CNT-modified PLE working electrodes to 11 different NFX concentrations in the range 1.0 to 100 μM was measured in robotic manner. Figure 4.21 displays the result of such a typical automated calibration run through the wells of the microtiter plate and, as expected, the values of DPV peak current, i_p^a , increased progressively with increasing concentration of the NFX. In good agreement with the trial in normal beakers, a linear range of about 1.0 to 10 μM was available for the methodology. In further system tests both the precalibration and the standard addition method were then employed for robotic voltammetric quantifications of NFX in spiked model solutions and in solutions made of dissolved NFX tablets.

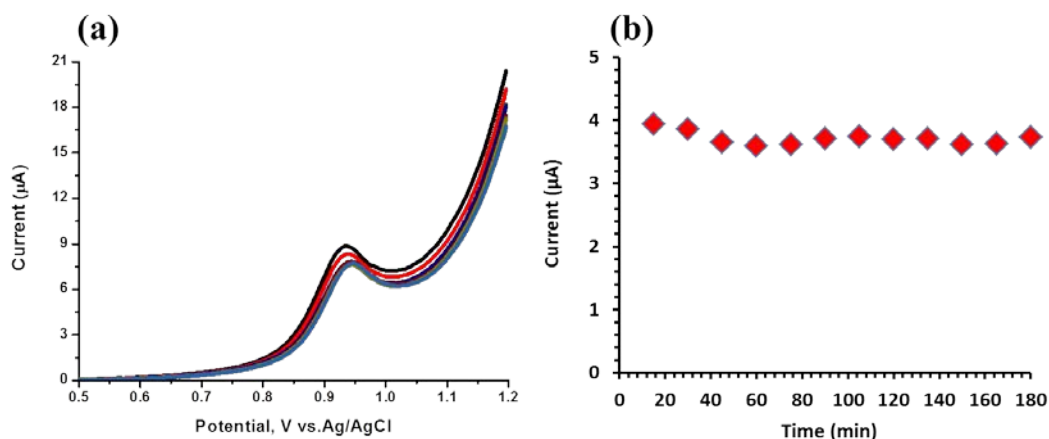


Figure 4.20 NFX stability test in the robotic electrochemical system. The addressed microtiter plate well was filled with 8 μM NFX in 0.1 M acetate buffer (pH 4.5). Robotic voltammetry used an electrode assembly with a CNT-modified PLE (WE), an Ag/AgCl (RE) and a Pt-spiral (CE), and the parameters for DPV acquisition were as listed before in the manual procedure. DPVs were recorded and stored every 15 min for a period 3 h. (a) The twelve DPVs of the trial. (b) A plot of the baseline-corrected anodic NFX peak currents as a function of time.

For calibration curve establishment, a microtiter plate was loaded with (i) 4.0 M HNO_3 in well #1 for the working (PLE) electrode pretreatment, (ii) water for the electrode cleaning in all wells with odd numbers of 3 and above, (iii) bare measuring electrolyte (0.1 M acetate buffer pH 4.5 in 0.1 M KCl) in well #2 for base line according, (iv) eleven calibration solutions of known NFX concentration (1, 2, 4, 6, 8, 10, 20, 40, 60, 80 and 100 μM) in the wells with even numbers of #4 and above for the acquisition of the data for calibration curve construction. The microtiter plate load for the robotic NFX calibration trial is schematically illustrated in Figure 4.22.

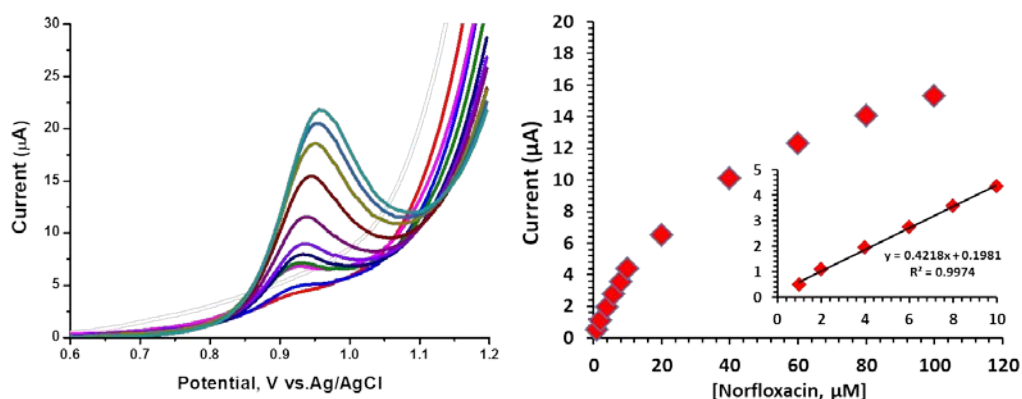


Figure 4.21 Robotic NFX calibration measurements in a 24-well microtiter plate. (a) The 11 sample wells of the loaded microtiter plate carried analyte solutions of 1.0 to 100 μM and they were sequentially subjected to DPV measurement. (b) The full calibration curve and, as inset, the linear range of the NFX voltammetry.

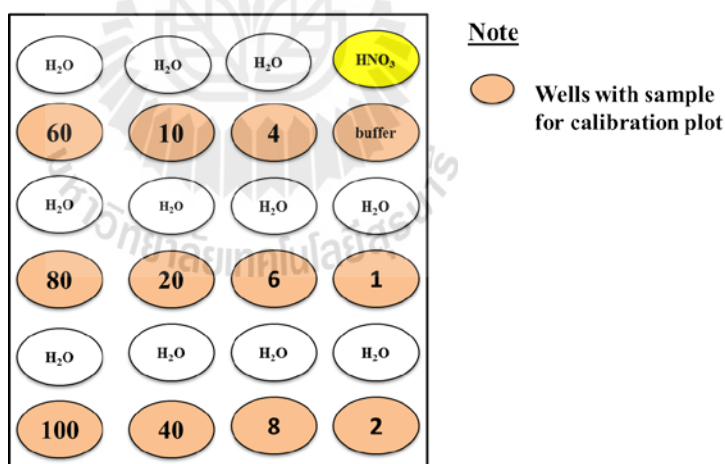


Figure 4.22 Schematic representation of the load of a microtiter plate as it was used for a robotic NFX calibration measurement.

Figure 4.23, shows the load of a microtiter plate as designed and routinely used for measuring with four-fold repetition ($n=4$) the NFX level of

spiked model sample solutions with an adjusted 2.0 μM of the target compound. Figure 4.24(a) then is displaying for one of the four loaded samples the DPVs in (1) the bare buffer, (2) the sample itself, and (3) the sample but including the supplementations with known levels of NFX. Figure 4.24(b) is the translation of the measurement in Figure 4.24(a) into the typical analytical standard addition plot that allows analyte concentration assessment via extrapolation of the regression line towards the x-axis or from the regression line equation. Worth mentioning that the completion of the robotic DPV measurements in the microtiter plate format took about 2 ½ hours, however, without any operator involvement. For the particular case presented in Figure 4.24(a) and (b), the analysis of the plot of peak currents vs. added NFX in part (b) revealed a determined NFX sample level of 2.03 μM . As the adjusted sample concentration was exactly 2 μM , the recovery rate for this measurement was 101.5%. For sixteen robotic determinations (4 plate runs with 4 samples each) of the 2.0 μM NFX model solution the average recovery rate for the analysis in the standard addition mode was $101.5\% \pm 1.5\%$ (see also Table 4.3).

The robotic NFX voltammetry procedure was finally applied to real sample analysis and measurements were made with solutions of commercial NFX tablets and with serum samples, respectively. The microtiter plate load for the robotic tablet and serum trials was similar to the one illustrated in Figure 4.23, but the 4 sample wells carried of course the right target, namely either a tablet or a spiked serum solution. Figure 4.25(a) is displaying for one of the four loaded NFX tablet samples the DPVs in (1) the bare buffer, (2) the tablet sample itself, and (3) the tablet sample but with the supplementations with known levels of NFX. Figure 4.25(b) is the display of the corresponding analytical standard addition plot that allows sample

analyte concentration, for instance, via x axes extrapolation of the regression line. For the particular case presented in Figure 4.25(a) and (b), the analysis of the plot of peak currents vs. added NFX in part (b) revealed a determined NFX sample level of 1.30 μM . Taking the dilution factor in course of sample preparation into account, the determined tablet content was computed as 392.38 mg/tablet which with the listed value of 400 mg/tablet corresponds to a recovery rate of 101.9%. For 8 repetitive robotic tablet NFX determinations (2 plate runs with 4 samples each) the average recovery rate for the analysis in the standard addition mode was $101.9\% \pm 1.9\%$ (see also Table 4.3). The completion of one set of four robotic tablet DPV measurements in the microtiter plate format took about 2½ hours, however, without any operator involvement.

The measurements on the commercial NFX tablet samples were followed by assessments of the NFX content in spiked human serum samples. The microtiter plate load again followed the design demonstrated in Figure 4.23 but the model sample was replaced by the serum sample. And as before for the tablet trials the standard addition method was in charge of quantification. Serum was spiked with 2 μM NFX and 100 μL of the spiked serum solution was then diluted into 3 mL of (0.1 M acetate buffer (pH 4.5) in 0.1 M KCl) buffer solution and transferred to designated vials in the 24-wells microtiter plate.

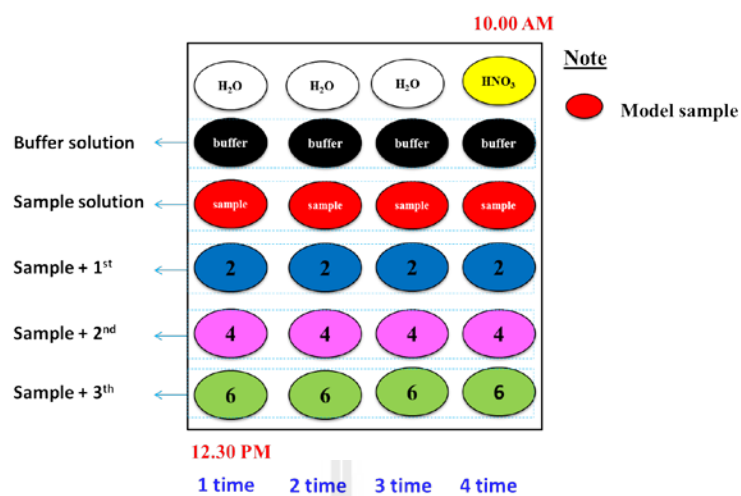


Figure 4.23 Schematic display of the load of a microtiter plate as used for the concentration determination of a model (spiked) sample solution with an adjusted NFX level of 2.0 μM . The load is designed for the application of the standard addition method for quantitative NFX analysis. The time of a complete robotic analytical run through all wells of the microtiter plate was usually about 2½ h.

Figure 4.26(a) is displaying for one of the four loaded NFX-spiked serum samples the DPVs in (1) the bare buffer, (2) the spiked serum sample itself, and (3) the spiked serum sample but with additional supplementations of known levels of NFX for standard addition realization. Figure 4.26(b) is the display of the corresponding analytical standard addition plot that allows sample analyte concentration determination, for instance, via x axes extrapolation of the regression line. For the particular case presented in Figure 4.26(a) and b, the analysis of the plot of peak currents vs. added NFX in part (b) revealed a determined NFX sample level of 2.10 μM . Taking the dilution factor in course of spiked serum sample preparation into account, the determined serum content was computed as 2.10 μM -

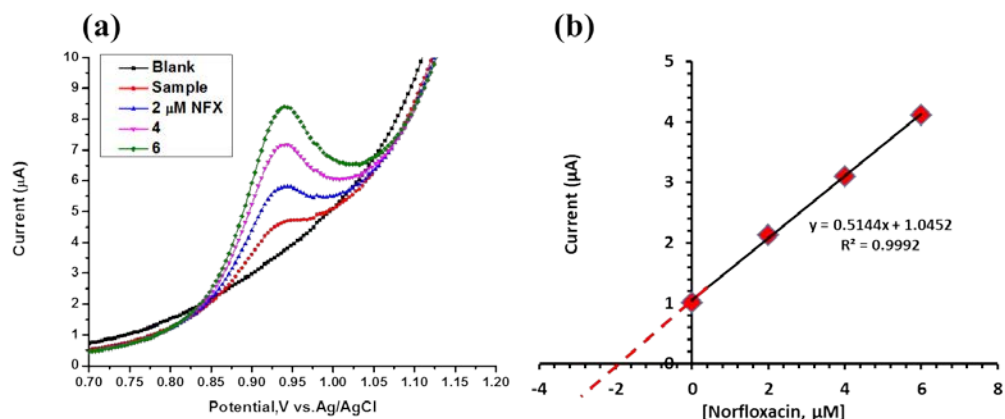


Figure 4.24 Microtiter plate-based quantification of NFX in a spiked, 2.0 μM, NFX model samples by the automated standard addition method with voltammetric detection. Measuring buffer was in 0.1 M acetate buffer (pH 4.5) in 0.1 M KCl. (a) A typical set of the NFX DPVs for the blank solution (black trace), the bare sample (red trace) and for sample with three sequential additions of small aliquots of a NFX stock solution. (b) Sample NFX quantification in the standard addition mode with the extrapolation of the linear regression line to the x axes and the utilization of the x-axes interception for sample concentration identification.

-which with the adjusted value of 2 μM corresponds to a recovery rate of 105.5%. For 4 repetitive robotic tablet NFX determinations (1 plate run with 4 samples each) the average recovery rate for the analysis in the standard addition mode was 105.5% ± 5.0% (see also Table 4.3). The completion of one set of four robotic serum DPV measurements in the microtiter plate format took about 2½ hours, however, without any operator involvement.

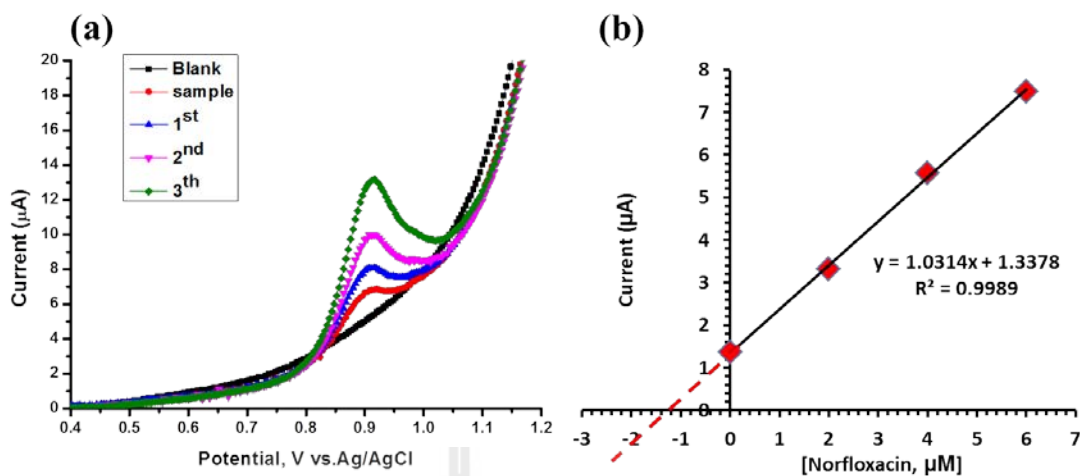


Figure 4.25 Microtiter plate-based quantification of NFX in a dissolved tablet (real) sample by the automated standard addition method with voltammetric detection. Measuring buffer was in 0.1 M acetate buffer (pH 4.5) in 0.1 M KCl. (a) A typical set of the NFX DPVs for the blank solution (black trace), the bare tablet sample solution (red trace) and for sample with three sequential additions of small aliquots of a NFX stock solution. (b) Sample NFX quantification in the standard addition mode with the extrapolation of the linear regression line to the x axes and the utilization of the x-axes interception for sample concentration identification.

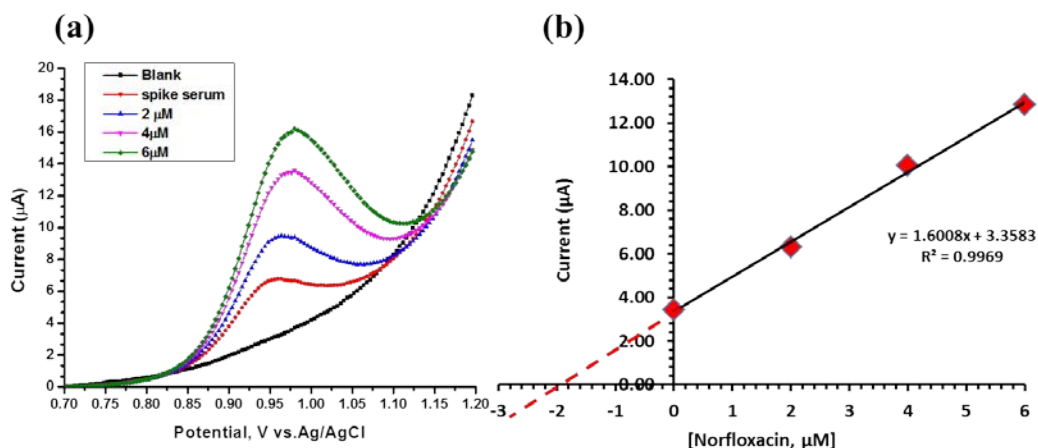


Figure 4.26 Robotic voltammetric quantification of NFX in spiked serum sample in microtiter plate wells by the standard addition method. (a) A representative set of four DPVs for bare buffer, a spiked serum sample and the solution with known level of NFX supplementation, all acquired as part of an automated run through a loaded microtiter plate. (b) Standard addition curve and linear regression plot.

In summary of the NFX part of this study it can be said that a sensitive voltammetric assay for this antibiotic has been achieved in form of DPV at CNT-modified PLE electrodes and an incorporation of these sensors into a microtiter plate-based robotic electrochemical workstation. The automated in-well NFX differential pulse voltammetry achieved a linear response between 1.0 to 10.0 μM and a detection limit of 0.3 μM NFX. Spiked model samples, dissolved NFX tablet samples and spiked serum samples were about equally well analyzed with the robotic drug voltammetry and results compared also well with the ones from standard manual assessments in beaker-type electrochemical cells. As multiple samples can be processed automatically in a single analytical run through a loaded microtiter plate

format the methodology is time-saving and convenient and thus expected to be a useful option for drug quality control in the pharmaceutical industry.

Table 4.3 Norfloxacin (NFX) quantification in spiked model samples, in NORFA tablets (400 mg/tablet) and intentionally spiked serum sample. Compared are results from manual beaker-type voltammetric measurements with the outcome of automated NFX voltammetry in microtiter plates.

Sample	Voltammetry				Recovery	
	Manual		Robotic		Manual	Robotic
	Added	Found	Added	Found		
Model sample test, μM	2.0	1.96 ± 0.3	2.0	2.03 ± 0.21	99.0 ± 5.2	101.5 ± 1.5
NORFA 400 (mg/tablet)	-	412.8 ± 0.1	-	392.38 ± 0.1	103.2 ± 3.2	101.9 ± 1.9
Serum sample, μM	-	-	2.0	2.10 ± 0.02	-	105 ± 5.0

4.2.3 Work with respect to the target analyte ciprofloxacin (CFX)

4.2.3.1 Conventional CFX voltammetry tests, calibration measurements and sample analysis

CFX is another widely applied synthetic broad spectrum antibiotic and used for treating infections caused by various bacteria. According to the scientific literature, HPLC is the most widely used method for the determination of CFX (Neckel, Joukhadar, Frossard, Jager, Muller and Mayer, 2003). However, electrochemical methods have been proposed for CFX analysis and they are linked to

a number of advantages including high sensitivity, rapid sensor response, low cost and a pronounced simplicity.

From the earlier reviewed literature (see Chapter II) it was known that in a voltammetric scan CFX is getting oxidized just above 1 V vs. reference and, though not very well expressed at bare electrodes, a current peak may there be visible. As for norfloxacin, better voltammetric peaks were observed at CNT-modified electrodes and they enabled, for instance, the analysis of CFX in eye drop solutions (Zhang and Wei, 2007). Published conditions could that be taken here as starting point for setting up an optimal procedure for CFX detection in the robotic electrochemical workstation. Representative cyclic and differential pulse voltammograms for the oxidation of 10 μM CFX in 0.1 M phosphate buffer (pH 4.0) with 0.1 M KCl at bare and CNT-modified PLEs working electrodes are shown in Figure 4.27. Important practical observation was that only at the CNT-modified PLE an analytically useful CFX DPV peak was obtained in the voltammograms. As for NFX also for CFX the presence of the graphitic surface modification was essential for the ability to establish a quantitative robotic CFX electroanalysis.

Figure 4.28(a) shows a set of DPV curves that were recorded with a stationary PLE/Pt/AgAgCl three electrode assembly in one and the same well of a microtiter plate but solutions with increasing concentration of analyte, following a 120 s long preconcentration of CFX at the CNT-modified working electrode. At levels above 100 μM a deviation from linearity was noticed but below that critical concentration the current response to CFX addition scaled well linear with the CFX concentration. Typically, the detection limit of CFX for the manual measurements

with stationary electrodes was found to be $1.6 \mu\text{M}$, with 120 s employed as preconcentration time.

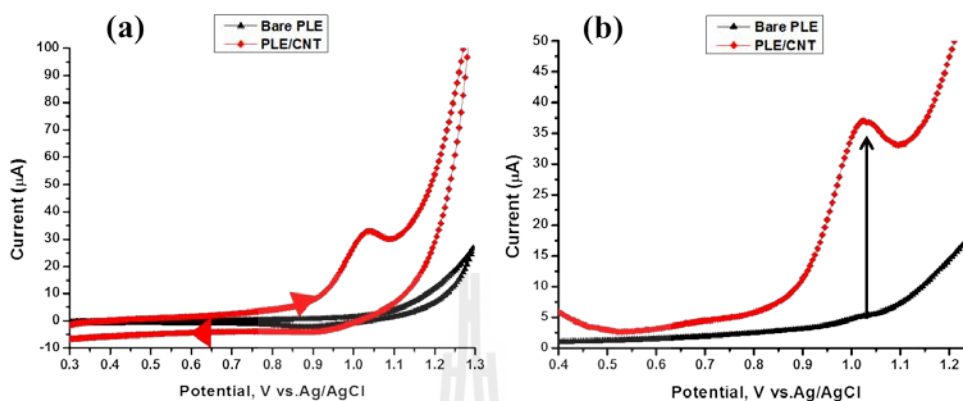


Figure 4.27 CVs (a) and DPVs (b) of $10 \mu\text{M}$ CFX in 0.1 M phosphate buffer pH 4.0/ 0.1 M KCl at a bare PLE (black curve) and a CNT-modified PLE (red curve) working electrode. Voltammetry parameters were: scanned potential range: 0.3 to 1.3 V , E_{step} : 5 mV , E_{pulse} : 50 mV , scan rate: 20 mVs^{-1} , t_{pulse} : 0.07 s and t_{dep} : 120 s .

Figure 4.29 displays the outcome of a typical quantification of CFX in a spiked model sample with $10.0 \mu\text{M}$ analyte and DPV in conjunction with the standard addition method in charge for analysis. Figure 4.29(a) actually provides the DPVs in the bare buffer, the CFX-spiked model sample, and the CFX sample but with additional supplementations of known levels of CFX for standard addition establishment. Figure 4.29(b) is the display of the corresponding analytical standard addition plot that allows sample analyte concentration determination, for instance, via x axes extrapolation of the regression line. For the particular case presented in 4.29a and b, the analysis of the plot of peak currents vs. added CFX in part (b) revealed a

determined CFX sample level of 10.21 μM . With the adjusted level of 10.0 μM CFX in mind, the determined level corresponds to a recovery rate of 102.1%. For six repetitive determinations the average recovery rate for the CFX analysis in the manual standard addition mode was $102.1\% \pm 0.17\%$ (see also Table 4.4). A similar quality of analysis was obtained when measuring with the same manual approach samples originating from the dissolution of commercial CFX tablets with a content of 500 mg/tablet (Figure 4.30(a) and (b)). In this case, the average recovery rate was found to be $98.4\% \pm 1.62\%$ ($n = 6$, see also Table 4.4). Apparently, DPV at CNT-modified PLEs was sensitive and reliable enough for the task of CFX quantification in aqueous solution of this species.

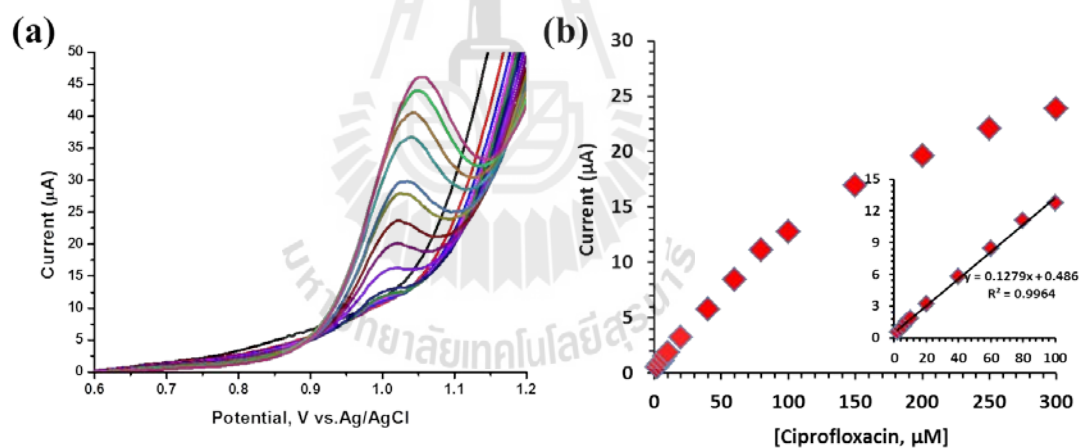


Figure 4.28 DPVs in solutions of increasing CFX concentrations as used for calibration curve data acquisition, analysis and final standard addition curve plotting. For CFX in 0.1 M phosphate buffer (pH 4.0) with 0.1 M KCl the linear range of the voltammetric procedure is from about 2.0 to 100 μM . The optimum DPV conditions were: potential range, 0.3 - 1.3 V.; E_{step} , 5 mV; E_{pulse} , 50 mV; scan rate, 20 mV s^{-1} and t_{pulse} , 0.07 s.

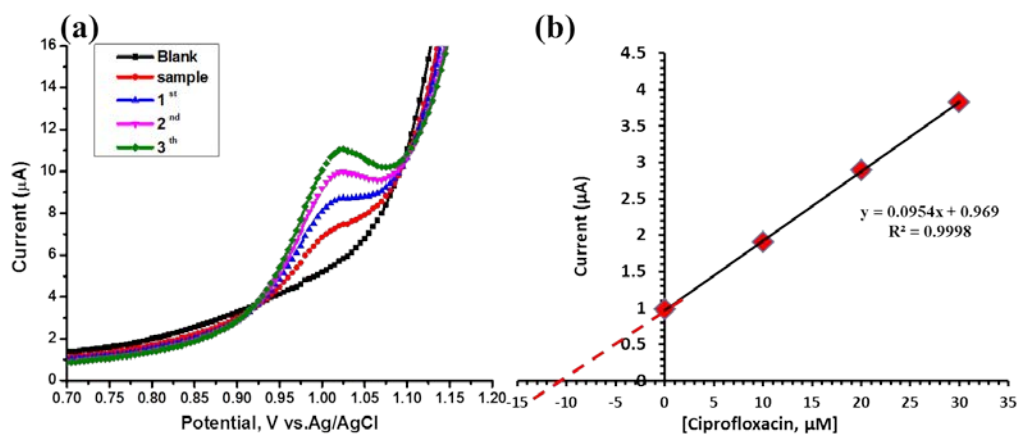


Figure 4.29 Quantification of CFX in a spiked model sample by application of the manually performed standard addition method with voltammetric detection. (a) DPVs were recorded in 0.1 M phosphate buffer (pH 4.0)/0.1 M KCl, one for the blank solution (black trace), one for the 10 μM spiked model sample, and three for the spiked sample plus proper aliquots of CFX stock solution. (b) The regression line in the standard addition curve for the CFX model sample assessed in (a).

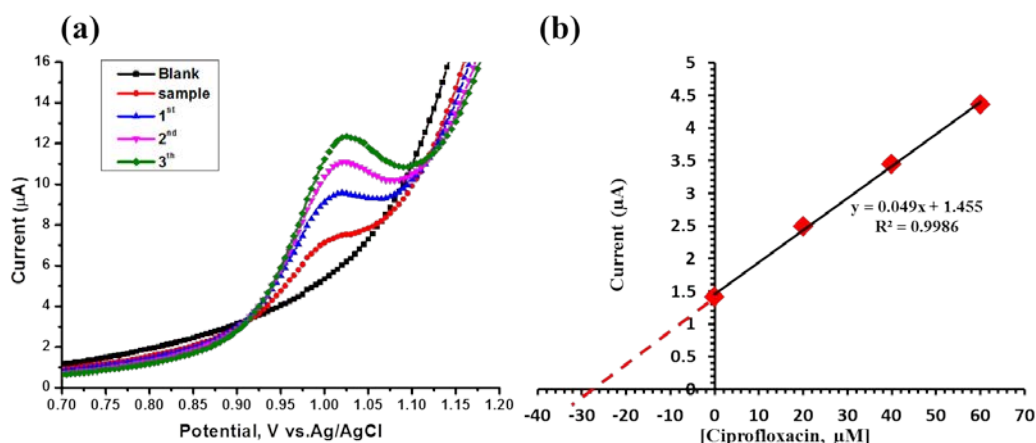


Figure 4.30 Quantification of CFX in a dissolved CFX tablet sample by application of the manually performed standard addition method with voltammetric detection. (a) DPVs were recorded in 0.1 M phosphate buffer (pH 4.0)/0.1 M KCl, one for the blank solution (black trace), one for the dissolved CFX table sample, and three for the spiked sample plus proper aliquots of CFX stock solution. (b) The regression line in the standard addition curve for the CFX tablet sample assessed in (a).

4.2.3.2 Robotic CFX voltammetry in the microtiter plate format:

Establishment, calibration measurements and sample analysis

The quality check for manual voltammetric CFX analysis was followed by a move to trials in the robotic mode. Figure 4.31(a) shows the outcome of the requisite stability test under the conditions of optimal CFX voltammetry. CFX DPVs were recorded at a stationary CNT-modified PLEs over a period of 2 h in a microtiter plate well containing 50 μM CFX at intervals of 10 min. The CFX peaks were seen at about 1.02 V vs. reference electrode as tiny signals that superimposed the anodic current curve for oxygen evolution Figure 4.31(b) is a plot of the extracted

CFX peak current as function of time and a reasonably stable response is confirmed. Apparently, a degradation of the drug analyte and/or a detrimental coverage of the CNT working electrode surface with reaction products of the electrochemical oxidation and related electrode fouling is not a problem, at least not within the 2 h time of inspection.

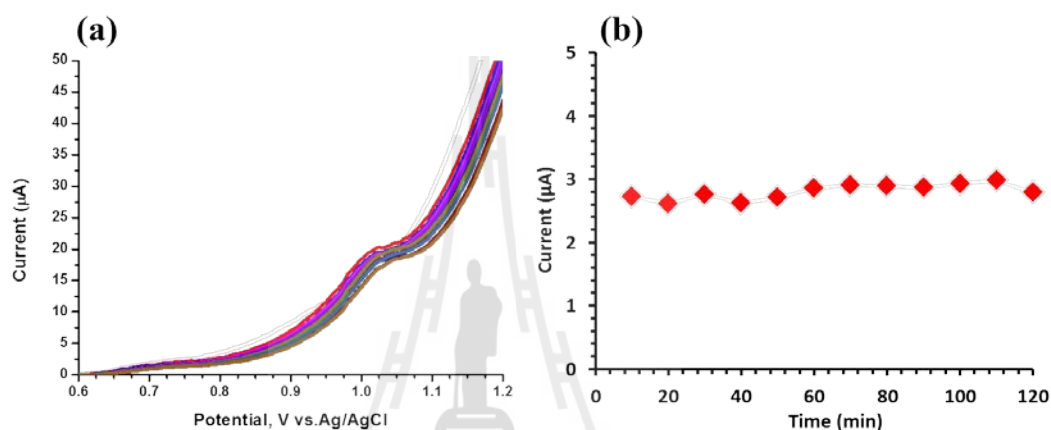


Figure 4.31 The electrochemical detection of 50 μM of the CFX in a microtiter plate well, with an electrode assembly incorporating a CNT-modified PLE (WE), an Ag/AgCl (RE) and a Pt spiral (CE). Supporting electrolyte was 0.1 M phosphate buffer (pH 4.0), the scan speed for DPV acquisition was 20 mVs^{-1} with other parameter as listed before for CFX DPV measurements. One DPV was recorded every 10 min for a period of 2 h.

In the robotic system, automated DPV was used to evaluate the response of the CNT-modified PLEs to ten CFX concentrations in the range of 2.0 to 100 μM . The microtiter plate load for the experiment is shown in Figure 4.32 while Figure 4.33(a) and (b) displays the collection of DPVs that were acquired in the automated plate run and the corresponding calibration curve, respectively. As

expected, the values of the CFX DPV peak currents, i_p^a , increased progressively with increasing concentration of the CFX. The linear range turned out to be about 2.0 to 100 μM , which is similar to the performance of the conventional manual CFX voltammetry. Robotic CFX voltammetry could thus in the further experiments be used for model and real sample analysis.

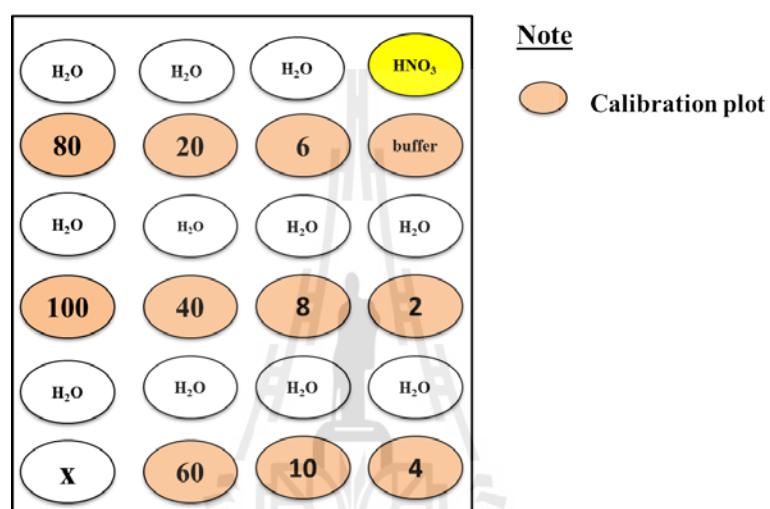


Figure 4.32 The microtiter plate load CFX calibration measurement. The numbers refer to concentrations of CFX in μM .

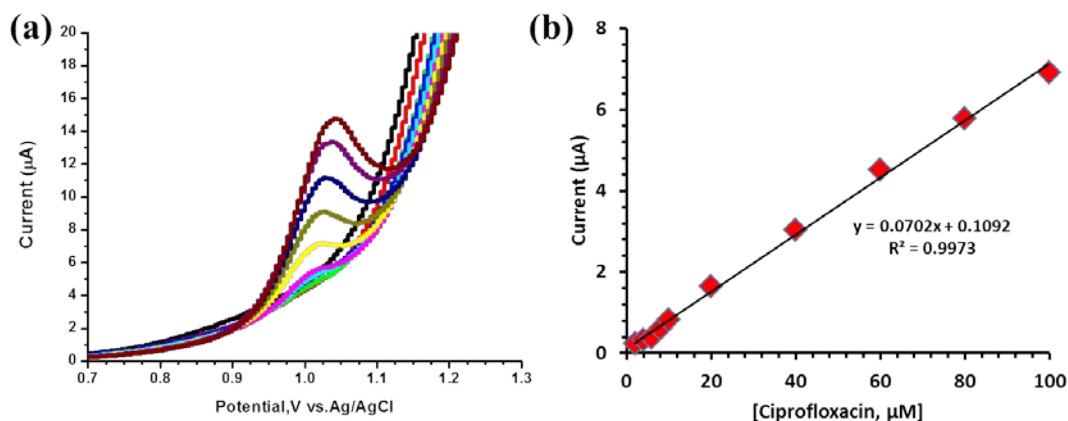


Figure 4.33 Robotic CFX calibration measurements in a 24-well microtiter plate format. 10 wells of the microtiter plate were filled. As shown in Figure 4.33 with analyte solutions of 2.0 to 100 μM and sequentially subjected by the system software to DPV measurements. Parameters for DPV acquisition were potential range: 0.3 - 1.3 V vs. reference, E_{step} : 5 mV, E_{pulse} : 50 mV, scan rate: 20 mV s^{-1} and t_{pulse} : 0.07 s.

Robotic microtiter plate voltammetry in the standard addition mode was then used to determine the CFX level in model and real samples with a four times repetition accomplished in one plate run, Figure 4.34 shows the load of a microtiter plate as designed for such a trial on spiked model sample solutions with an adjusted 10.0 μM of the target compound. Figure 4.35(a) then is displaying for one of the four loaded samples the DPVs in (1) the bare buffer, (2) the sample itself, and (3) the sample but with supplementations with known levels of NFX. Figure 4.35(b) is the translation of the measurement in Figure 4.35(a) into the typical analytical standard addition plot that allows sample analyte concentration via extrapolation of the regression line towards the x-axes or from the regression line equation. Worth mentioning that the completion of the robotic CFX DPV measurements in the

microtiter plate format took about 1 hours without any operator involvement. For the particular case presented in Figure 4.35(a) and (b), the analysis of the plot of peak currents vs. added CFX in part (b) revealed a determined CFX sample level of 9.92 μM . As the adjusted sample concentration was exactly 10.0 μM , the recovery rate for this measurement was thus 99.2%. For eight robotic determinations (2 plate runs with 4 samples each) of the 10.0 μM CFX model solution the average recovery rate for the analysis in the standard addition mode was 99.2% \pm 2.5% (see also Table 4.4).

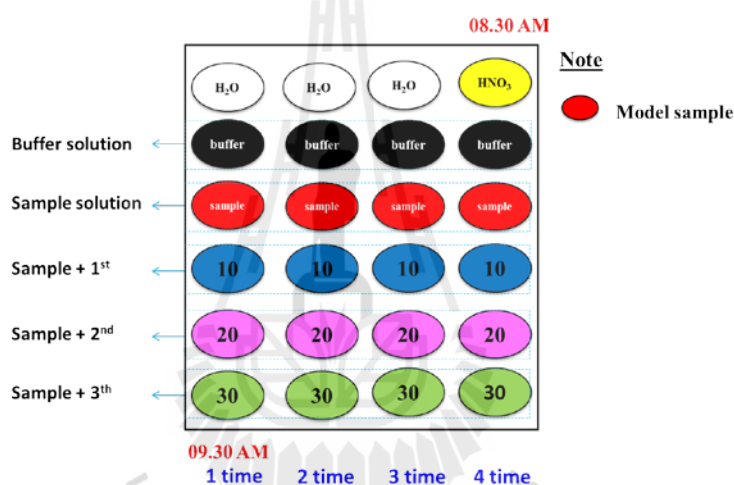


Figure 4.34 Schematic display of the load of a microtiter plate as used for the concentration determination of a model (spiked) sample solution with an adjusted CFX level of 10.0 μM . The load is designed for the application of the standard addition method for quantitative CFX analysis. The time of a complete robotic analytical run through all wells of the microtiter plate was usually about 1 h.

With a microtiter plate design similar to the one shown in Figure 4.34, also real sample CFX analysis was approached and again measurements were made for solutions of a commercial CFX tablets from a local pharmacy shop of

Thailand. The average obtained recovery rate was found to be $97.7\% \pm 3.3\%$ (see also Table 4.4). Apparently, DPV at CNT-modified PLEs was sensitive and reliable enough for the task of CFX quantification in aqueous solution of this species.

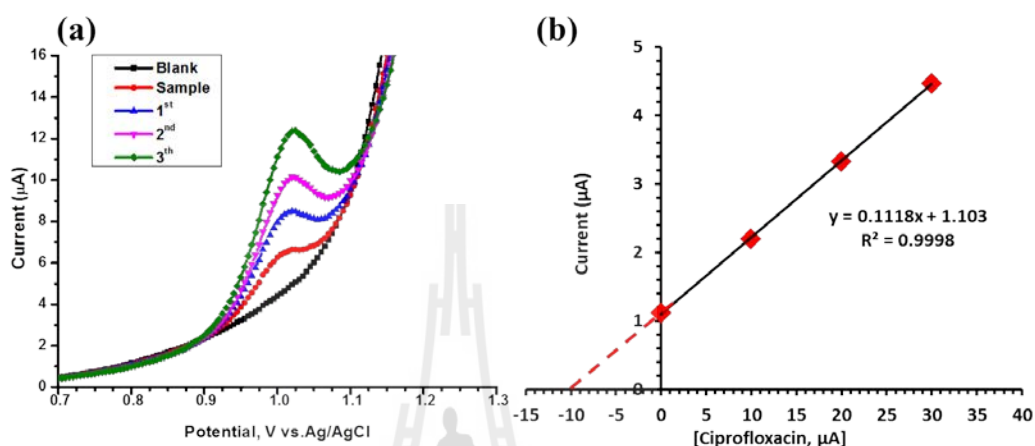


Figure 4.35 Microtiter plate-based quantification of CFX in spiked, $10.0 \mu\text{M}$, CFX model samples by the automated standard addition method with voltammetric detection. Measuring buffer was 0.1 M phosphate buffer/ 0.1 M KCl ($\text{pH } 4.0$). (a) A typical set of the CFX DPVs for the blank solution (black trace), the bare sample (red trace) and for sample with three sequential additions of small aliquots of a CFX stock solution. (b) Sample CFX quantification in the standard addition mode with the extrapolation of the linear regression line to the x axes and the utilization of the x-axes interception for sample concentration identification.

Figure 4.36(a) shows a representative set of automatically recorded DPVs as used for the quantification of CFX in tablet samples with a listed content of 500 mg/tablet via the standard addition method in the robotic electrochemical device. It was assumed that CFX was the main contributor to the

electrochemical signal. Typically the anodic peak for CFX oxidation occurred at about 0.95 V vs. Ag/AgCl reference electrode. Figure 4.36(b) show the standard addition plot corresponding to the measurement in (a) and the linear regression line through the data points ($R = 0.9989$). The extrapolation to the x axis, led in this specific case to a concentration of CFX in the tablet of 488.57 mg/tablets and with 500 mg/tablet listed on the tablet package the recovery rate here was 97.7%. Table 4.4 is a summary of the manual and robotic CFX assessments as obtained for replicate measurements ($n = 8$) and provides the average recovery rates as a performance parameter. In summary of the CFX part of this study it can be said that a sensitive voltammetric assay for this antibiotic has been achieved in form of DPV at CNT-modified PLE electrodes and an incorporation of these sensors into a microtiter plate-based robotic electrochemical workstation. The automated in-well CFX differential pulse voltammetry achieved a linear response between 2 to 100 μM and a detection limit of 1.6 μM NFX. Spiked CFX model samples and dissolved CFX tablet samples were well analyzed with the robotic drug voltammetry and results compared well with the ones from standard manual assessments in beaker-type electrochemical cells. As several samples can be processed automatically in a single analytical run through a loaded microtiter plate format the methodology is time-saving and convenient and expected to be useful for CFX quality control in the pharmaceutical industry.

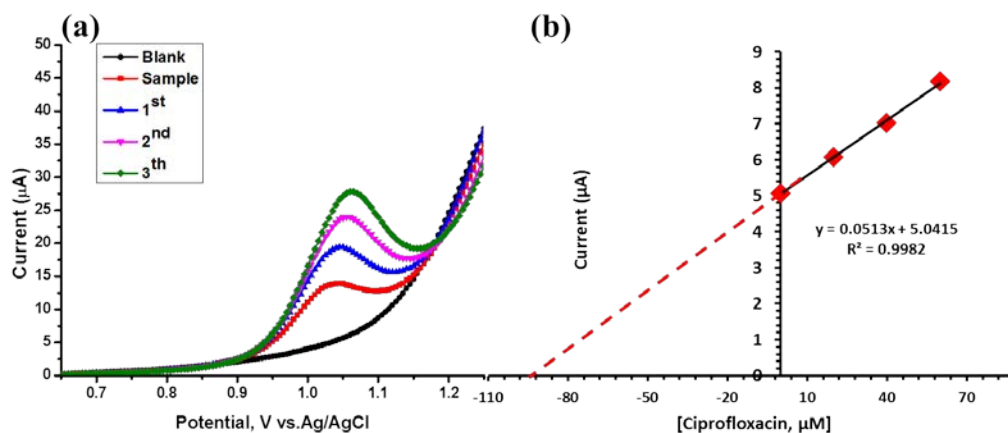


Figure 4.36 Microtiter plate-based quantification of CFX in commercial CFX tablet samples by the automated standard addition method with voltammetric detection. Measuring buffer was 0.1 M phosphate buffer/ 0.1 M KCl (pH 4.0). (a) A typical set of the CFX DPVs for the blank solution (black trace), the bare tablet sample (red trace) and for the tablet sample with three sequential additions of small aliquots of a CFX stock solution. (b) Tablet sample CFX quantification in the standard addition mode with the extrapolation of the linear regression line to the x axes and the utilization of the x-axes interception for sample concentration identification. Computation of the tablet content took the dilution factor for the sample preparation onto account.

Table 4.4 Ciprofloxacin (CFX) quantification in spiked model samples and in COBAY tablets (500 mg/tablet). Compared are results from manual beaker-type voltammetric measurements with the outcome of automated CFX voltammetry in microtiter plates.

Sample	Voltammetry				Recovery	
	Manual		Robotic		Manual	Robotic
	Added	Found	Added	Found		
Model sample test, μM	10.0	10.21 ± 0.24	10	9.92 ± 0.39	102.1 ± 0.17	99.2 ± 2.5
COBAY 500 (mg/tablet)	-	491.88 ± 1.41	-	488.57 ± 5.52	98.4 ± 1.6	97.7 ± 3.3

4.2.4 Work with respect to the target analyte PCT

4.2.4.1 Conventional PCT voltammetry tests, calibration measurements and sample analysis

As mentioned earlier, paracetamol (PCT; acetaminophen) is one of most commonly used analgesics and described for the reduction of fever and pain such as headache, backache, arthritis and postoperative or inflammatory pain. PCT has been demonstrated as electroactive (Miner, Rice, Riggins and Kissinger, 1981; Navarro, Gonzalez-Arjona, Roldan and Rueda, 1988; Lau, Luk, and Cheung, 1989; Bramwell, Cass, Gibbins and Green, 1990; Gilmarin, and Hart, 1994; Erdogdu and Karagozler and Zen and Ting, 1997; Wang et al., 2001; Ozkan, Uslu, and Aboul-Enein, 2003) and quite a number of voltammetric PCT studies at various electrode

materials have been reported (Tan et al., 2003) (Boopathi et al., 2004) (ShangGuan, et al., 2008) (Tungkananurak et al., 2005) (Jia, Zhang, Li and wang, 2007) (Fanjul-Bolado et al., 2007 and Nair et al., 2009) (Goyal et al., 2010) (Zidan et al., 2011). Here, CNT-modified PLE's were chosen as sensors for PCT determination in the robotic system and the following is a description of comparative manual (first) and then robotic electrochemical PCT analysis in a variety of samples. Based on the experience with CNT-enhanced AA, NFX and CFX electro-oxidation the expected advantage of the CNT modification was here a sensitivity improvement for the electroanalysis of the target molecule PCT. This effect would be similar to what was earlier observed by others with nanoparticle modified carbon electrodes and utilized for the voltammetric analysis of PCT in pharmaceutical and urine samples (Goyal et al., 2010). Representative CVs and DPVs for the faradaic reaction of 100 μ M PCT in 0.1 M KH_2PO_4 / 0.1 M KCl (pH 4.5) at bare PLE and CNT-modified PLEs working electrodes are shown in Figure 4.37. As for AA, NFX, and CFX the voltammetric PCT peaks were much better pronounced at the PLE working electrodes that had a thin layer of CNT on their surface with the peak potentials shifted positively to more cathodic values and the peak maxima increased. In particular useful for PCT electroanalysis was the about tenfold boost in the peak current in the DPV mode of detection and thus DPV was the method of choice for electrochemical PCT quantifications and the optimum parameters for PCT DPV were an E_{pulse} of 25 mV, E_{step} of 5 mV and t_{pulse} of 0.07 s.

Figure 4.38 shows a set of four DPV curves as typically obtained at the CNT-modified PLEs under optimum conditions for increasing concentration of PCT. A linear relationship became evident between the oxidation

peaks current (i_p^a) and concentration (c) of PCT in the range from about 5.0 to 150 μM . The linear range regression equation for the particular example shown in Figure 4.38 is $i_p^a = 5.9284c + 40.404$, $R = 0.9944$, where i_p^a is the anodic peak current (μA) and C is the PCT concentration (μM); the detection limit of PCT was found to be in the order of 1.5 μM .

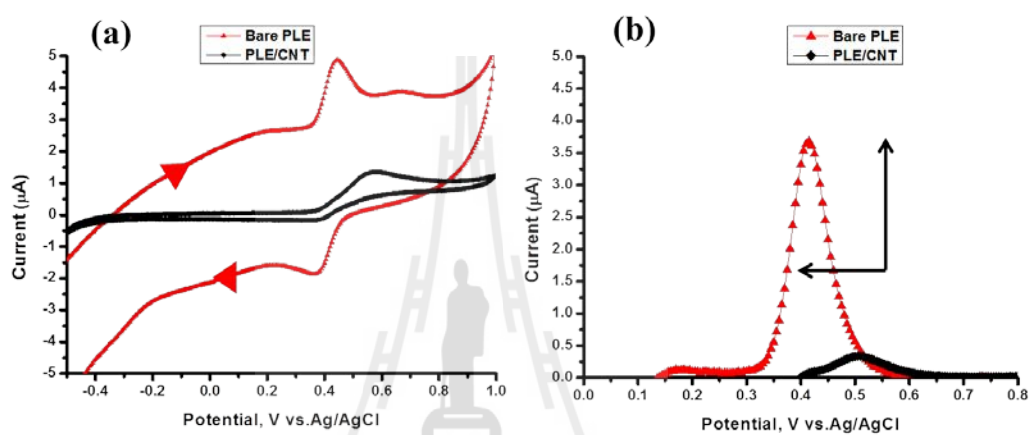


Figure 4.37 Comparison of CVs (a) and DPVs (b) of 100 μM PCT in 0.1 M KH_2PO_4 / 0.1 M KCl (pH 4.5) acquired with the bare (black curves) and CNT-modified PLEs (red curves). Potential was scanned from -0.1 to 1.0 V, and for the DPVs used were $E_{\text{step}} 5\text{mV}$, $E_{\text{pulse}} 25\text{mV}$, scan rate 20mVs^{-1} and $t_{\text{pulse}} 0.07\text{s}$.

After revealing a reasonable linearity through PCT calibration experiments, the standard addition method was successfully applied for the manual voltammetric quantification of PCT in beaker-type electrochemical cells. Figure 4.39 is displaying the outcome of a typical quantification of PCT in a spiked model sample with an adjusted 10 μM analyte. DPV was used in conjunction with the standard addition method for the recovery of the test concentration. Figure 4.39(a) actually provides the DPVs in the bare buffer, the PCT-spiked model sample, and the PCT

sample but with additional supplementations of known levels of PCT for standard addition establishment. Figure 4.39(b) is the display of the corresponding analytical standard addition plot that allows sample analyte concentration determination, for instance, via x axes extrapolation of the regression line. For the particular case presented in Figure 4.39(a) and (b), the analysis of the plot of peak currents vs. added PCT in part Figure 4.39(b) revealed a determined PCT sample level of 10.66 μM . With the adjusted level of 10 μM PCT in mind, the determined level corresponds to a recovery rate of 106.6%. For replace by number value repetitive determinations the average recovery rate for the PCT analysis in the manual standard addition mode was 106.6% \pm 6.6% (see also Table 4.5) A similar quality of analysis was obtained when measuring with the same manual approach samples originating from the dissolution of commercial PCT tablets with a content of 500 mg/tablet; for this situation the original DPV data and the standard addition plot are shown in Figure 4.40. In this case, the average recovery rate was found to be 94.3% \pm 5.7% (see also Table 4.5). Apparently, beaker-type measurement DPV at CNT-modified PLEs was DPV data and the standard addition plot are shown in Figure 4.40. In this case, the average recovery rate was found to be 94.3% \pm 5.7% (see also Table 4.5). Apparently, beaker-type measurement DPV at CNT-modified PLEs was sensitive and reliable enough for the task of PCT quantification in aqueous solution of this species and was related to a good average assay recovery rate.

Voltammetric PCT quantifications in the conventional beaker-type configuration were followed by a transfer of the methodology into the available robotic electrochemical device of the already mentioned design for automation of the procedure.

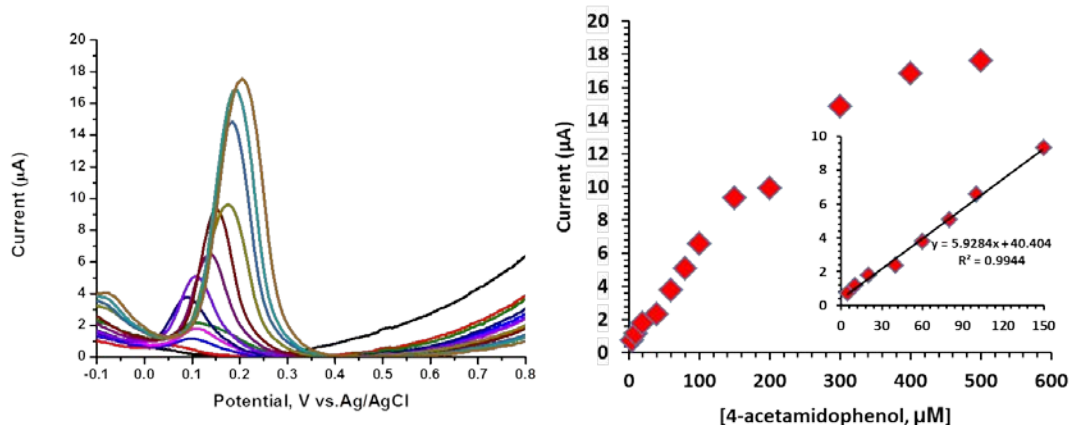


Figure 4.38 (a) DPVs for increasing concentrations of PCT in 0.1 M $\text{KH}_2\text{PO}_4/0.1$ M KCl (pH 4.5). (b) The calibration curve extracted from the measurements in (a) with a linear range from about 5.0 to 150 μM ; DPV recording conditions: Potential scanned from -0.1 - 1.0 V, E_{step} 5mV, E_{pulse} 25mV, scan rate 20mV/s, t_{pulse} 0.07 s.

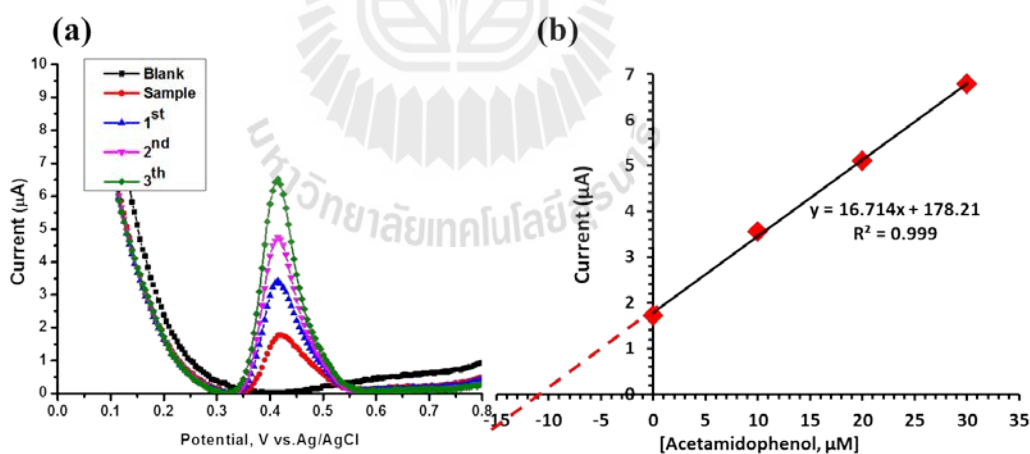


Figure 4.39 Quantification of PCT in spiked model samples by manually performed DPV in the standard addition mode. Adjusted PCT concentration of the sample was 10.0 μM and the supporting electrolyte was 0.1 M $\text{KH}_2\text{PO}_4/0.1$ M KCl (pH 4.5). (a) The acquired DPV collection and (b) the linear regression plot that made available sample PCT level computation.

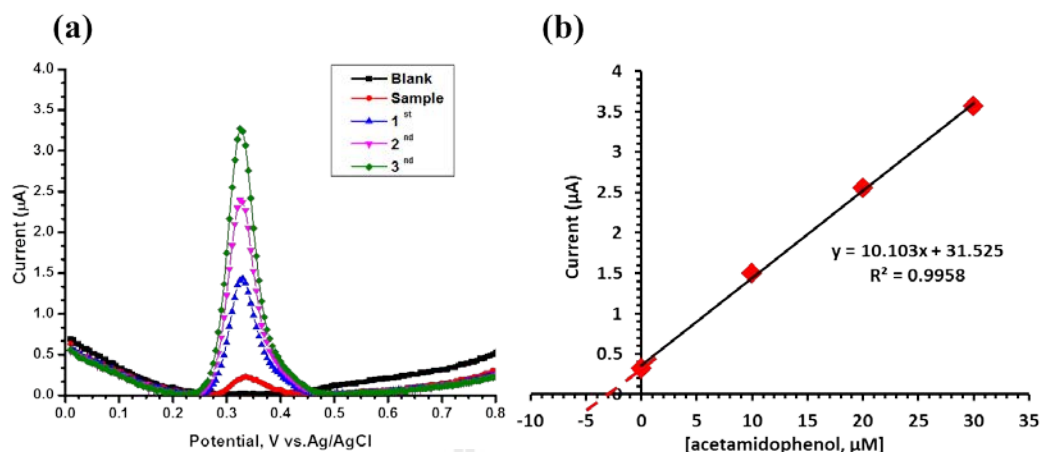


Figure 4.40 Quantification of PCT a dissolved tablet sample by manually performed DPV in the standard addition mode. Reported PCT concentration on the package was 500 mg/tablet. The supporting electrolyte for the measurements was 0.1 M $\text{KH}_2\text{PO}_4/0.1$ M KCl (pH 4.5). (a) The acquired DPV collection and (b) the linear regression plot that made available sample PCT level computation.

4.2.4.2 Robotic PCT voltammetry in the microtiter plate format:

Establishment, calibration measurements and sample analysis

Figure 4.41(a) shows the outcome of the requisite stability test under the conditions of optimal PCT voltammetry. PCT DPVs were recorded at a stationary CNT-modified PLEs during over a period of 1 h, with the voltammetric trial executed at intervals of 10 min in a microtiter plate well containing 20 μM PCT. Reproducibly the PCT DPVs appeared as well bell-shaped I/E curves with a reasonably symmetrical peak current at about 0.25 V vs. reference electrode. Figure 4.41(b) is a plot of the extracted PCT peak current as function of time and a reasonably stable response is confirmed. Apparently, a degradation of the PCT drug

analyte and/or a detrimental coverage of the CNT working electrode surface with reaction products of the electrochemical PCT oxidation and related electrode fouling was not turning up as a problem, at least over within the 1 h of inspection.

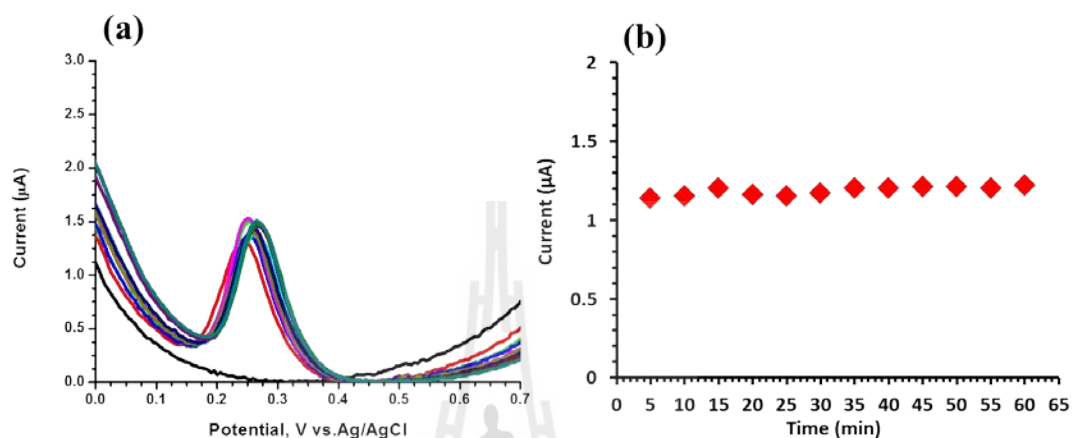


Figure 4.41 Response stability test for PCT voltammetry. The electrochemical detection of 20 µM of PCT in a microtiter plate wells, with an electrode assembly incorporating a CNT-modified PLE (WE), an Ag/AgCl (RE) and a Pt spiral (CE). One DPV was recorded every 5 min for a period of 1 h. The supporting electrolyte for the measurements was 0.1 M KH_2PO_4 /0.1 M KCl (pH 4.5) and the DPV parameter set as listed before.

In the robotic system, automated DPV was used evaluate the response of the CNT-modified PLEs to eight PCT concentrations in the range of 5.0 to 150 µM. The microtiter plate load for the experiment was shown in Figure 4.42 while Figures 4.43(a) (b) displayed the collection of DPVs that were acquired in the automated plate run and the corresponding calibration curve, respectively. As expected from the experience with the manual PCT trials, the values of the PCT DPV

peak currents, i_p^a , in the automatically recorded voltammograms increased progressively with increasing concentration of the PCT. The linear range turned out to be about 5.0 to 150 μM , which is similar to the achievement of the conventional manual PCT voltammetry. Robotic PCT voltammetry could thus in the further experiments be used for quantitative model and real sample analysis.

The microtiter plate load as used for PCT quantification via robotic voltammetry in the standard addition mode is shown in Figure 4.44. Usually (i) 4.0 M HNO_3 was in well #1 for the pretreatment, (ii) water in the three other top wells for the electrode cleaning, (iii) four samples in the four wells of the third row, and (iv) three additionally spiked solutions in the remaining wells of rows four, five and six.

Figure 4.45 then is displaying for one of the four loaded PCT model samples the DPVs in (1) the bare buffer, (2) the sample itself, and (3) the sample but the supplementations with known levels of PCT. Figure 4.45(b) is the translation of the measurement in Figure 4.45(a) into the typical analytical standard addition plot that allows sample analyte concentration via extrapolation of the regression line towards the x-axis or from the regression line equation. Worth mentioning that the completion of the robotic PCT DPV measurements in the microtiter plate format took about 40 minutes for one plate with four replicate samples without any operator involvement

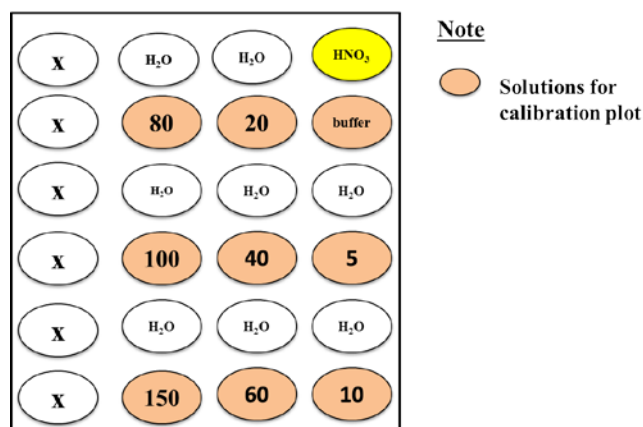


Figure 4.42 The microtiter plate load as used for robotic electrochemical PCT calibration measurement.

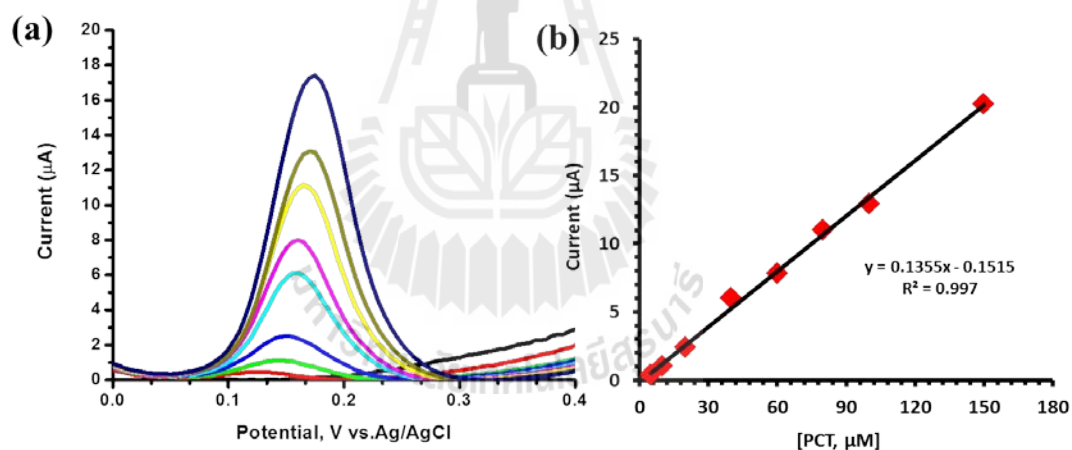


Figure 4.43 Robotic PCT calibration measurements via 24-well microtiter plate voltammetry. Shown 10 DPVs (a) are that were acquired in wells of the microtiter plate with PCT analyte solution of 5.0 to 150 μM levels. (b) Shows the linear calibration plot as extracted from the displayed voltammograms in (a). Recording conditions: Potential scan range: $-0.1 - 1.0$ V vs. reference, E_{step} : 5 mV, E_{pulse} : 50 mV, scan rate: 20 mV s^{-1} and t_{pulse} : 0.07 s.

For the particular case presented in Figure 4.45(a) and b, the analysis of the plot of peak currents vs. adjusted PCT level, in part Figure 4.45(b) revealed a determined PCT sample level of 10.42 μM . As the adjusted sample concentration was exactly 10.0 μM , the recovery rate for this measurement appeared as 104.2%. For eight robotic determinations (2 plate runs with 4 samples each) of the 10.0 μM PCT model solution the average recovery rate for the analysis in the standard addition mode was 104.2% \pm 4.2% (see also Table 4.5).

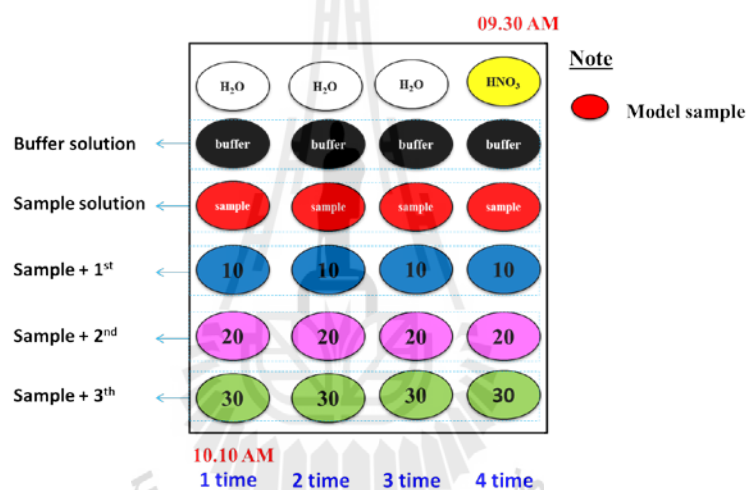


Figure 4.44 The microtiter plate load as used for robotic electrochemical PCT determination with automated standard addition method in charge of quantification. A full run took about 40 min.

The robotic PCT voltammetry procedure was also applied to real sample analysis and measurements were made with solutions of a commercial PCT tablet from a local pharmacy shop and with urine samples of a volunteer consuming a drug dose. For all trials of this kind the microtiter plate had (i) 4.0 M HNO₃ in well #1 for the pretreatment, (ii) water in well #7, 13 and 19 for the

electrode cleaning, (iii) measuring electrolyte (0.1 M KH_2PO_4 /0.1 M KCl, pH 4.5) in well #2, 8, 14 and 20 for base line according, (iv) sample solutions in well #3, 9, 15 and 21, and (v) samples plus suitable supplement of a PCT stock solution as requisite for the acquisition of the standard addition curve (step-wise increase in PCT concentration was 10, 20 and 30 μM for tablet samples and 20, 40 and 60 μM for urine samples) in well #4-6, 10-12, 16-18 and 22-24. A schematic of the load is shown in Figure 4.46.

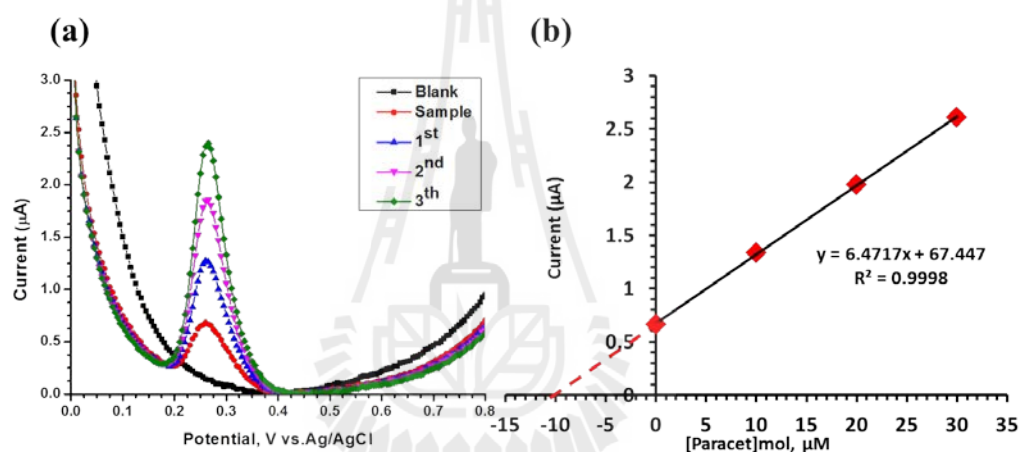


Figure 4.45 Robotic voltammetric quantification of PCT in microtiter plate wells and using the strategy of standard addition method for final computation. (a) One of the four model samples PCT, DPVs acquired in an automated run through a loaded microtiter plate. (b) Standard addition assessment of the adjusted PCT concentration.

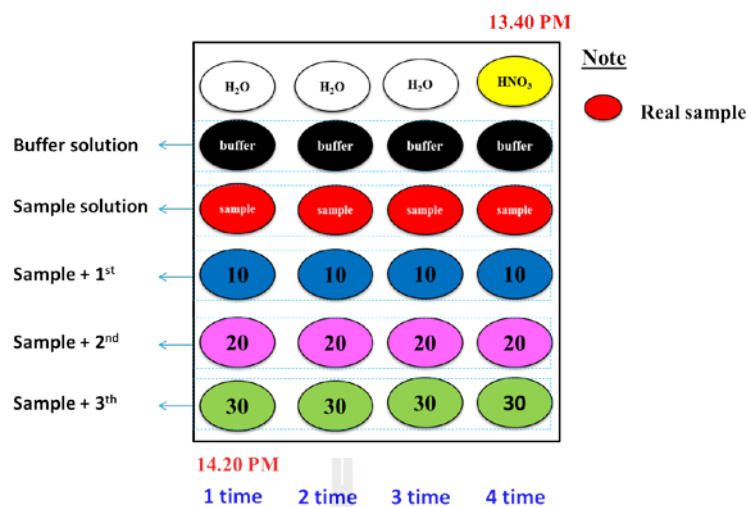


Figure 4.46 Microtiter plate load as used for PCT determination in tablet sample solutions via robotic DPV and the standard addition method (n=4). The time for completion of one analytical plate run was about 40 min.

Figure 4.47(a) is displaying for one of four loaded PCT tablet samples the DPVs in (1) the bare buffer, (2) the sample itself, and (3) the sample but with the supplementations of known levels of PCT. Figure 4.47(b) is then the translation of the measurement in Figure 4.47(a) into the typical analytical standard addition plot that allows sample PCT quantification via extrapolation of the regression line towards the x-axis or from the regression line equation. Worth mentioning that the completion of the robotic PCT DPV measurements in the microtiter plate format took about 40 minutes for four samples without any personal participation. For the particular case presented in Figures 4.47(a) (b), the analysis of the plot of peak currents vs. added PCT in part Figure 4.47(b) revealed a determined PCT sample level of 16.49 μM , which, taking dilution factors for sample preparation via tablet dissolution into account, equaled an amount of 498.49 mg PCT for a tablet. As the

listed PCT content of a tablet was exactly 500 mg, the recovery rate for this assessment was 97.7%. For eight robotic tablet content determinations (2 plate runs with 4 samples each, $n=8$) the average recovery rate for the analysis in the standard addition mode was found to be $97.7\% \pm 0.3\%$ (see also Table 4.5).

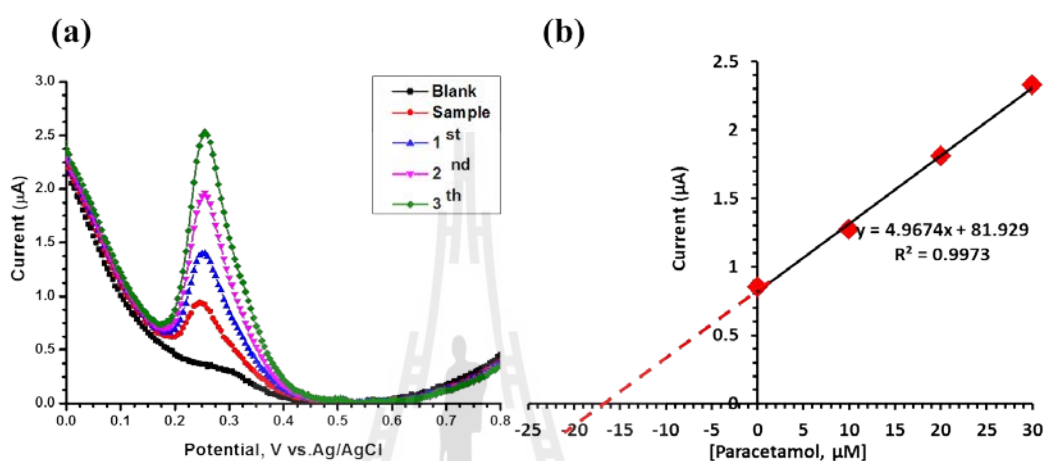


Figure 4.47 Robotic voltammetric PCT level assessment of tablet samples in microtiter plate format with the standard addition method employed as analysis approach. (a) One representative example of the four sample analyte DPVs acquired in an automated run through a loaded microtiter plate. (b) Standard addition curve extracted from the measurement shown in (a).

Finally, the robotic PCT voltammetry assay was applied to the determination of the analyte in the urine of a volunteer that had eaten 2 Tylenol tablets (= 1000 mg PCT) obtained from a local pharmacy shop. In the literature, the onset of analgesic action is reported to take place approximately 11 minutes after oral administration of PCT, maximum effective body drug level is reached after 40-60 minutes, and substantial clearance happens already after about 3-4 hours, depending

of curves on body weight and metabolic condition (Tylenol[®] professional product information, 2010) Here, urine samples were taken from the volunteer before drug uptake (t_0), and then 45 (t_{45}) and 240 (t_{240}) minutes after drug uptake, respectively. Figure 4.48 is a comparison of the DPVs of the different samples and demonstrates that there is virtually no measurable PCT in the “ t_0 ” urine sample. Drug consumption led then to body uptake and internalization and in accordance to the expected appearance of the usual PCT peak in the “ t_{45} ” sample The PCT peak was found to be significantly suppressed in the “ t_{240} ” sample, indicating the onset of body clearance and decrease in free PCT level.

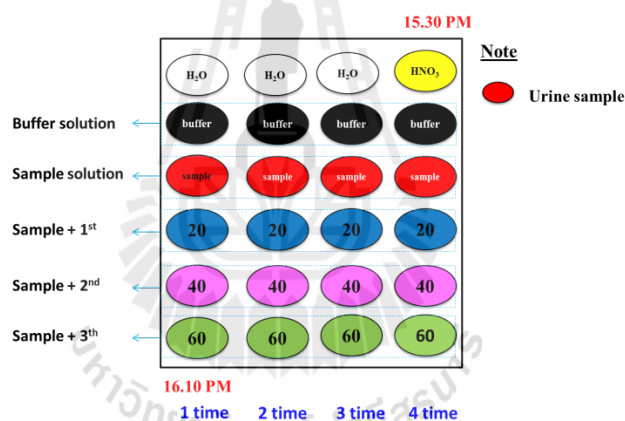


Figure 4.48 The microtiter plate load as used for robotic electrochemical PCT determinations in urine samples with automated standard addition method in charge of quantification. A full analytical plate run took about 40 min.

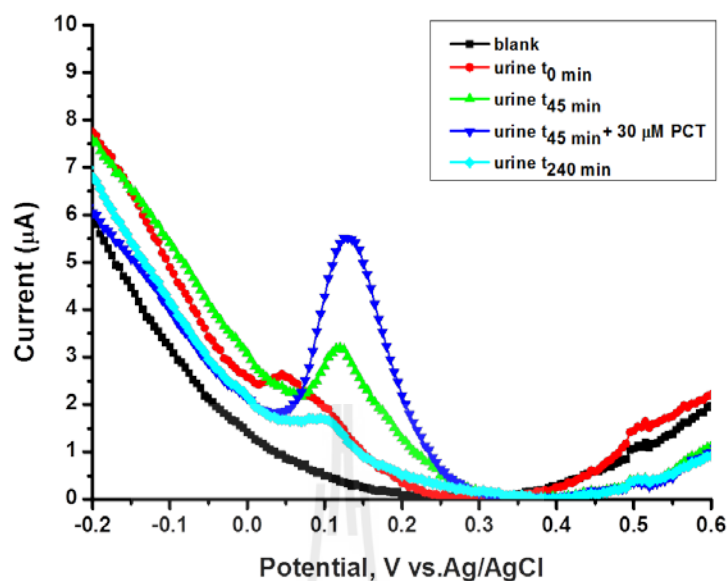


Figure 4.49 PCT DPVs acquired in different urine samples before and after uptake of a 1000 mg dose of PCT through tablet consumption. t_0 , t_{45} and t_{240} (minutes) refer to urine samples taken before and 45 and 240 min after uptake, respectively.

Figure 4.49 is displaying the microtiter plate load for the analysis of the PCT content of urine. Figure 4.50(a) is showing for one of the four loaded urine samples the DPVs in (1) the bare buffer, (2) the sample itself, and (3) the sample but the supplementations with known levels of PCT. Figure 4.50(b) is then the translation of the measurement in Figure 4.50(a) into the typical analytical standard addition plot that allows sample PCT quantification via extrapolation of the regression line towards the x-axis or from the regression line equation. For the particular case presented in Figures 4.50(a) (b), the analysis of the plot of peak currents vs. added PCT in part 4.50(b) revealed a determined PCT urine level in the “ t_{45} ” sample of

31.38 mg/L. For eight robotic urine PCT content determinations (2 plate runs with 4 samples each). The average computed level of recovers was found to be $90.0\% \pm 2.5\%$ (see also Table 4.5). In literature 35 mg/L have been mentioned for the sensor experimental condition (Tylenol[®] professional product information, 2010), which compares well with the value obtained in this study.

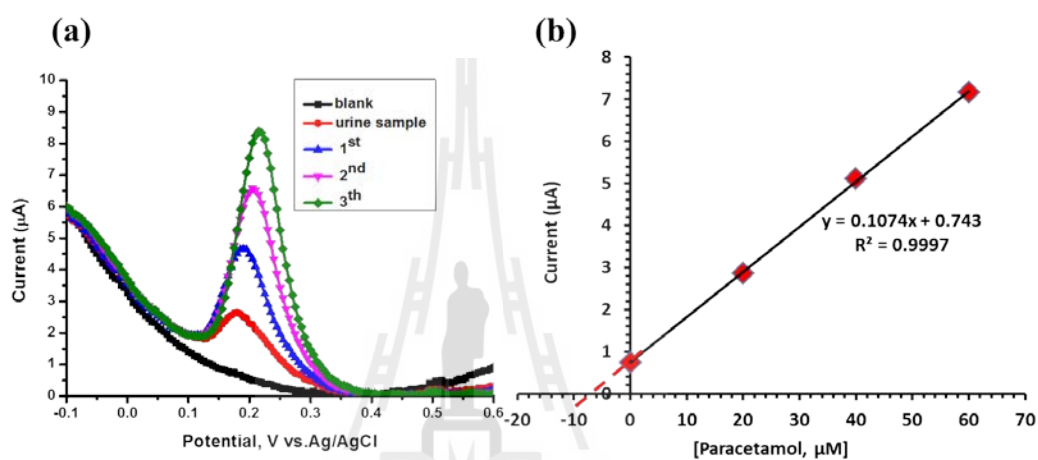


Figure 4.50 Robotic voltammetric urine PCT level assessment in microtiter plate format with standard addition method. (a) One representative example of the three sets of sample analyte DPVs acquired in an automated run through a loaded microtiter plate. (b) Standard addition curve extracted from the measurement shown in (a).

To summarize this part of the thesis a sensitive voltammetric PCT assay was successfully incorporated into the microtiter plate-based robotic electrochemical workstation. With the system measurements of the target analyte could be accomplished in automated manner with a linear response between 5.0 to 150.0 μM and a detection limit of 1.6 μM PCT. This analytical performance compared well to the one of manual voltammetric PCT quantification in beaker-type

electrochemical cells. The developed novel methodology produced accurate assessments of the PCT content of commercial PCT tablets and also led to meaningful results on a urine sample from a volunteer with PCT ingestion. Associated with the opportunity of a convenient multi sample handling the developed robotic PCT electroanalysis could be a useful complementary analytical option for clinical laboratories that are on routine basis in the need of many PCT sample assessments.

Table 4.5 Paracetamol (PCT) quantification in spiked model samples, dissolved Tylenol tablet samples, and in urine samples after tablet intake. Compared are results from manual beaker-type voltammetric PCT measurements with the outcome of automated PCT voltammetry in microtiter plates.

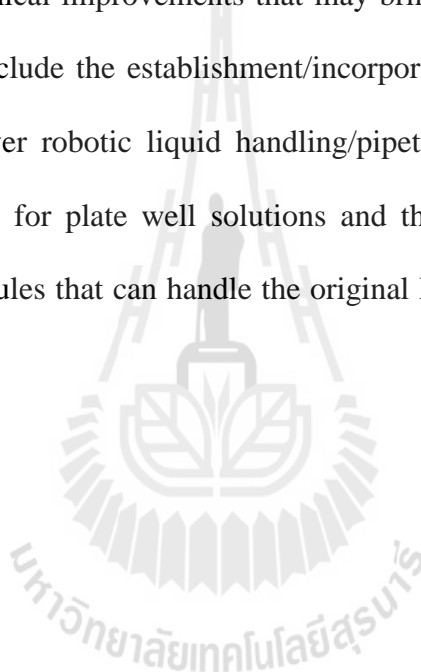
Sample	Voltammetry				Recovery	
	Manual		Robotic		Manual	Robotic
	Added	Found	Added	Found		
Model sample test, μM	10.0	10.66 ± 0.2	10.0	10.42 ± 1.2	102.1 ± 0.17	104.2 ± 4.2
Tylenol 500 (mg/tablet)	-	471.30 ± 0.7	-	498.49 ± 0.55	97.7 ± 0.3	97.7 ± 0.3
Urine sample ($t_{45 \text{ min}}$), mg/L	-	-	-	31.38 ± 0.20	-	90.0 ± 2.5

CHAPTER V

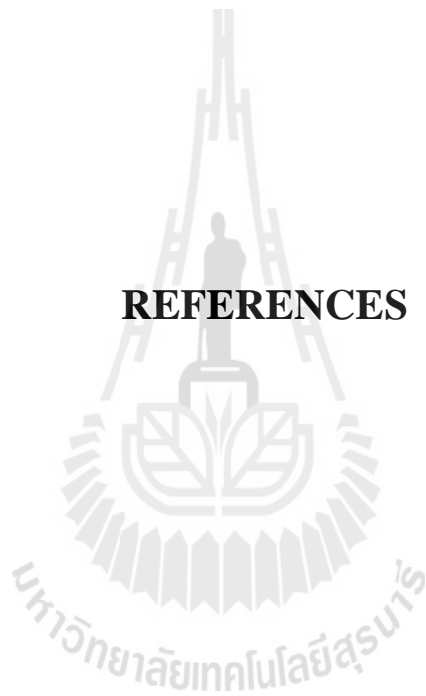
CONCLUSIONS AND OUTLOOK

Sensitive differential pulse voltammetry of an antioxidant (AA), two antibiotics (NFX and CFX) and of an analgesic (PCT) has been successfully incorporated into a microtiter plate-based robotic electrochemical workstation for automated analyte quantification. Measurement of the target analyte used a suitably sized movable three electrode assembly with properly adjusted sensing properties. For all analytes a modification of the working electrode with an electrocatalytic carbon nanotube thin film was identified as essential for reaching good enough sensitivity of the voltammetric assay for low level analyte detection. In-well DPV achieved a linear response up to 10 mM (AA), 10 μ M (NFX), 100 μ M (CFX) and 150 μ M (PCT) and a detection limit of 0.05 mM (AA), 0.3 μ M (NFX), 1.6 μ M (CFX) and 1.56 μ M (PCT), respectively. Apparently, the calibration and the standard addition method worked equally well for analyte quantification via the automated voltammetry and delivered a reasonable accuracy and good recovery rates for measurements on model samples, dissolved tablet samples, and real samples such as urine of drug consumers. Definite strength of the developed methodology is that with reasonably cheap and easy to use instrumentation it can work off multiple samples automatically in a single microtiter plate run. Trials are convenient and do not need a personal operator involvement once the microtiter plate is placed and the device started. Benefits are cost- and time saving

as well as a release of usually well trained and thus expensive laboratory personnel to other duties. It is therefore assumed that robotic electrochemical drug analysis in a microtiter plate format is a good complementary option for all laboratories that face the task of handling large drug sample libraries, which is particularly true for the pharmaceutical business but also a reality in the clinical laboratories of hospitals and environmental laboratories dealing with drug pollution of water, soil, plant and food samples. Further technical improvements that may bring robotic drug electroanalysis to highest standard include the establishment/incorporation of automated microtiter-plate loading via clever robotic liquid handling/pipetting, the implementation of a stirring/heating option for plate well solutions and the automatic data analysis via adapted software modules that can handle the original DPV recordings in appropriate way.



REFERENCES



REFERENCES

- Abbas, M. N. and Radwan, A. A. (2008). Novel lipoate-selective membrane sensor for the flow injection determination of α -lipoic pharmaceutical preparation and urine. **Talanta**. (74): 1113-1121.
- Ad-el-Maali, N. (2004). Voltammetric analysis of drug. **Bioelectrochemistry**. 1(64): 99-107.
- Bagotsky, V. S. (2006). **Fundamentals of electrochemistry**. 2nded. New York: John Wiley & Sons, Inc. p 388.
- Banks, CE. And Compton, RG. (2006). New electrodes for old: from carbon nanotubes to edge plane pyrolytic. **Analyst**, 131(1): 15-21.
- Bard, A. and Faulkner, L. (2001). **Electrochemical methods: Fundamentals and applications**. 2nd ed. New York: John Willey & Sons, Inc. pp 261-301.
- Belal, F., Al-Majed, A. A. and Al-Obaic, A. M. (1999). Method of analysis of 4-quinilone antibacterials. **Talanta**. (50): 765-786.
- Blum, D., Leyffer, W. and Holze, R. (1996). Pencil-leads as new electrodes for abrasive stripping voltammetry. **Electrochem**. 3(8): 296-297.
- Boccacini, A. R., Cho, J., Roether, A. A., Thomas, B. J. C., Minay, E. J. and Shaffer, F. S. P. (2006). Electrophoretic deposition of carbon nanotubes. **CARBON**. (44): 3149-3160.
- Boonsong, K., Chuanuwatanakul, S., Wangfuengkanakul, N. and Chailapakul, O. (2005). Electroanalysis of lincomycin using boron-doped diamond thin film electrode applied to flow injection system. **Sens. Actuators. B**. 108: 627-632.
- Boopathin, M., Won, M-S. and Shim, Y. (2004). A sensor for acetaminophen in a blood

- medium using a Cu(II)-conducting polymer complex modified electrode. **Anal. Chim. Acta.** 512: 191-197.
- Bokros, J. C. (1977). Carbon biomedical devices. **CARBON**, (15): 353-371.
- Bramwell, H., Cass, A.E.G., Gibbs, P. N. B. and Green, M. J. (1990) Method for Determining Paracetamol in Whole Blood by Chronoamperometry following Enzymatic Hydrolysis, **Analyst.** (115): 185-188.
- Campbell, J.K., Sun, L. and Crooks, R.M. (1999). Electrochemistry using single carbon nanotubes. **J. Am. Chem. Soc.** 121(15): 3779-3780.
- Campos Prado Tavares, P. H. and Sanches Barbeira, P. J. (2008). Influence of pencil lead hardness on voltammetric response of graphite reinforcement carbon electrodes. **Appl. Electrochem.** 6(38): 827-832.
- Chang, E. E., Hsu, T.-J., Kao, W. Y. and Yang, C. C. (1982). Study on the ion-exchange chromatographic separation of L-ascorbic acid and oxalic acid. **Chinese Chem. Soc.** 29: 93-98.
- Chauhan, N., Narang, J. and Pundir, C. S. (2011). Fabrication of multiwalled carbon nanotubes/polyaniline modified Au electrode for ascorbic determination. **Analyst.** 136(9): 1938-1945.
- Crespo, G., Macho, S., Bobacka, J. and Rius, F. X. (2009). Transduction mechanism of carbon nanotubes in solid-contact ion-selective electrodes. **Anal. Chem.** (81): 676-681.
- Csöregi, E., Gorton, L. and Marko-Varga, G. (1993). Carbon fibres as electrode materials for the construction of peroxidase-modified amperometric biosensors. **Anal. Chim. Acta.** 273: 59-70.
- Demetriades, D., Economou, A. and Voulgaropoulos, A. (2004). A study of pencil-lead

bismuth-film electrodes for the determination of trace metals by anodic stripping voltammetry. **Anal. Chim. Acta.** (519): 167-172.

Devaraj, M. Deivasigamani, R. K. and Jeyadevan, S. (2013). Enhancement of the electrochemical behavior of CuO nanoleaves on MWCNTs/GC composite film modified electrode for the determination of norfloxacin. **Biointerfaces.** (122): 554-561.

Dominguez, R. O., Alonso-Lomillo, M. A. and Arcos Martinez, M. J. (2007). Recent developments in the field of screen-printed electrodes and their related applications. **Talanta.** 2(73): 202-219.

Erdogdu, G. and Karagozler, A. E. (1997) Investigation and Comparison of the Electrochemical Behavior of Some Organic and Biological Molecules at Various Conducting Polymer Electrodes, **Talanta.** 44: 2011-2018.

Erichsen, T., Reiter, S., Ryabova, V., Bonsen, E. and Schuhmanna, W. (2005). Combinatorial microelectrochemistry development an evaluation of an electrochemical robotic system. **Rev. Sci. Instrum.** 76: 062204-11.

Esseghaire, C., Helali, S., Fredj, H. B., Tlili, A. and Abdelghani, A. (2008). Polypyrrole-neutravidin layer for impedimetric biosensor. **Sens. Actuators. B.** (131): 584-589.

Fanjul-Bolado, P., Lamas-Ardiasana, P. J., Hernandez-Santos, D. and Costa-Garcia, A. (2009). Electrochemical study and flow injection analysis of paracetamol in pharmaceutical formulations based on screen-print electrode and carbon nanoyubes. **Anal. Chim. Acta.** 638: 133-138.

Fawzi, A., Yazbi, E., Hammund, H. H. and Assi, A. A. (2006). Derivative-ratio spectrophotometric method for the determination of ternary mixture of aspirin, paracetamol and salicylic acid. **Spectrochem. Acta A.** (68): 275-278.

- Fotouhi, L. and Alahyari, M. (2010). Electrochemical behavior and analytical application of ciprofloxacin using a multiwall carbon nanotube composite film-glassy carbon electrode. **Biointerfaces**. 1(81): 110-114.
- Fu, G-r., Hu, Z-a., Xie, L-j., Jin, X-q., Xie, Y-l., Wang, Y-x., Zhang, Z-y., Yang, Y-y. and Wu, H-y. (2009). Electrodeposition of nickel hydroxide films on nickel foil and its electrochemical performances for supercapacitor. **Electrochem. Sci.** (4): 1052-1062.
- Gabrielli, C. (1995). **Physical electrochemistry: Principles, methods and application monographs in electroanalytical chemistry and electrochemistry**. Israel Rubinstein. New York: Marcel Dekker, Inc. pp 249-297.
- Gamry instruments. (2010). **Application note: Basic of electrochemical impedance spectroscopy**. USA Warminster. Gamry instruments, Inc. pp 1-13.
- Ghoneim, M., M., Radi, A. and Beltagi, A. M. (2000). Determination of norfloxacin by square-wave adsorptive voltammetry on a glassy carbon electrode. **JPBA**. 25: 205-219.
- Gilmartin, M. A. T. and Hart, J. P. (1994) Rapid detection of paracetamol using a disposable, surface-modified screen-printed carbon electrode, **Analyst**. (119): 2431-437.
- Goyal, R. N., Gupa, V. K. and Chatterjee, S. (2010). Voltammetric biosensor determination of paracetamol at carbon nanotube modified pyrolytic graphite electrode. **Sens. Actuators. B**. 149: 252-258.
- Goyal, R. N. and Singh, S. P. (2006). Voltammetric determination of paracetamol at C₆₀-modified glassy carbon electrode. **Electrochim. Acta**. 51: 3008-3012.
- Guldi, GM., Rahman, GM., Sgobba, V. and Ehli, C. (2006). Multifunctional molecular

- carbon materials from fullerenes to carbon nanotubes. **Chem. Soc. Rev.** 35(5): 471-487.
- Gupta, V. K., Jain, A. K. and Shoorra, S. K. (2013). Multiwall carbon nanotube modified glassy carbon electrode as voltammetric sensor for the simultaneous determination of ascorbic acid and caffeine. **Electrochim. Acta**, (93): 248-253.
- Hardy and Paul, A. J. (1997). **Chronic pain management: The essentials**. UK: Gloucestershire Royal Hospital, Inc. pp 1-10.
- Hecht, DS., Hu, L. and Irvin, G. (2011). Emerging transparent electrodes based on thin films of carbon nanotubes grapheme and metallic nanostructures. **Sci. Adv. Mater.** 13(23): 1482-1513.
- Hoffer, A. (1989). The discovery of vitamin C. **JOM**. (4): 24-26.
- Huang, M-Z., Shentu, J-Z., Chen, J-C., Liu, J. and Zhou, H-I. (2008). Determination of risperidone in human plasma by HPLC MS/MS and its application to a pharmacokinetic study in chines volunteers. **JZUS**. 9(2):114-120.
- Huang, K. J., Liu, X., Xie, W. Z. and Yuan, H. X. (2008). Electrochemical behavior and voltammetric determination of norfloxacin at glassy carbon electrode modified with multi walled carbon nanotubes/Nafion. **Colloids Surf. B**. (64): 269-274.
- Huffman, HL. and Venton, B. J. (2009). Carbon-fiber microelectrodes for in vivo applications. **Analyst**. 1(134): 18-24.
- Intarakamhang, S. and Schulte, A. (2012). Automated electrochemical free radical scavenger screening dietary samples. **Anal. Chem.** (84): 6767-6774.
- Intarakamhang, S., Leson, C., Schuhmann, W. and Schulte, A. (2011). A novel automated electrochemical ascorbic acid assay in the 24-well microtiter plate format. **Anal. Chim. Acta**. (687): 1-6.

- Intarakamhang, S. Schuhmann, W. and Schulte, A. (2013). Robotic heavy metal anodic stripping voltammetry: ease and efficacy for trace lead and cadmium electroanalysis. *J. Solid State Electrochem.* DOI 10. 1007/s 10008-013-2018-2: 1-8.
- Jaber, A. M. Y. and Lounici, A. (1994). Polarographic behavior and determination of norfloxacin in tablets. *Anal. Chim. Acta.* 291(1-2): 53-64.
- Jacobs, CB., Peairs, MJ. And Venton, BJ. (2010). Carbon nanotube based electrochemical sensor for biomolecules. *Anal. Chim Acta.* 662(2): 105-27.
- Jia, L., Zhang, X. -H., Li, Q. and Wang, S. -F. (2007). Determination of acetaminophene by square voltammetry at a gold electrode by 4-amino-2-mercaptopyrimidine self-assemble monolayers. *Anal. Chem.* (62): 266-269.
- Kauffmann, J-M. and Vire, J-C. (1993). Pharmaceutical and biomedical applications of electrophoresis: A critical review. *Anal. Chim. Acta*, 1-2(64):99-107.
- Koryta, J., Dvorak, J. and Kavan, L. (1993). **Principles of electrochemistry**. 2nded. New York: John Wiley & Son, Inc. pp 100-101.
- Lau, O.-W., Luk, S.-F. and Cheung, Y. P. M. 1989 Simultaneous Determination of Ascorbic Acid, Caffeine and Paracetamol in Drug Formulations by Differential-Pulse Voltammetry Using a Glassy Carbon Electrode, *Analyst.* (114): 1047-1051.
- Li, M., Li, Y., Li, D-W. and Long, Y-T. (2012). Recent developments and applications of screen-printed electrode in environmental assays-A review. *Anal. Chim. Acta.* (734): 31-44.
- Lindner, E., Lu, Z.-L., Mayer, H. A., Speiser, B., Tittel, C. and Warad, I. (2005). Combinatorial micro electrochemistry. Part 4: Cyclic voltammetric redox screening of homogeneous ruthenium(II) hydrogenation catalysts. *Electrochem.*

Commun. (7): 1013-1020.

Leon, L. E. and Catapano, J. (1993). Indirect flow-injection analysis of ascorbic acid by photochemical reaction of methylene blue. **Anal. Lett.** (26): 1741.

Lin, W-Y., Deng, Y-J., Liao, W-S., Sun, S-W., Lin, W-Y. and Chen, C-C. (2004). Electrophoretic behavior and pKa determination of quinolone with a piperazinyl substituent by capillary zone electrophoresis. **Chromatography A.** (1051): 283-290.

Loveday, D., Peterson, P. and Rodgers, B. (2004). Evaluation of organic coatings with electrochemical impedance spectroscopy. Part 1: Fundamentals of electrochemical impedance spectroscopy. **J. Coat. Technol. Res.** 46-52.

Markle, W., Speiser, B., Tittel, C. and Vollmer, M. 2005. Combinatorial micro electrochemistry Part 1. Automated micro electrosynthesis of iminoquinol ether and [1,2,4]triazolo[4,3-*a*]pyridinium perchlorate collections in the wells of microtiter plates. **Electrochim. Acta.** (50): 2753-2762.

Mastos, R. C., Angnes, L., Araujo, M. C., U. and Salanha, T. c. B. (2000). Modified microelectrodes and multivariate calibration for flowinjection amperometric simultaneous determination of ascorbic acid, dopamine and epinephrine. **Electrochem.** 14: 1102-1107.

Meissam, N. Mozhgan, K-M. and Hamed, T. (2013). Electrochemical determination of ascorbic acid using modified glassy carbon electrode by multiwall carbon nanotube-Nafion in Chloroacetic acid media. **Chem. ASIAN J.** 1(25): 119-124.

Miner, D. J., Rice, J. R., Riggin, R. M. and Kissinger, P. T. (1981). Voltammetry of Acetaminophen and Its Metabolites, **Anal. Chem.** 53: 2258-2263.

Nair, S. S., John, A. and Sagara, T. (2009). Simultaneous determination of paracetamol

and ascorbic acid using tetraoctylammonium bromide capped gold nanoparticles immobilized on 1,6-hexanedithiol modified Au electrode **Electrochim. Acta.** (54): 6837-6843.

Nascimento, VB. and Angnes, L. (1998). Screen-printed electrodes. **Quim. Nova**, 5(21): 614-629.

Navarro, I., Gonzalez-Arjona, D., Roldan, E. and Rueda, M. (1988). Determination of Paracetamol in Tablets and Blood Plasma by Differential Pulse Voltammetry, **J. Pharm. Biomed. Anal.** (6): 969-976.

Nayssonen, K., Pikkarainen, S., Parviainen, M. T., Heinonen, K. and Mononen, I. (1988). Quantitative estimation of dehydroascorbic acid and ascorbic acid by high-performance liquid chromatography-application of human milk, plasma and leukocytes. **Liq. Chromatogr.** (11): 1717.

Noroozifar, M., Mozghan, K-M. and Hamed, T. (2011). Preparation of tetraheptyl ammonium iodide-iodine graphite-multiwall carbon nanotube paste electrode: electrolytic determination of ascorbic acid in pharmaceuticals and foods. **Anal. Sci.** 9(27): 929-935.

Ozkan, S. A., Uslu, B. and Aboul-Enein, H. Y. (2003). Analysis of Pharmaceuticals and Biological Fluids Using Modern Electroanalytical Techniques. **Anal. Chem.** 33: 155-181.

Pachla, LA., Reynolds, DL. And Kissinger, PT. (1985). Analytical methods for determining ascorbic acid in biological samples, food products and pharmaceuticals. **Anal. Chem.** 68(1): 1-12.

Padayatty S. J., Katz, A., Wang, Y., Eck, P., Kwon, O., Lee, J-H., Chen, S., Corpe, C., Dutta, A., Dutta, K. and Levine, N. (2003). Vitamin C as an antioxidant:

- Evaluation of its role in disease prevention. **JACN**. 22: 18-35.
- Patriarche. (1986). New trends on modified electrodes: applications of drug analysis. **Pharm. Biomed. Anal.** 4(6): 789-97.
- Preantoni, C., B., Carbogim. L. G. S., Semaan, F. S., Matos, R. C. and Lowinsohn, D. (2011). Flow injection analysis of ethambutol in antituberculosis drugs using a graphite-paraffin electrode as amperometric detector. **Electroanalysis**. (23): 2582-2585.
- Petersen, P. (1999). **Diagnosis and management of infectious diseases**. Wordnet. Rochedale South Qld 4123, Australia. pp 1-67.
- Pletcher, D. (1991). **Microelectrodes: Theory and applications**. Netherlands: Kluwer Academic Publishers. pp 3-16.
- Raouf, J. B., Kiani, A., Ojani, R. and Valiollahi, R. (2011). Electrochemical determination of dopamine using banana-MWCNTs modified carbon paste electrode. **Anal. Bioanal. Chem.** 1(3): 59-66.
- Reiter, S., Ruhligh, D., Ngounou, B., Neugebauer, S., Janiak, S., Vilkanauskite, A. and Schuhmann, W. (2004). An electrochemical robotic system for the optimization of amperometric glucose biosensors based on a library of cathodic electrodeposition paints. **Macromol. Rapid Commun.** 25: 348-354.
- Richard, L. and McCreery. (2008). New electrodes fold: from carbon nanotubes to edge plane pyrolytic graphite. **Chem. Rev.** 108(7): 2646-2787.
- Ryabova, V., Schulte, A., Erichsen, T. and Schuhmann, W. (2005). Robotic sequential analysis of a library of metalloporphyrins as electrocatalysts for voltammetric nitric oxide sensors. **Analyst**. 130: 1245-1252.

- Salem, H. (2005). Spectrofluorimetric, atomic absorption spectrometric and spectrophotometric determination of some fluoroquinolones. **J. Appl. Sci.** 2(3): 219-229.
- ShangGuan, X., Zhang, H. and Zheng, J. (2008). Electrochemical behavior and differential pulse voltammetric determination of paracetamol at a carbon ionic liquid electrode. **Anal. Bioanal. Chem.** 391: 1049-1055.
- Snell, E. E., Strong, F. M. and Peterson, W. H. Growth factors for bacteria viii. Pantothenic and nicotinic acids as essential growth factors for lactic and propionic acid bacteria', **J. Am. Chem. Soc.** 61: 293-308.
- Spraul, M., Hofmann, M., Lindon, L. C., Farrant, M. D., Seddon, M. J., Nicholson, J. K. and Wilson, I. D. (1994). Evaluation of liquid chromatography coupled with high-field ¹H NMR spectroscopy for drug metabolites in urine and bile. **NMR Biomed.** 7: 295-303.
- Solangi, A. R., Huhawar, M. R. and Bhangar, M. I. (2005). Adsorptive stripping voltammetric determination of fluoroquinolones in pharmaceuticals. **JFDA.** 13:201-204.
- Skoog, D., Holler, F. and Nieman, T. (1997). **Principles of Instrumental Analysis.** 5th ed. USA: Thomson Learning, Inc. pp 876-877.
- Stumpf, M. Ternes, T. A., Wilken, R-R., Rodrigues, S. and Baumann, W. (1999). Polar drug residues in sewage and natural waters in the state of Rio De Janeiro, Brazil. **Sci. Total Environ.** 225: 135-141.
- Tan, W. T., Bond, A. M., Ngooi, S. W., Lim, E. B. and Goh, J. K. (2003). Electrochemical oxidation of l-cysteine mediated by a fullerene-C60-modified

- carbon electrode. **Anal. Chim. Acta.** 491: 181-191.
- Ternes, T. A., Bonerz, M. and Schmidt, T. (2001). Determination of neutral pharmaceutical in waste water and rivers by liquid chromatography-electrospray tandem mass spectrometry. **Chromatography A.** 938: 175-185.
- Ternes, T. A., Hirsch, R., Mueller, I. and Haberer, K. (1998). Method for the determination of neutral as well as betablockers and β_2 -sympathomimetics in aqueous matrices using GC/MS and LC/MS. **Anal. Chem.** 362: 329-340.
- Truong, L. T. N., Chikae, M., Ukita, Y. and Takamura, Y. (2011). Labelless impedance immunosensor based on polypyrrole-pyrolecarboxylic acid copolymer for hGG detection. **Talanta.** 85: 2576-2580.
- Tsierkezos, N. G. and Ritter, U. (2010). Synthesis and electrochemistry of multiwalled carbon nanotube films directly attached on silica substrate. **J. Solid State Electrochem.** 14: 1101-1107.
- Tungkanauruk, K., Tungkanauruk, N. and Burns, D. T. (2005). Cyclic voltammetric determination of acetamidophene in paracetamol tablets. **Sci. Tech. J.** 5: 457-551.
- Uslu, B. and Ozkan, S.H. (2007). Solid electrodes in electroanalytical chemistry: present applications and prospects for high throughput screening of drug compounds. **Comb. Chem. High T. Scr.** 10: 495-513.
- Varadharaj, S., Watkins, T., Cardounel, A. J., Garcia, J. G. N., Zweire, J. L., Kuppusamy, P., Natarajan, V. and Parinandi, N. L. (2005). Vitamine C-induced loss of redox-dependent viability in lung micro vascular endothelial cells. **Antioxid. Redox Signaling.** 7: 287-300.
- Vashist, S. K., Zheng, D., Al-Rubeaan, K., Luong, J. H. T. and Sheu, F-S. (2011). Advances in carbon nanotube based electrochemical sensors for bioanalytical

- applications. **Biotechnol. Adv.** 2(29): 169-188.
- Vire, J-C., Kauffmann, J-M. and Pafriarche. (1989). Adsorptive stripping voltammetry applied to drug analysis: A powerful tool. **Pharm. Biomed. Anal.** 12(7): 1323-1335.
- Wang, C., Hu, C.X., Leng, Z., Yang, G. and Jin, G. (2001). Differential Pulse Voltammetry for Determination of Paracetamol at a Pumice Mixed Carbon Electrode, **Analyt. Lett.** 34: 2747-2759.
- Wangfuengkanagul, N. and Chailapakul, O. (2001). Electrochemical analysis of acetamidophene using a boron-doped diamond thin film electrode applied to flow injection system. **Pharm. Biochem. Anal.** 28: 841-847.
- Wangfuengkanagul, N., Siangproh, W. and Chailapakul, O. (2004). A flow injection method for the analysis of tetracycline antibiotics in pharmaceutical formulations using electrochemical detection at anodized boron-doped diamond thin film electrode. **Talanta.** 64: 1183-1188.
- Wang, J. (2000). **Analytical electrochemistry.** 2nd ed. New York: John Wiley & Son, Inc. p 141.
- Wang, J. (2006) **Analytical electrochemistry.** 3th ed. New York: John Wiley & Son, Inc. p 165.
- Wang, SH. (1989). Advances in liquid chromatography and related methodologies for therapeutic drug monitoring. **Pharm. Biomed. Anal.** 7(9): 1011-32.
- Wang. (1999). Amperometric biosensors for clinical and therapeutic drug monitoring: A review. **Pharm. Biomed. Anal.** 1-2(19): 47-53.
- Washko, P. W., Hartzell, W. o. and Levine, M. (1989). Ascorbic acid determination using high-performance liquid chromatography with coulometric electrochemical

- detection. **Anal. Biochem.** (181): 276-282.
- Wikipedia. **Norfloxacin** [on-line]. Available: <http://en.wikipedia.norfloxacin.html>.
- Yamanaka, J., Yoshida, H., Koga, T., Ise, N. and Hashimoto, T. (1998). Reentrant solid-Liquid transition in ionic colloidal dispersions by varying particle charge density. **Phys. Rev. Lett.** 80: 5806-5809.
- Yang, Z-h. and Wu, H-q. (2001). The electrochemical measurements of carbon nanotubes. **Chem. Phys. Lett.** 324: 235-340.
- Yang, Y-L., Unnikrishnan, B. and Chem, S-M. (2011). Amperometric Determination of 4-Nitrophenol at Multi-Walled Carbon Nanotube-Poly (Diphenylamine) Composite Modified Glassy Carbon Electrode. **Electrochem. Sci.** 6: 3902-3912.
- Yardim, Y. (2011). Cathodic adsorptive stripping voltammetry of ascorbic acid using pencil lead bismuth-film electrode. **Anal. Chem. Rev.** 1(30): 37-43.
- Yogesworan, U. and Chen, S-M. (2008). Recent trends in the application of carbon nanotubes-polymer composite modified electrodes for biosensors: A review. **Anal. Lett.** 2(41): 210-243.
- Yu, S-H. and Zhao, G-C. (2012). Preparation of platinum nanoparticles-graphene modified electrode and selective determination of rutin. **Int. J. Electrochem.** (2012): 1-6.
- Zagal, JH., Griveau, S. Ozoemena, KJ., Nyokong, I. and Bedioui, F. (2009). Carbon nanotube, phthalocyanines and porphyrins: attractive hydride materials for electrocatalysis and electroanalysis. **Nanosci. Nanotechnol.** 9(4): 2201-14.
- Zen, J.-M. and Ting, Y-S. (1997). Simultaneous Determination of Caffeine and Acetaminophen in Drug Formulations by Square-Wave Voltammetry Using a Chemically Modified Electrode, **Analyt. Chim. Acta.** 342: 175-180.

- Zidan, M., Tee, T. W., Abdullah, A. H., Zainal, Z. and Kheng, G. J. (2011). Electrochemical oxidation of paracetamol mediated by nanoparticle bismuth oxide modified glassy carbon electrode. **Electrochem. Sci.** 6: 279-288.
- Zhang, S. and Wei, S. (2007). Electrochemical determination of ciprofloxacin based on the enhancement effect of sodium dodecyl benzene sulfonate. **Bull. Korean Chem. Soc.** 28: 543-546.
- Zhu, Q-G., Sujari, A. M. A. and Ghani, S. A. (2012). Electrophoretic deposition MWCNT composite graphite pencils and its uses to determine hyperin. **J. Solid State Electrochem.** 16: 3179-3187.



APPENDICES



APPENDICE A

SOLUTION PREPARATION FOR DRUG SCREENING



A.1 Preparation of supporting electrolytes

1. A dispersion of CNT of 20 mg/ml carbon nanotube (P3-SWNT) in water; it is used for the electrophoretic deposition of the PLE (preparation of WE):

20 mg of CNT was dissolved in DI water in 1 mL eppendorf tube. The solution was suspended in ultrasonic bath.

2. Potassium chloride solution of 0.1 M of KCl as supporting electrolyte of AA determination.

3.7278 g of KCl was dissolved in DI water and transfer in to a 500 mL volumetric flask. The solution was made up to volume with water.

3. Acetate buffer solution of 0.1 M of $\text{CH}_3\text{COONa}\cdot\text{H}_2\text{O}$ and CH_3COOH (pH 4.5) as supporting electrolyte of NFX determination:

3.4025 g of $\text{CH}_3\text{COONa}\cdot\text{H}_2\text{O}$ was dissolved in DI water and transferred in to a 250 mL volumetric flask (A), 2.8736 mL of CH_3COOH was dissolved in DI water and transferred in to 500 mL volumetric flask (B) and 3.7278 g of KCl was added. Third of them were mixed up to the volume 500 mL (196 mL (A):304 mL (B)). The solution was adjusted to pH of 4.5 levels by NaOH solution addition.

4. Phosphate buffer solution of 0.1 M of $\text{C}_8\text{H}_5\text{KO}_4$ and HCl (pH 4.0) as supporting electrolyte of CFX determination:

5.11 g of $\text{C}_8\text{H}_5\text{KO}_4$ was dissolved in DI water and transferred in to a 500 mL volumetric flask and 0.5 mL of 0.1 M HCl and 3.7278 g of KCl were added. The solution was made up to volume with water and pH was adjusted to 4.0 by HCl solution addition.

5. A solution of 0.1 M KH_2PO_4 in water (pH 4.5) as supporting electrolyte of PCT determination:

3.4013 g of KH_2PO_4 was dissolved in 0.1 M KCl and transferred in to 500 mL volumetric flask. The solution was made up to volume with 0.1 M KCl and pH was adjusted to 4.0 by HCl solution addition.

A.2 Preparation of stock standard solution

1. A stock standard solution of 1mM Norfloxacin in 0.01 M HCl:

32 mg of $\text{C}_{16}\text{H}_{18}\text{FN}_3\text{O}_3$ (NFX) was dissolved in 0.01 M and transferred in to a 10 mL volumetric flask. The solution was made up to the volume with 0.01 M HCl.

2. A stock standard solution of 1 mM Ciprofloxacin in 0.01 M HCl:

33 mg of $\text{C}_{17}\text{H}_{18}\text{FN}_3\text{O}_3$ (CFX) was dissolved in 0.01 M and transferred in to 10 mL volumetric flask. The solution was made up to the volume with 0.01 M HCl.

3. A stock standard solution of 1 M ascorbic acid in water:

1.76 g of L(+) Ascorbic acid (AA) was dissolved in DI water and transferred in to a 10 mL volumetric flask. The solution was made up to the volume with DI water.

4. A stock standard solution of 1 mM a 4-cetamidophenol (paracetamol) in water:

15 mg of $\text{C}_8\text{H}_9\text{NO}_2$ (PCT) was dissolved in DI water and transferred in to 10 mL volumetric flask. The solution was made up to the volume with DI water.

5. A solution of 0.1 M $\text{K}_3\text{Fe}(\text{CN})_6$ in 0.1 M KCl; it is used as reversible redox mediator standard solution.

1.6463 g of $\text{K}_3\text{Fe}(\text{CN})_6$ was dissolved in 0.1 M KCl and transferred in to a 50 mL volumetric flask. The solution was made up to volume with 0.1 M KCl.

A.3 Preparation of stock sample solution

1. A stock sample solution of 400 mg Norfloxacin tablets was obtained by dilution in 100 ml of 0.01 M HCl (sample preparation):

400 mg of NOFAR was dissolved in 0.01 M and transferred in to a 100 mL volumetric flask. The solution was made up to the volume with 0.01 M HCl.

2. A stock sample solution of 500 mg Ciprofloxacin tablets was obtained by dilution in 50 ml of 0.01 M HCl (sample preparation):

500 mg of Cobay was dissolved in 0.01 M and transferred in to a 50 mL volumetric flask. The solution was made up to the volume with 0.01 M HCl.

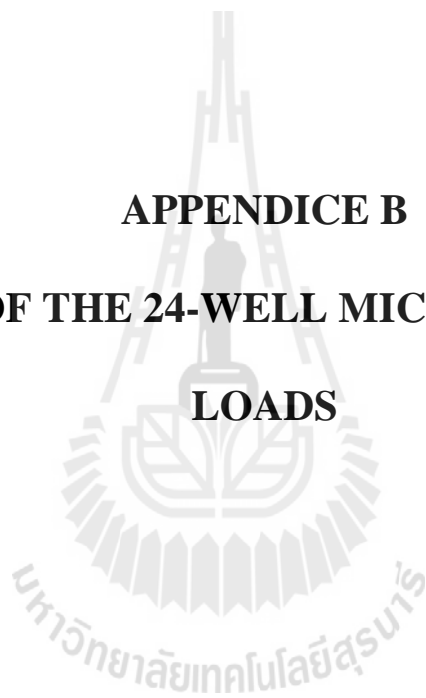
3. A stock sample solution of 500 mg vitamin C tablets was obtained by dilution in 50 ml water (sample preparation):

500 mg of Hicee was dissolved in DI water and transferred in to a 50 mL volumetric flask. The solution was made up to the volume with DI water.

4. A stock sample solution of 500 mg Paracetamol of Tylenol or Sara was obtained by dilution in 100 ml water (sample preparation):

500 mg of Tylenol was dissolved in DI water and transferred in to a 100 mL volumetric flask. The solution was made up to the volume with DI water.

APPENDICE B
SCHEMES OF THE 24-WELL MICROTITER PLATE
LOADS



B.1 Ascorbic acid

Table B.1 is listing the volumes of solutions of AA to be loaded in to the 24 wells microtiter plates for robotic quantification. Wells #1 had 4 M HNO₃ for electrode pretreatment, well #2 and 7 were water-filled for electrode cleaning, well #3 had bare 0.1 M KCl, well #4 to 9 were for AA calibration, well #10 to 16 were for model sample measurement of AA and well #14 to 16 were for real sample measurement. Automated DPV AA measurement in the model and real samples used six times repetition in one microtiter plate run.

Table B.1 Solution volumes of AA for calibration and sample measurement in 24-well microtiter plates.

Well- No.	Solution			Well- No.	Solution		
	0.1 M KCl (μL)	AA 1 mM (μL)	real sample (μL)		0.1 M KCl (μL)	AA 1 mM (μL)	real sample (μL)
3	3000	–	–	14	2997	3	–
4	2997	3	–	15	2997	3	–
5	2994	6	–	16	2997	3	–
6	2991	9	–	17	2940	–	60
8	2988	12	–	18	2940	–	60
9	2985	15	–	20	2940	–	60
10	2997	3	–	21	2940	–	60
11	2997	3	–	22	2940	–	60
12	2997	3	–	23	2940	–	60

Note - Well #1 is containing 4 M HNO₃ solution.

- Well #2 and 7 are containing H₂O.

- Real sample is 500 mg/tablet Hicee (Vitamin C) dissolved in water.

B.2 Norfloxacin (NFX)

Table B.2 is listing of the solution volumes of NFX to be loaded in to the 24 well microtiter plates for robotic calibration measurement. Wells #1 had 4 M HNO₃ for electrode pretreatment, well #3 to 23 were water-filled for electrode cleaning, well #2 had bare 0.1 M acetate buffer pH 4.5, well #4 to 24 are of NFX calibration. Automated DPV of NFX measurement in one microtiter plate run.

Table B.3 is listing of the solution volumes of NFX to be loaded in to the 24 well microtiter plates for robotic commercial samples measurement. Wells #1 had 4 M HNO₃ for reproducible electrode, well #2, 7, 13 and 19 were water-filled for cleaning electrode, well #2, 8, 14 and 20 had bare 0.1 M acetate buffer pH 4.5, well #3 to 21, #4 to 22, #5 to 23, and #6 to 24 were for standard addition of NFX measurement with four times repetition in one of microtiter plate run (the model sample got measured 16 times for accurately of NFX). And also the solution volumes for the serum sample and spike serum sample are presented in the Table B.4.

Table B.2 Solution preparation of NFX for calibration measurement in 24-well microtiter plates.

Well- No.	Well-Solution		Well No.	Well-Solution	
	AC buffer pH 4.5 (μL)	1 mM NFX (μL)		AC buffer pH 4.5 (μL)	1 mM NFX (μL)
2	3000	–	14	2970	30
4	2997	3	16	2940	60
6	2994	6	18	2880	120
8	2988	12	20	2820	180
10	2982	18	22	2760	240
12	2976	24	24	2700	300

Note - Well #1 is a containing 4 M HNO₃ solution.

- Well #3, 5, 7, 9, 11, 13, 15, 17, 19, 21 and 23 are containing of water.

Table B.3 Sample solution volumes of NFX measurement in 24-well microtiter plates.

Well-No.	Solution (model sample)		Well-No.	Solution (real sample)		
	AC buffer pH 4.5 (μL)	1 mM NFX (μL)		AC buffer pH 4.5 (μL)	1 mM NFX (μL)	real sample (μL)
2, 8, 14, 20	3000	–	2, 8, 14, 20	3000	–	–
3, 9, 15, 21	2994	6	3, 9, 15, 21	2999.5	–	0.5
4, 10, 16, 22	2988	12	4, 10, 16, 22	2990.5	9	0.5
5, 11, 17, 23	2982	18	5, 11, 17, 23	2981.5	18	0.5
6, 12, 18, 24	2976	24	6, 12, 18, 24	2972.5	27	0.5

Note - Well #1 is containing 4 M HNO₃ solution

- Well #2, 7, 13 and 19 are containing of water and Real sample is 400 mg/tablet NOFAR (Norfloxacin) drug dissolved in 0.01 M HCl

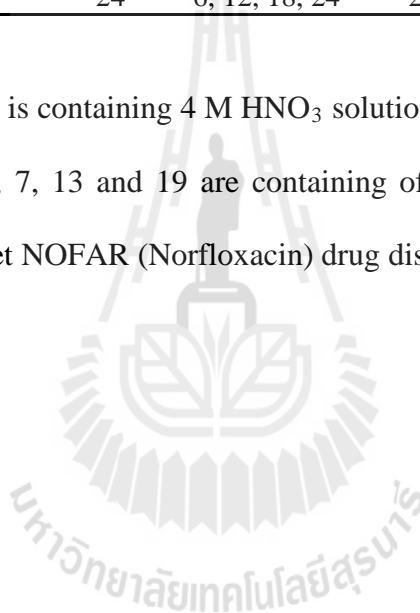


Table B.4 Serum sample solution volumes of NFX measurement in 24-well microtiter plates.

Well-No.	Solution (serum sample)			Well-No.	Solution (spike serum sample)		
	AC buffer pH 4.5 (μL)	1 mM NFX (μL)	Serum sample (μL)		AC buffer pH 4.5 (μL)	1 mM NFX (μL)	Serum sample (μL)
2, 8, 14, 20	3000	-	-	2, 8, 14, 20	3000	-	-
3, 9, 15, 21	2894	-	100	3, 9, 15, 21	2894	6	100
4, 10, 16, 22	2888	6	100	4, 10, 16, 22	2888	12	100
5, 11, 17, 23	2884	12	100	5, 11, 17, 23	2882	18	100
6, 12, 18, 24	2882	18	100	6, 12, 18, 24	2876	24	100

- Note
- Well #1 is containing 4 M HNO₃ solution
 - Well #2, 7, 13 and 19 are containing of water
 - Serum sample from volunteer in our laboratory

Table B.4 is explaining of the solutions preparation of NFX to be loaded in to the 24 well microtiter plates for robotic quantification of spike serum samples. Wells #1 had 4 M HNO₃ for reproducible electrode, well #2, 7, 13 and 19 were water-filled for cleaning electrode, well #2, 8, 14 and 20 had bare 0.1 M acetate buffer pH 4.5, well #3 to 21, #4 to 22, #5 to 23, and #6 to 24 were of standard addition of NFX measurement for represent four times in one of microtiter plate run.

B.3 Ciprofloxacin (CFX)

Table B.5 is listing of the solution volumes of CFX to be loaded in to the 24 well microtiter plates for robotic quantification. Wells #1 had 4 M HNO₃ for electrode pretreatment, well #3 to 23 were water-filled for electrode cleaning, well #2 had bare 0.1 M PBS buffer pH 4.0, well #4 to 24 are of CFX calibration. Automated DPV of CFX measurement in one microtiter plate run.

Table B.6 is listing of the solution volumes of CFX to be loaded in to the 24 well microtiter plates for robotic quantification. Wells #1 had 4 M HNO₃ for electrode pretreatment, well #2, 7, 13 and 19 were water-filled for electrode cleaning, well #2, 8, 14 and 20 had bare 0.1 M acetate buffer pH 4.5, well #3 to 21, #4 to 22, #5 to 23, and #6 to 24 were of standard addition of CFX measurement for represent four times in one of microtiter plate run. And also for the solution volume for the real sample, is listed in Table 6.

Table B.5 Solution volumes of CFX for calibration measurement in 24-well microtiter plates.

Well- No.	Solution		Well- No.	Solution	
	PBS buffer pH 4.0 (μL)	1 mM CFX (μL)		PBS buffer pH 4.0 (μL)	1 mM CFX (μL)
A2	3000	–	C2	2940	60
A4	2994	6	C4	2980	120
A6	2988	12	C6	2820	180
B2	2982	18	D2	2760	240
B4	2976	24	D4	2700	300
B6	2970	30			

Note - Well 1 is containing 4 M HNO₃ solution.

- Well 3, 5, 7, 9, 11, 13, 15, 17, 19 and 21 are containing water.

Table B.6 Sample solution volumes for CFX measurement in 24-well microtiter plates.

Well-No.	Solution (model sample)		Well-No.	Solution (real sample)		
	PBS buffer pH 4.0 (μL)	1 mM CFX (μL)		PBS buffer pH 4.0 (μL)	1 mM CFX (μL)	real sample (μL)
2, 8, 14, 20	3000	–	2, 8, 14, 20	3000	–	–
3, 9, 15, 21	2970	30	3, 9, 15, 21	2990	–	10
4, 10, 16, 22	2940	60	4, 10, 16, 22	2930	60	10
5, 11, 17, 23	2910	90	5, 11, 17, 23	2870	120	10
6, 12, 18, 24	2880	120	6, 12, 18, 24	2810	180	10

Note - Well 1 is containing 4 M HNO_3 solution

- Well 2, 7, 13 and 19 are containing of water

- Real sample is 500 mg/tablet COBAY (Ciprofloxacin) drug dissolved in
0.01 M HCl

B.4 Paracetamol (PCT)

Table B.7 is listing the solution volumes of PCT to be loaded in to the 24 well microtiter plates for robotic quantification. Wells #1 had 4 M HNO_3 for electrode pretreatment, well #3 to 23 were water-filled for electrode cleaning, well #2 had bare 0.1 M KH_2PO_4 buffer pH 4.5, well #4 to 24 are of PCT calibrations. Automated DPV of PCT measurement in one microtiter plate run.

Table B.8 is listing the solution volumes of PCT to be loaded in to the 24 well microtiter plates for robotic (model sample) quantification. Wells #1 had 4 M HNO_3 for electrode pretreatment, well #2, 7, 13 and 19 were water-filled for electrode cleaning, well #2, 8, 14 and 20 had bare 0.1 M KH_2PO_4 buffer pH 4.5, well #3 to 21, #4 to 22, #5 to 23, and #6 to 24 are for standard addition of PCT measurement for represent four times repetition in one microtiter plate run. And the solution volumes for the real sample, is

listed in Table B.8. And the solution volumes for the urine sample after contribution of two tablets (1000 mg for dosage) of paracetamol, (keep the urine sample at $t_{0\text{min}}$, $t_{45\text{min}}$ and $t_{4\text{h}}$ for confirm the peak current), is listed in the Table B.9.

Table B.7 Solution volumes of PCT for calibration measurement in 24-well microtiter plates.

Well- No.	Solution		Well- No.	Solution	
	KH ₂ PO ₄ pH 4.0 (μL)	1 mM PCT (μL)		KH ₂ PO ₄ pH 4.0 (μL)	1 mM PCT (μL)
2	3000	–	12	2820	180
4	2985	15	14	2760	240
6	2970	30	16	2700	300
8	2940	60	18	2550	450
10	2880	120			

Note - Well 1 is containing 4 M HNO₃ solution.

- Well 3, 5, 7, 9, 11, 13, 15 and 17 are containing of water.

Table B.8 Sample solution preparation of PCT measurement in 24-well microtiter plates.

Well-No.	Solution (model sample)		Well-No.	Solution (real sample)		
	KH ₂ PO ₄ pH 4.0 (μL)	1 mM PCT (μL)		KH ₂ PO ₄ pH 4.0 (μL)	1 mM PCT (μL)	real sample (μL)
2, 8, 14, 20	3000	–	2, 8, 14, 20	3000	–	–
3, 9, 15, 21	2970	30	3, 9, 15, 21	2998.5	–	1.5
4, 10, 16, 22	2940	60	4, 10, 16, 22	2968.5	30	1.5
5, 11, 17, 23	2910	90	5, 11, 17, 23	2938.5	60	1.5
6, 12, 18, 24	2880	120	6, 12, 18, 24	2908.5	90	1.5

Note - Well 1 is a containing 4 M HNO₃ solution

- Well 2, 7, 13 and 19 are containing of water

- Real sample is 500 mg/tablet Sara (Paracetamol) drug dissolved in water

Table B.9 is listing the solutions volumes of PCT to be loaded in to the 24 well microtiter plates for robotic (urine sample) quantification. Wells #1 had 4 M HNO₃ for electrode pretreatment, well #2, 7, 13 and 19 were water-filled for electrode cleaning, well #2, 8, 14 and 20 had bare 0.1 M KH₂PO₄ buffer pH 4.5, well #3 to 21, #4 to 22 and #5 to 23 were standard addition of PCT measurement for represent three times repetition in one microtiter plate run.

Table B.9 Sample solution preparation of PCT in urine sample measurement in 24-well microtiter plates.

Well-No.	Solution (urine sample)		
	KH ₂ PO ₄ pH 4.0 (μ L)	1 mM PCT (μ L)	urine sample (μ L)
2, 8, 14, 20	3000	–	–
3, 9, 15, 21	2900	–	100
4, 10, 16, 22	2840	60	100
5, 11, 17, 23	2780	120	100
6, 12, 18, 24	2720	180	100

Note - Well 1 is containing 4 M HNO₃ solution

- Well 2, 7, 13 and 19 are containing of water

- Urine sample from volunteer in our laboratory

APPENDICE C

DESIGN OF SOFTWARE FOR THE EXECUTION OF

ROBOTIC ELECTROCHEMICAL ANALYSIS IN 24-WELL

MICROTITER PLATES



C.1 Robotic electrochemical parameter for robotic script writing to execute robotic electrochemical system using microtiter plate format

A description of the software and abbreviations used for script design for voltammetry and the command of x, y and z micro-positioning system control robotic software are provided in Table C.1. The software scripts for cyclic, differential pulse voltammetry and amperometry and for electrode movement were written in Notepad (see Table C.2)

Table C.1 Listed parameters and abbreviations of voltammetric techniques used in software script of the robotic electrochemical device.

Abbreviation	Implication
E begin	Potential where a scan starts. The applicable range of the potential is -2V to +2V.
E start	Potential where a CV scan starts. The value must be between E vtx1 and E vtx2.
E vtx1	Potential where a scan direction is reversed (CV only). The applicable range of the potential is -2V to +2V.
E end	Potential where a measurement stops.
E vtx2	Potential where a scan direction is reversed (CV only). The applicable range of the potential is -2V to +2V.

Table C.1 Listed parameters and abbreviations of voltammetric techniques used in software script of the robotic electrochemical device (Continued).

Abbreviation	Implication
E step	Step potential (not for CP).
E pulse	Pulse potential (DPV only).
E cond	Potential applied before the deposition stage. Is only relevant when $t_{dep} > 0$ s.
E dep	Potential applied during the deposition stage. Is only relevant when $t_{dep} > 0$ s.
E stby	Potential applied after the measurement is finished.
I strip	Stripping current (CP only). If specified as 0, the method is called chemical stripping otherwise it is constant current stripping. The applicable range is $\pm 0.001 \mu\text{A}$ to $\pm 2 \text{ mA}$. The applicable range of the potential is -2 V to $+2 \text{ V}$.
Scan rate	The applied scan rate. The applicable range depends on the value of E step. In case the scan rate is so low that the time between two measured points is longer than approx. 0.05 s, the measured data points are displayed during the measurement. In other cases the measurement is completed before the points are shown.

C.2 The quantification AA in Vitamin C tablet via calibration method

Table C.4 The data for the AA measurement.

No.	Volume AA (μL)	Calculation [AA] (mM)	Calculation [AA] (mg/Tablet)
1	60	1.13	
2	60	1.15	
3	60	1.12	
4	60	1.11	495.61
5	60	1.12	
6	60	1.13	
average	60	1.13	

Involved calculation;

The concentration of AA 500 mg/50 mL (molecular weight AA are 176.13 g/mole)

$$[\text{AA}] = \frac{500 \text{ mg}}{50 \text{ mL}} = 10 \text{ g/L}$$

Therefore, the concentration of AA dilution in robotic system is:

$$C_1 V_1 = C_2 V_2$$

$$C_1 = \text{AA concentration, g/L}$$

$$V_1 = \text{AA volume, } \mu\text{L}$$

$$C_2 = \text{final concentration of AA, g/L}$$

$$V_2 = \text{final volume of AA in well (3 mL)}$$

$$(10 \text{ g/L}) \times (60 \mu\text{L}) = C_2 \times (3 \text{ mL})$$

$$C_2 = 200 \text{ mg/L}$$

The Molar concentration of AA can be calculated from:

$$[\text{AA}] = \frac{200 \text{ mg/L}}{176.13 \text{ g/mol}}$$

$$[\text{AA}] = 1.14 \text{ mM/3mL}$$

Table C.6 The Notepad software script for NFX quantification via standard addition method for the plate layout in to Figure 4.23 (Continued).

1			2	3	4	5	7	8	9	10	11	15	16	17
Well- No.			Ebeg in (V)	Eend (V)	Estep (mV)	Epulse (mV)	Econd (V)	Edep (V)	Estant (V)	scan rate (mV/s)	tpulse (s)	tcond (s)	tdep (s)	tstant (s)
D4	POT	DPV	0	1.2	4	50	0	0	0	20	0.07	10	300	0
A1	WAIT	10												
D1	WAIT	5												
D5	POT	DPV	0	1.2	4	50	0	0	0	20	0.07	10	300	0
A1	WAIT	10												
D1	WAIT	5												
D6	POT	DPV	0	1.2	4	50	0	0	0	20	0.07	10	300	0
D1	WAIT	5												
A1	WAIT	10												
# stop the script execution with a stop-command														
A1	STOP													

C.5 The quantification NFX in NORFA tablet and spike serum samples via standard addition method

Table C.8 The data for the NFX measurements.

NFX in tablet				Spike serum		
No.	Volume NFX (μL)	Calculation [NFX] (mM)	Calculation [NFX] (mg/Tablet)	No.	Volume NFX (μL)	Calculation [NFX] (μM)
1	0.50	2.01		1	2.0	2.10
2	0.50	1.96		2	2.0	2.10
3	0.50	2.03		3	2.0	2.07
4	0.50	2.20		4	2.0	2.05
5	0.50	2.05	392.38			
6	0.50	2.10				
7	0.50	2.03				
8	0.50	2.10				
average	0.50	2.06		average	2.0	2.10

1 The calculation NFX in tablet sample

Involved calculation;

The concentration of NFX 400 mg/100 mL (molecular weight NFX are 319.331 g/mole)

$$[\text{NFX}] = \frac{400 \text{ mg}}{100 \text{ mL}} = 4 \text{ g/L}$$

Therefore, the concentration of NFX dilution in robotic system is:

$$C_1V_1 = C_2V_2$$

C_1 = NFX concentration, g/L

V_1 = NFX volume, μL

C_2 = final concentration of NFX, g/L

V_2 = final volume of NFX in well (3 mL)

$$(4 \text{ g/L}) \times (0.5 \mu\text{L}) = C_2 \times (3 \text{ mL})$$

$$C_2 = 0.67 \text{ mg/L}$$

The Molar concentration of NFX can be calculated from:

$$[\text{NFX}] = \frac{0.67 \text{ mg/L}}{319.331 \text{ g/mol}}$$

$$[\text{NFX}] = 2.10 \mu\text{M}/3\text{mL}$$

0.5 μL from 4 g/L of NFX have 2.10 $\mu\text{M}/3\text{mL}$ (400 mg/tablet)

Therefore, 2.06 $\mu\text{M}/3\text{mL}$ of NFX (from measurement) have 392.38 mg/tablet

2. The calculation NFX in spike serum sample

Involved calculation;

The linear range regression from standard addition is:

$$y = 1.6008x + 3.3583 \quad (R^2 = 0.9969)$$

y = Current, μA

x = Concentration, μM

$x = 2.10 \mu\text{M}$ (or intercepted extrapolation on the x-axis was proportional to the concentration of NFX)

C.6 The software script for microtiter plate-based assessment of CFX and PCT calibration curve

The software scripts for the calibrations of the CFX and PCT drugs are similar with NFX, as listed in Table C.2, but for the corresponding parameters of them it different follow by below:

Table C.9 The corresponding parameters for CFX and PCT.

Parameters (DPV)	CFX	PCT
E_{begin} (V)	0.3	-0.1
E_{end} (V)	1.3	1.0
E_{step} (mV)	5	5
E_{pulse} (mV)	50	25
E_{cond} (V)	0	0
E_{dep} (V)	0	0
E_{stan} (V)	0	0
scan rate (mV/s)	20	20
t_{pulse} (s)	0.07	0.07
t_{cond} (s)	10	10
t_{dep} (s)	120	0
t_{stan} (s)	0	0

C.7 The software script for microtiter plate-based assessment of CFX and PCT quantification via the standard addition method

The software scripts for the samples measurement of the CFX and PCT drugs that are similar with NFX, as list in Table C.3 and for the corresponding parameters of them it can be used the same with appendix C.4 (four times in one microtiter plates run)

C.8 The quantification CFX in Cobay tablet via standard addition method

Table C.10 The data for the CFX measurements.

No.	CFX in tablet		Calculation [CFX] (mg/Tablet)
	Volume CFX (μL)	Calculation [CFX] (mM)	
1	10	101.64	488.57
2	10	97.08	
3	10	95.87	
4	10	97.58	
5	10	100.25	
6	10	98.50	
7	10	97.70	
8	10	97.60	
average	10	98.28	

The calculation CFX in tablet sample

Involved calculation;

The concentration of CFX 500 mg/50 mL (molecular weight CFX are 331.346 g/mole)

$$[\text{CFX}] = \frac{500 \text{ mg}}{50 \text{ mL}} = 10 \text{ g/L}$$

Therefore, the concentration of CFX dilution in robotic system is:

$$C_1V_1 = C_2V_2$$

C_1 = CFX concentration, g/L

V_1 = CFX volume, μL

C_2 = final concentration of CFX, g/L

V_2 = final volume of CFX in well (3 mL)

$$(10 \text{ g/L}) \times (10 \mu\text{L}) = C_2 \times (3 \text{ mL})$$

$$C_2 = 33.33 \text{ mg/L}$$

The Molar concentration of CFX can be calculated from:

$$[\text{CFX}] = \frac{33.33 \text{ mg/L}}{331.346 \text{ g/mol}}$$

$$[\text{CFX}] = 100.59 \mu\text{M}/3\text{mL}$$

10 μL from 10 g/L of CFX have 100.59 $\mu\text{M}/3\text{mL}$ (500 mg/tablet)

Therefore, 98.28 $\mu\text{M}/3\text{mL}$ of CFX (from measurement) have 488.57 mg/tablet

C.9 The quantification PCT in Tylenol tablet via standard addition method

Table C.11 The data for the PCT measurements

PCT in tablet			PCT in urine		
No.	Volume PCT (μL)	Calculation [PCT] (mM)	Calculation [PCT] (mg/Tablet)	No.	Calculation [PCT] (μM)
1	1.50	16.10		1	6.37
2	1.50	16.82		2	7.02
3	1.50	16.60		3	7.10
4	1.50	16.50		4	7.20
5	1.50	16.00	498.49	5	6.81
6	1.50	17.00		6	6.90
7	1.50	16.50		7	6.70
8	1.50	16.40		8	7.25
average	1.50	16.49		average	6.92

1. The calculation PCT in tablet sample

Involved calculation;

The concentration of PCT 500 mg/100 mL (molecular weight PCT are 151.16 g/mole)

$$[\text{PCT}] = \frac{500 \text{ mg}}{100 \text{ mL}} = 5 \text{ g/L}$$

Therefore, the concentration of PCT dilution in robotic system is:

$$C_1V_1 = C_2V_2$$

C_1 = PCT concentration, g/L

V_1 = PCT volume, μL

C_2 = final concentration of PCT, g/L

V_2 = final volume of PCT in well (3 mL)

$$(5 \text{ g/L}) \times (1.5 \mu\text{L}) = C_2 \times (3 \text{ mL})$$

$$C_2 = 2.5 \text{ mg/L}$$

The Molar concentration of PCT can be calculated from:

$$[\text{PCT}] = \frac{2.5 \text{ mg/L}}{151.16 \text{ g/mol}}$$

$$[\text{PCT}] = 16.54 \mu\text{M}/3\text{mL}$$

1.5 μL from 5 g/L of PCT have 16.54 $\mu\text{M}/3\text{mL}$ (500 mg/tablet)

Therefore, 16.49 $\mu\text{M}/3\text{mL}$ of PCT (from measurement) have 498.49 mg/tablet

2. The calculation PCT in urine sample

Involved calculation;

The linear range regression from standard addition is:

$$y = 0.1074x + 0.743 \quad (R^2 = 0.9997)$$

y = Current, μA

x = Concentration, μM

$x = 6.92 \mu\text{M}$ (or intercepted extrapolation on the x-axis was proportional to the concentration of PCT)

C.10 Statistically

1. Sample standard deviation (SD)

$$\text{SD} = \sqrt{\frac{\sum(x-\bar{x})^2}{n-1}}$$

Note $x = 1, 2, 3, 4 \dots$

$$\bar{x} = x_1 + x_2 + x_3 + x_4 + \dots$$

$n =$ number of data items in sample

2. Relative standard deviation (%RSD)

$$\% \text{RSD} = \frac{\text{SD}}{\bar{x}} \times 100$$

3. Percent recovery

$$\% \text{ Recovery} = \frac{\text{detected amount}}{\text{adjusted amount}} \times 100$$

CURRICULUM VITAE

SOMJAI TEANPHONKRANG

Born: 24 May, 1987 in Nakhon Ratchasima, Thailand

Education:

2006-2010 B. Sc. (Chemistry), Rajamangala University of Technology Isan, Nakhon Ratchasima, Thailand

2010-2013 M. Sc. (Chemistry), Suranaree University of Technology, Nakhon Ratchasima, Thailand

Academic Conference:

2010 International Symposium of The Protein Society of Thailand, Chulabhorn Research Institute, Bangkok, Thailand. (Participant)

2010 Regional Electrochemistry Meeting of South-East Asia 2010, Chulalongkorn University, Bangkok, Thailand. (Participant)

2011 Teanphonkrang S, Intarakamhang S, Schulte A. German-Thai Symposium on Nanoscience and Nanotechnology 2011, Suranaree University of Technology, Nakhon Ratchasima, Thailand. (Participant with poster presentation)

2012 Teanphonkrang S, Winterhalter M, Weingart H, Schulte A. 13th FAOBMB International Congress of Biochemistry and Molecular Biology, Bangkok, Thailand. (Participant with poster presentation)

2013 Schulte A, Weingart H, Teanphonkrang S. International Society of Electrochemistry, Bochum, Germany, (Oral presentation of thesis work by supervisor Assoc. Prof. Dr. Albert Schulte)